Armed Services Technical Information Agency

AD 47616

UNCLASSIFIED

NEW YORK UNIVERSITY
COLLEGE OF ENGINEERING
RESEARCH DIVISION

NOTES ON CYCLONE DEVELOPMENT IN THE UNITED STATES

Technical Paper No. 2

Project SCUD

Contract No. Nonr-285 (09)

September 1954

NEW YORK UNIVERSITY
COLLEGE OF ENGINEERING
RESEARCH DIVISION

NOTES ON CYCLONE DEVELOPMENT IN THE UNITED STATES

Technical Paper No. 2

Project SCUD

Contract No. Nonr-285 (09)

September 1954

Department of
METEOROLOGY AND OCEANOGRAPHY
New York University

PREFACE

This is the second in a series of reports on some descriptive studies of cyclones which were carried out as part of a research project on cyclogenesis (Project SCUD) sponsored by the Office of Naval Research. (The first paper in the series, by E. L. Fisher, dealt with "Upper level temperature fields associated with east coastal cyclogenesis".)

There exists a need, both by the dynamicists, who are attempting the monumental task of weather forecasting by hydrodynamical methods, and the empirical forecasters, for quantitative information about the structure of cyclone development. Whether such information is used to construct new synoptic models, to provide parameters for statistical prediction schemes, or to suggest methods for solving the development problem in numerical forecasting, its essential importance is obvious.

One device for summarizing synoptically many facts about the structure of some atmospheric phenomenon is the composite map. Composite maps have been used rather rarely in meteorology. Yet they do provide a convenient way to test old models of the atmosphere and to construct new ones. In the first section of this report the composite map technique has been employed to construct some pictures of the average horizontal temperature distribution in the lower stratosphere over cyclones which do and cyclones which do not produce secondary lows along the east coast of the United States. This study in comparative analysis was undertaken by Mr. Emanuel M. Ballenzweig, Research Assistant, to test the hypothesis of Mr. E. L. Fisher that there may be found a characteristic anomaly in the 200 mb temperature field prior to the development of certain types of east coastal secondary cyclones. (The article by Mr. Ballenzweig is part of an M.S. thesis submitted to the Department of Meteorology and Oceanography at New York University.)

The routine analyses of upper level maps reveal that deep upper level cyclones, often with no corresponding sea level cyclone, occur frequently and play an important role in low level cyclogenesis. These systems are characterized by cold tropospheric cores and low warm stratospheric cores. The development and propagation of the thermal fields in these cyclones must be affected to an important degree by vertical motions in the atmosphere.

i

The second article in this report presents some calculations of the vertical velocity fields at 500 and 200 mb in such a deep cold cyclone. This research was done by Lieutenants Benjamin M. Herman and John J. R. Kinney, U. S. Air Force, while on temporary duty at New York University. (Although they were not employed on the project, Lieutenants Herman and Kinney worked in close collaboration with Project SCUD and have authorized the inclusion of an abridged version of their M.S. thesis in this report.)

Interest in the analysis of temperature fields at upper levels has been stimulated recently both by the revival of certain thermal theories of cyclogenesis as well as by theoretical developments in the use of baroclinic models in numerical forecasting. For a long time it has been customary in synoptic meteorology to assume that radiative temperature changes are negligible except within a few thousand feet off the ground and perhaps in the ozonosphere. Such an assumption (especially when coupled with the assumption that temperature is advected horizontally) leads to great simplification in theory and practice. However, it is of some importance to determine the magnitude of this neglected quantity. Some calculations of radiative temperature changes in cyclones are presented in the paper by Mr. George Ohring, Research Assistant. These calculations are helpful for the understanding of certain transient characteristics of cyclonic temperature fields, especially near cloud tops, and in the interpretation of lapse rates. (The paper by Mr. Ohring is an abridgment of an M.S. thesis presented to the Department of Meteorology and Oceanography at New York University.)

The last article in this report contains a supplement to James E. Miller's statistical study of east coastal cyclogenesis.

Jerome Spar
Project Director

ii

CONTENTS

COMPOSITE 200 MB TEMPERATURE FIELDS ABOVE
EXTRATROPICAL CYCLONES

EMANUEL M. BALLENZWEIG

Introduction

The suggestion has often been made that cyclogenesis is the result of high level density changes. Although this view is apparently supported by the well known observation that deep extratropical cyclones are characterized by warm stratospheres, the causal relationship between the cyclone and the warm stratosphere is still uncertain.

Stüve (1927) proposed the theory that cyclogenesis and anticyclogenesis are the result of meridional air motions in the stratosphere. In the troposphere the temperature gradient is negative from the equator to the poles; in the stratosphere the gradient is positive. According to Stüve, a surface pressure minimum is produced by the equatorward transport of warm, light stratospheric air over warm, light tropospheric air. This model stresses the stratospheric density changes, but neglects the compensating tropospheric density changes which were observed by Dines (1919).

Wulf and Obloy (1944) have also hypothesized that surface pressure changes are due to the interaction of stratospheric and tropospheric temperature changes. They visualize a warm artic stratosphere undercut by a warm tropical troposphere. According to their theory, this combination produces a pressure minimum; but this theory also does not quite account for the compensating effect of the tropospheric density changes.

The thermal theories of cyclogenesis (e.g., Austin 1952) are based largely on the principle of horizontal advection. However, it is well known from studies by Fleagle (1947) and others that, especially in the stratosphere, vertical motions play an important part in the development of temperature fields. The role of vertical motion is clearly illustrated in a recent paper by Fisher (1954) showing virtually stationary temperature fields at 200 mb embedded in rapidly moving air currents.

1

Although the exact causal connection between surface pressure changes and
stratospheric temperature changes is not known, there is reason to believe that
the stratospheric temperature fields may provide indications of surface devel-
opments. Fisher (1954) has suggested that there may be a characteristic anomaly
in the form of a tongue of warm air in the 200 mb temperature field prior to
the development of a secondary cyclone along the east coast of the United States.

This investigation was designed to study the 200 mb temperature field above
extratropical cyclones in the United States and to determine

(1) whether there is any difference between the 200 mb temperature
    fields and temperature change fields of those cyclones which
    develop secondaries and those which do not,

(2) the average structure of the 200 mb temperature field above
    moving extratropical cyclones, and

(3) the 200 mb temperature field above the newly formed cyclone.

The Composite Method

A study was made of six cyclones which formed secondaries to the south-
east of the primary cyclone and of seven cyclones which did not form secondar-
ies during the period December 1952 - February 1954. (see table 1). Those
cyclones which formed secondaries are called group 1 cyclones; those cyclones
which did not form secondaries are called group 2 cyclones.

The cyclones were tracked from the time they entered, or formed within,
the area bounded by 30°N latitude, 50°N latitude, 105°W longitude and the east
coast of the United States. (It was considered inadvisable to study cyclones
in the vicinity of the Rocky Mountains because large errors may result from
the use of nonrepresentative surface temperatures in making pressure reductions
to sea level. This difficulty is almost entirely eliminated east of the Rockies.)
Three-hourly positions of the cyclones were obtained from the United States
Weather Bureau maps at LaGuardia Field after they were detected on maps at
New York University. These positions and intensities were transferred to
blank maps. Tracks were drawn using only the 0330Z and the 1530Z positions.

A standard reference time (zero time) was needed in order to compare the
cyclones which formed secondaries with those which did not. Zero time for

those cyclones which formed secondaries was easily defined as the time closest to the RAOB time at which the secondary formed. However, there is no corresponding zero time for those cyclones which do not produce secondaries. The zero time for the latter group was defined in the following manner.

A map (fig. 1) was constructed showing the frequency distribution of the locations of primary cyclones at the time secondary cyclones first appeared.

This map was based on the data collected by Miller (1945) for type B or warm frontal secondaries which form to the southeast of the primary cyclone in the eastern United States. This is the type of development with which the present study is concerned.

The tracks of the group 2 primary cyclones were superimposed on figure 1. The position along the track at which the highest frequency value was found was designated as the zero position, and the corresponding time was considered to be the zero time. The zero time for this group of cyclones is thus the time at which a secondary is most likely to appear (although none did develop).

The method outlined above was tested on the six cyclones in group 1 which did produce secondaries. In five of the six cases the zero time obtained from figure 1 corresponded to the observed zero time.

The zero times for the cyclones studied are shown in table 1.

Table 1. Zero time of primary cyclones.

Group 1	Group 2
03 Z 21 December 1952	15 Z 24 January 1953
03 Z 11 February 1953	15 Z 16 February 1953
15 Z 12 February 1953	03 Z 21 February 1953
15 Z 23 March 1953	03 Z 4 March 1953
03 Z 11 April 1953	03 Z 8 March 1953
15 Z 28 October 1953	15 Z 4 December 1953
	15 Z 26 February 1954

In comparing the two groups of cyclones from the time they entered, or formed, within the area defined above, it was not possible to go back in time more than twenty-four hours from zero hour nor ahead more than twelve hours because the different cyclones had different life spans in the area as can be seen in table 2.
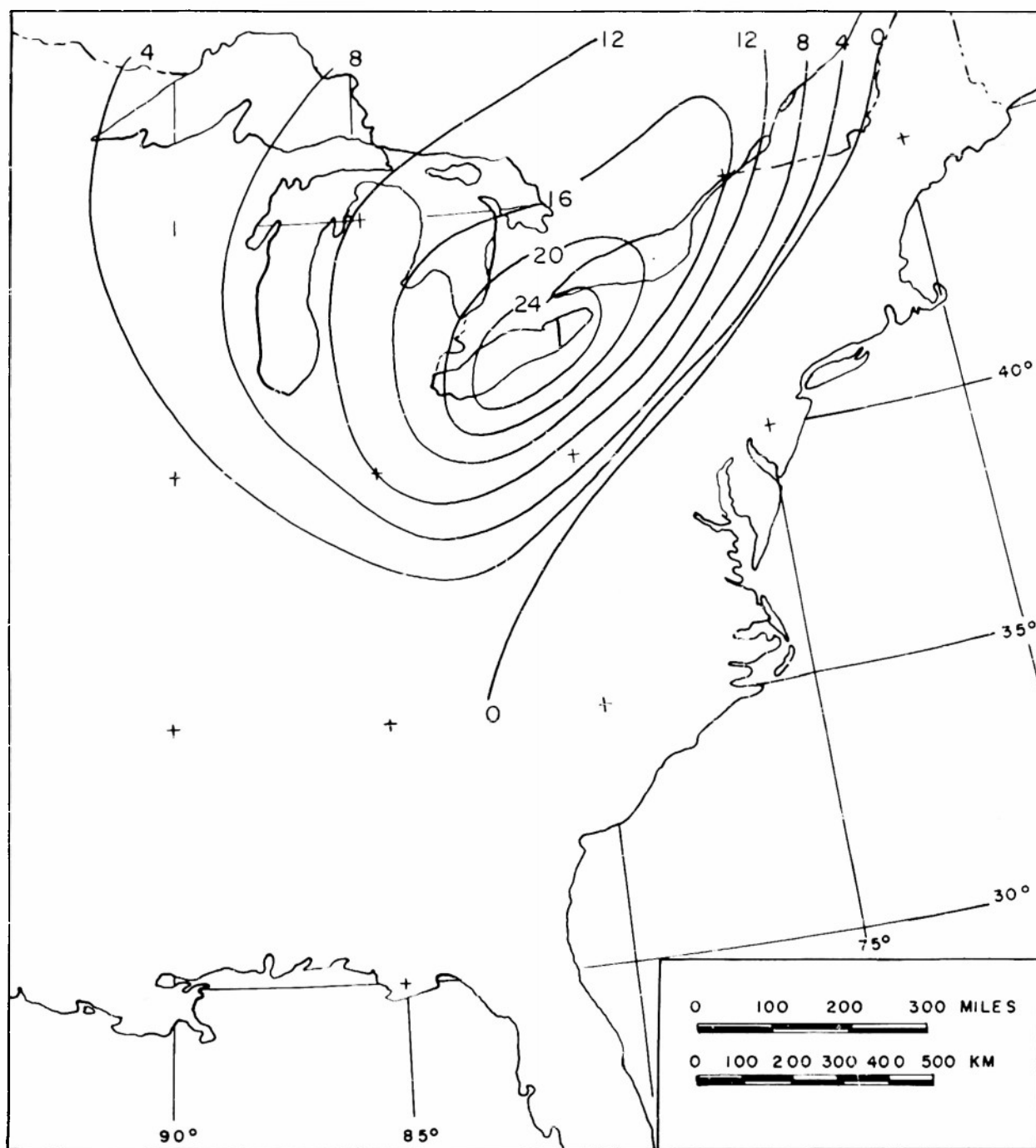
Fig. 1. Isopleths of frequency of location of primary cyclones at the time of secondary cyclogenesis.

Even the composite maps for group 1 at zero plus twelve hours and for group 2 at zero minus twenty-four hours are of dubious validity since they contain only about one-half the total number of cases.

Table 2. The number of primary cyclones in each
group at each time.

Group	0-48	0-36	0-24	0-12	0	0+12	0+24	hours
1	3	4	6	6	6	3	0	
2	0	1	4	7	7	7	3	

The following procedure was used to construct the composite maps:

1) The surface positions and central pressures of the cyclones were entered on the corresponding 200 mb charts.
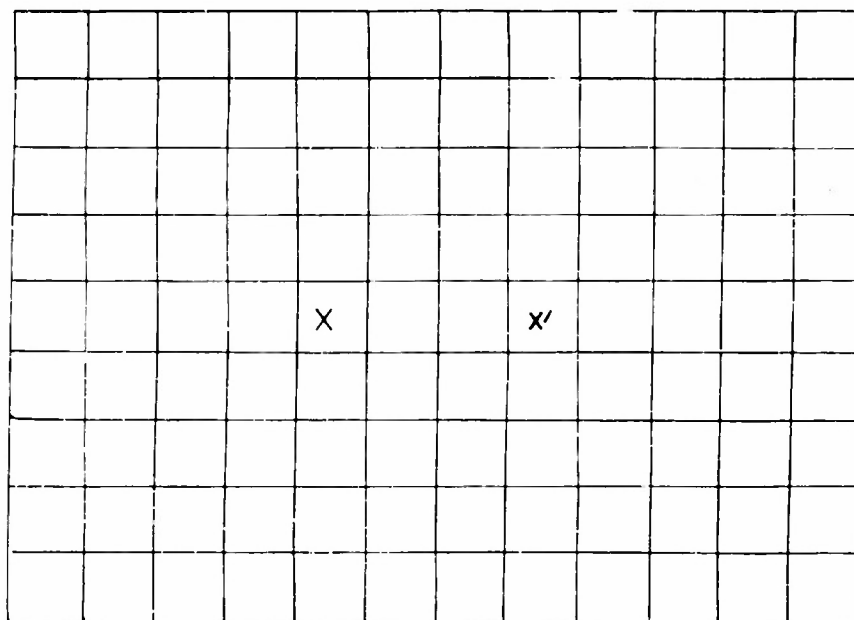
2) A grid of 2° squares, 18° in latitude and 24° in longitude, was placed on the 200 mb chart in such a way that the horizontal lines of the grid were on the odd latitude lines of the map, the vertical lines of the grid were on the even longitude lines of the map, and the cyclone was in the square marked X (see figure 2).

3) With the cyclone center as the reference point in each case, the temperatures at the intersections of the horizontal and vertical lines of the grid were interpolated to the nearest 0.5^oC and plotted on a corresponding grid.

4) The mean temperature at each grid point was determined and a set of 200 mb mean temperature charts was constructed for each group of cyclones. (A set consists of four charts: zero – 24 hours, zero – 12 hours, zero hour and zero + 12 hours).

5) Two sets of 200 mb mean temperature change maps were also constructed, one for each group of cyclones. (A set consists of three charts: zero-24 to zero-12 hours, zero-12 hours to zero hour and zero hour to zero + 12 hours).

6) The grid was also used to study the 200 mb temperature distribution above the secondary cyclones in group 1 at the time of cyclogenesis. The only difference in the application of the grid to the 200 mb chart was that the secondary cyclone was centered in the square marked X' (fig. 2).

Fig. 2. Grid used for obtaining 200 mb temperatures.
Primary cyclones were centered in box X;
secondary cyclones in Box X'.

Results

The results of the study are presented in the form of composite maps. These maps do not refer to a fixed geographical region but rather are constructed with the surface cyclone center as a common reference point. The scale of the map is indicated by the 2 degree square drawn about the reference point. The area studied is small enough so that a rectangular grid can be used without appreciable distortion of the picture.

The composite 200 mb temperature distributions relative to the primary surface cyclone at zero-minus-24 hours are shown in figures 3 and 4 for the group 1 and group 2 cyclones. At this time the differences between the two composite maps are rather slight. In both groups we find the cold pool about 10 degrees of longitude east of the cyclone center. The warm pool appears to the west of the cyclone in group 1 and west-southwest of the cyclone in group 2. There is as yet no indication in figure 3 of the protrusion of a tongue of warm air southeast of the primary cyclone or of the formation of a secondary warm pool which one might expect to accompany the development of the secondary low center in the group 1 cyclones.

At zero-minus-12 hours (figs. 5 and 6) a marked change occurs in the temperature field of the group 2 cyclones. However, a glance at table 2 shows that this change may be fictitious since only 4 cyclones were included in group 2 at zero-minus-24 hours, whereas this group includes seven cyclones at zero-minus-12 hours.

A comparison of figures 5 and 6 reveals some notable differences between the group 1 and group 2 cyclones. In the former the cold pool appears about 10 degrees of longitude to the east of the cyclone while in the latter the cold pool is found about the same distance from the cyclone, but to the southeast. The warm pool in group 1 lies about 5 degrees of longitude to the west of the cyclone. In group 2 the center of the warm pool appears about 10 degrees of longitude to the northwest of the cyclone. Finally, there is the obvious difference in the curvature of the isotherms between the two groups. The group 1 cyclones show the development of a tongue of warm air protruding southeast of the primary cyclone from the warm pool. The group 2 cyclones show quite the reverse, i.e., a cold tongue extending northwestward across the cyclone from the cold pool.
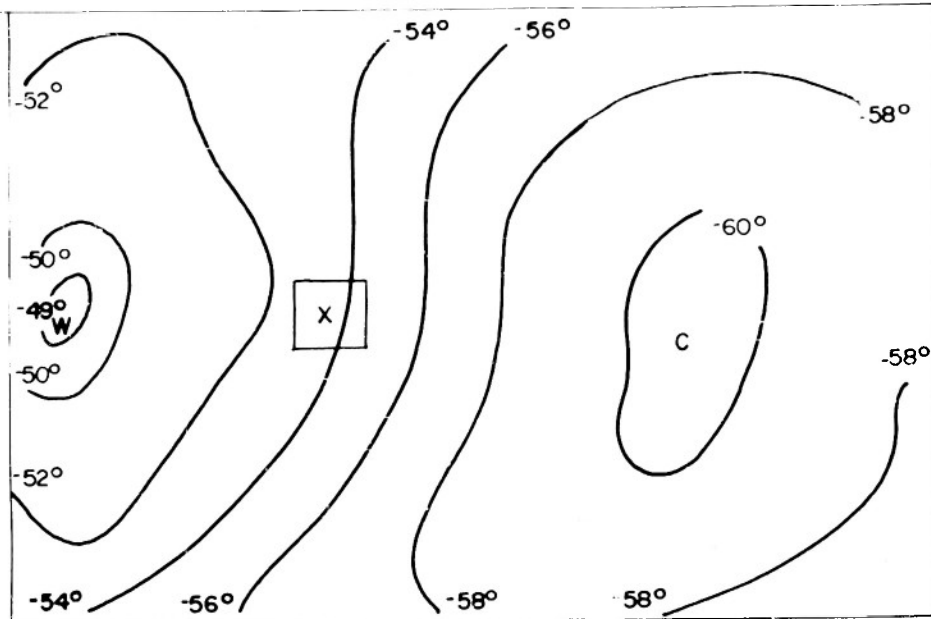
Fig. 3. Average 200 mb temperature above group 1 cyclones at zero - 24 hours.
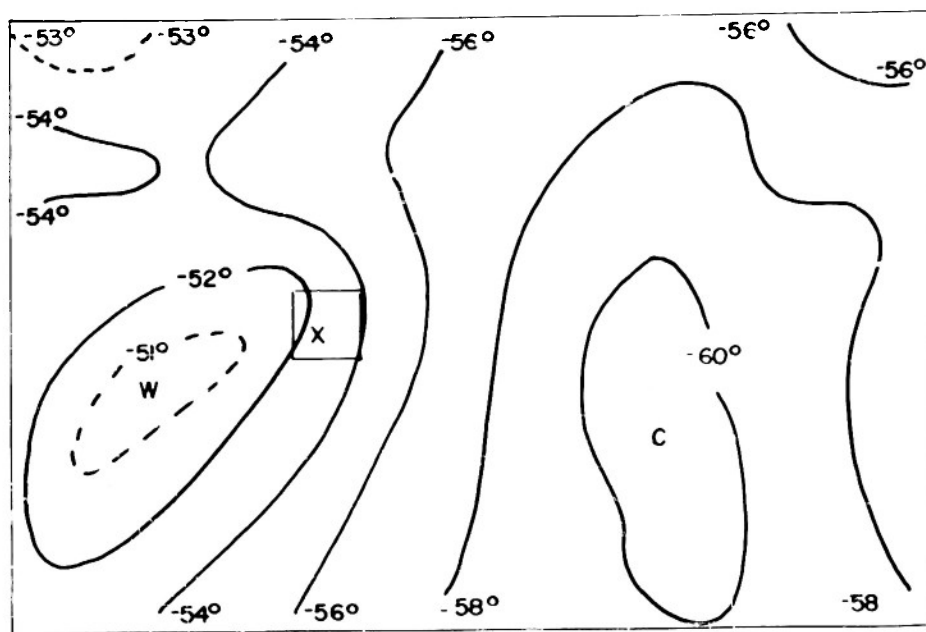

Fig. 4. Average 200 mb temperature above group 2 cyclones at zero - 24 hours.
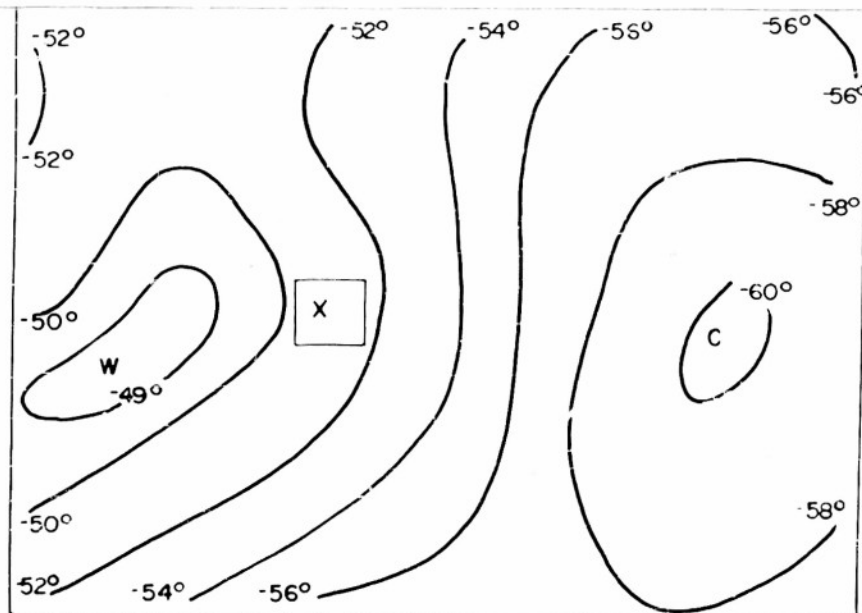
Fig. 5.   Average 200 mb temperature above group 1 cyclones
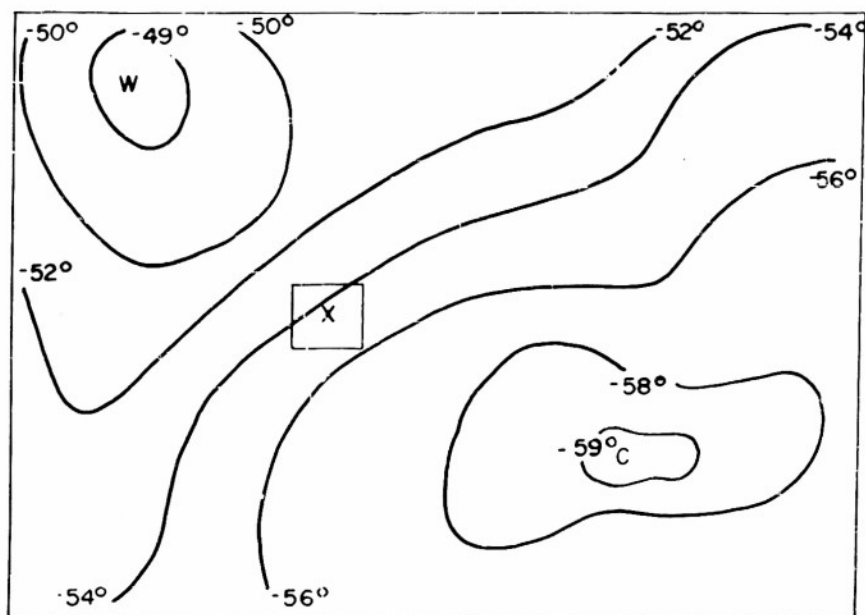   at zero - 12 hours.

Fig. 6.   Average 200 mb temperature above group 2 cyclones
           at zero - 12 hours.

In retrospect one can now see evidence of tne warm tongue in the secondary-producing lows as early as zero-minus-24 hours (fig. 3). However, it does not appear likely that precursory signs of secondary cyclogenesis can be recognized in the 200 mb temperature field much more than twelve hours before the development.

The temperature change maps for the period zero-minus-24 hours to zero-minus-12 hours (figs. 7 and 8) also exhibit some interesting differences between the group 1 and 2 cyclones. In the former we find warming at 200 mb to the east and southeast of the primary, whereas the latter show cooling taking place in the same region. Corresponding to the increasing temperature of the warm pool in the group 2 cyclones, we find rather considerable twelve hour warming northwest of the cyclone in figure 8. This warming is absent in the group 1 cyclones.

The development in the 200 mb temperature field associated with the formation of a secondary cyclone can be seen clearly in the zero hour map (fig. 9). Here the warm tongue is well developed southeast of the primary. The warm pool is rotating about the primary low and now lies to the southwest of the low. The cold pool has continued to retreat eastward away from the primary cyclone.

The characteristics of the group 1 cyclones at zero hour are even more striking when compared with those of group 2 (fig. 10). In group 2 there is no warm tongue development southeast of the low. The warm pool has moved southward relative to the low but still lies to the west-northwest. The cold pool shows no sign of retreating away from the cyclone.

The temperature change maps (figs. 11 and 12) again show marked differences between the two cyclone groups. Group 1 cyclones display a narrow band of local warming southeast of the primary cyclone corresponding to the formation of the secondary low center. The warming in group 2, on the other hand, is not confined to one quadrant and appears to be greatest over the surface primary cyclone itself.

Twelve hours after the formation of the secondary low, the temperature field at 200 mb (fig. 13) shows further development. The warm tongue east and southeast of the primary cyclone becomes more pronounced and the warm pool rotates to a position south of the primary. There is some indication of the formation of a secondary warm pool southeast of the primary cyclone. At the same time the group 2 cyclones (fig. 14) show no further movement of the warm pool relative to the primary low and no indication of the formation

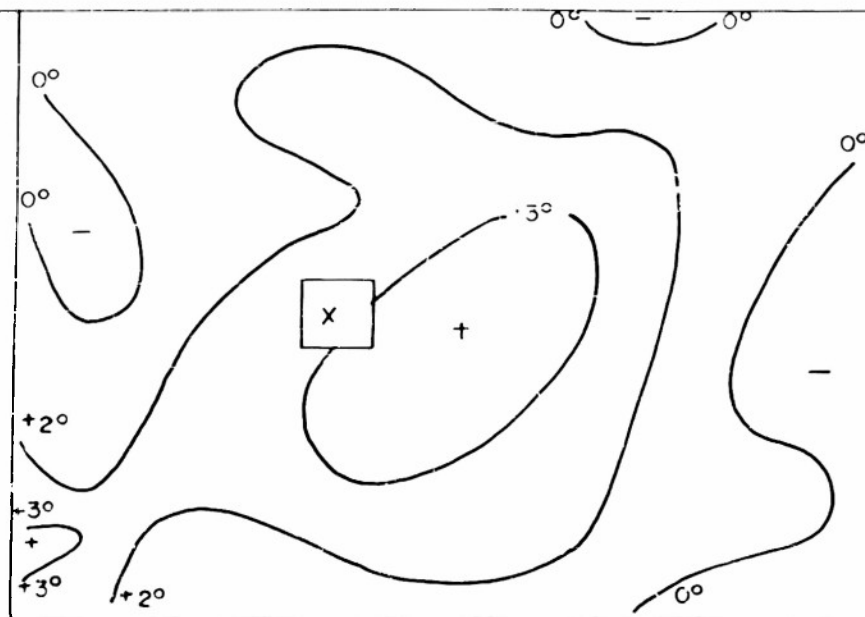Fig. 7. Average 200 mb temperature change above group 1
cyclones between zero – 24 hours and zero – 12 hours.

Fig. 8. Average 200 mb temperature change above group 2
cyclones between zero – 24 hours and zero – 12 hours.

Fig. 9.   Average 200 mb temperature above group 1 cyclones
          at zero hour.

Fig. 10.   Average 200 mb temperature above group 2 cyclones
          at zero hour.

Fig. 11.   Average 200 mb temperature change above group 1 cyclones
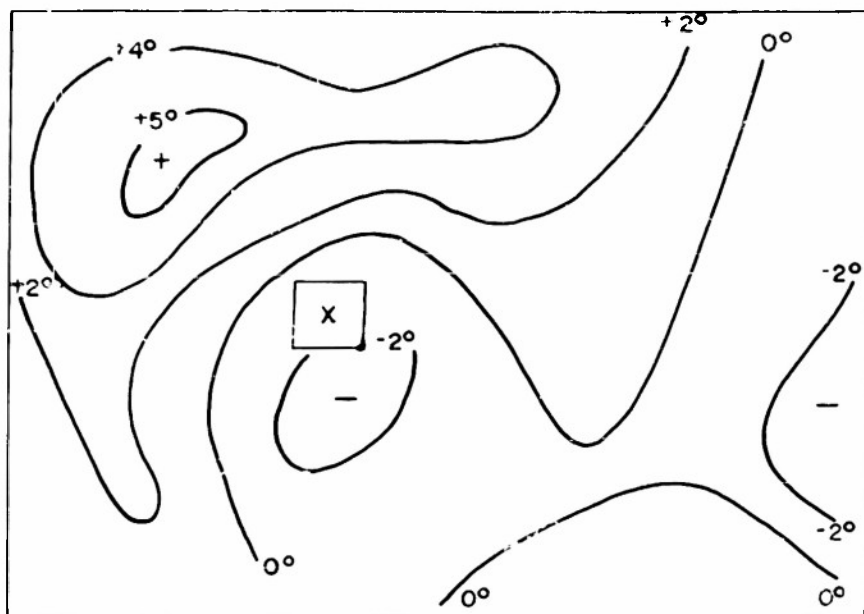between zero - 12 hours and zero hour.

Fig. 12.   Average 200 mb temperature change above group 2 cyclones
between zero - 12 hours and zero hour.

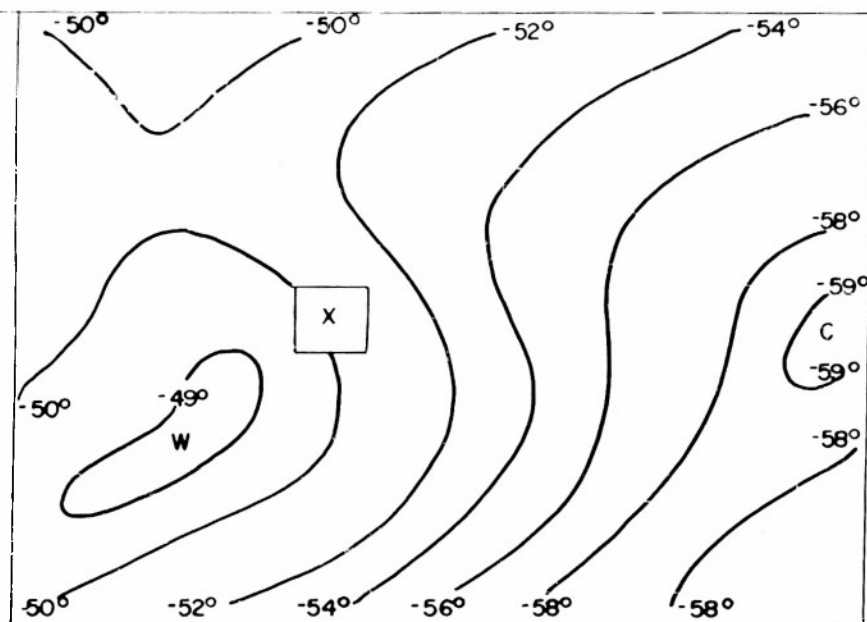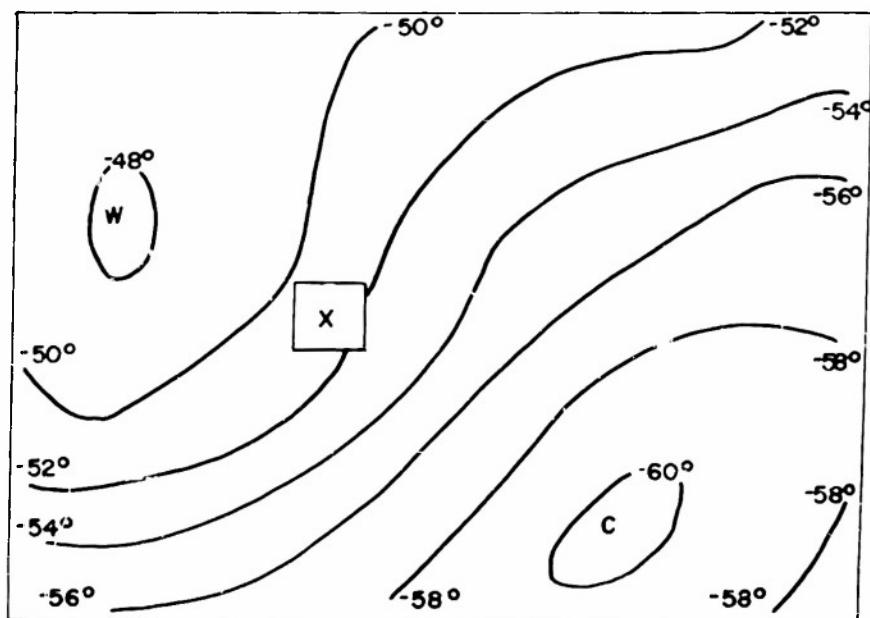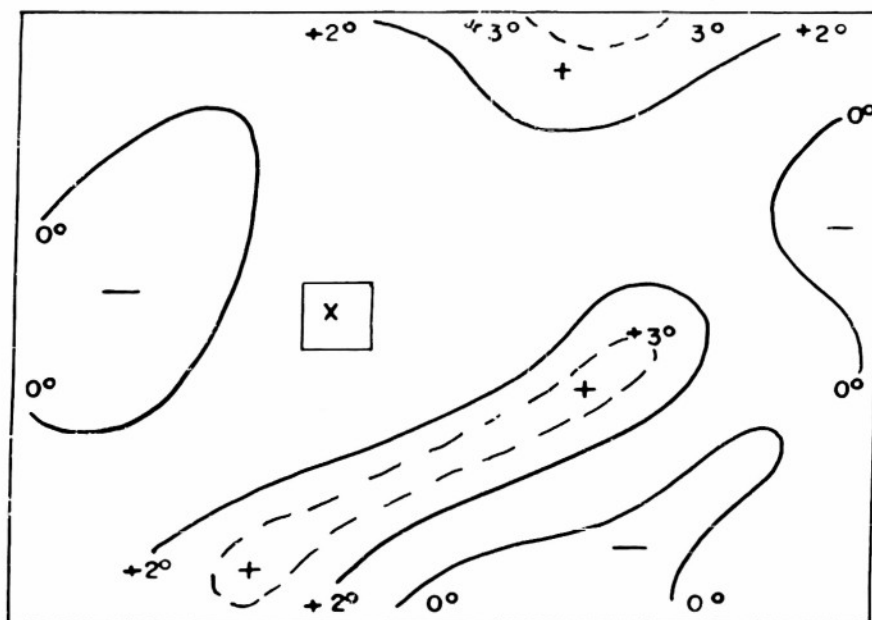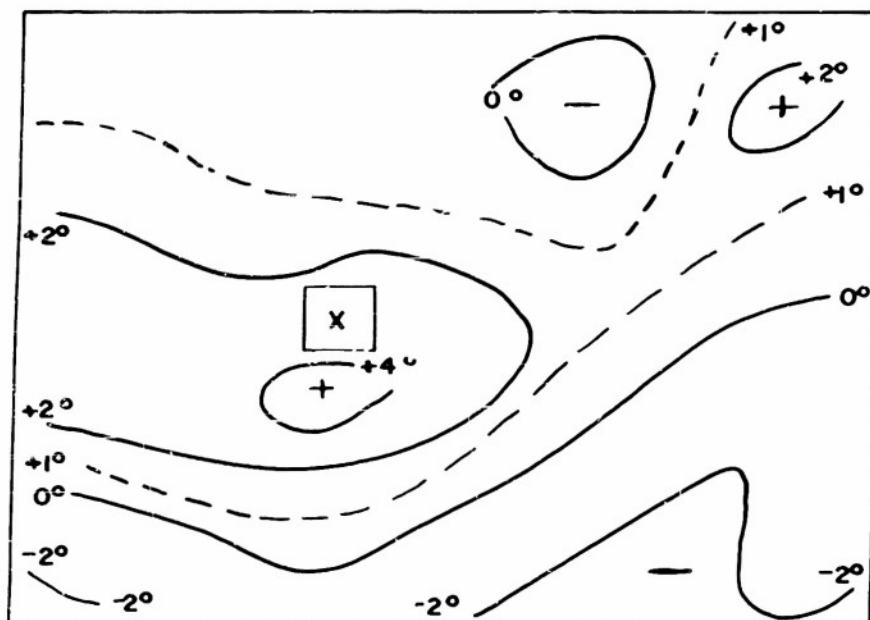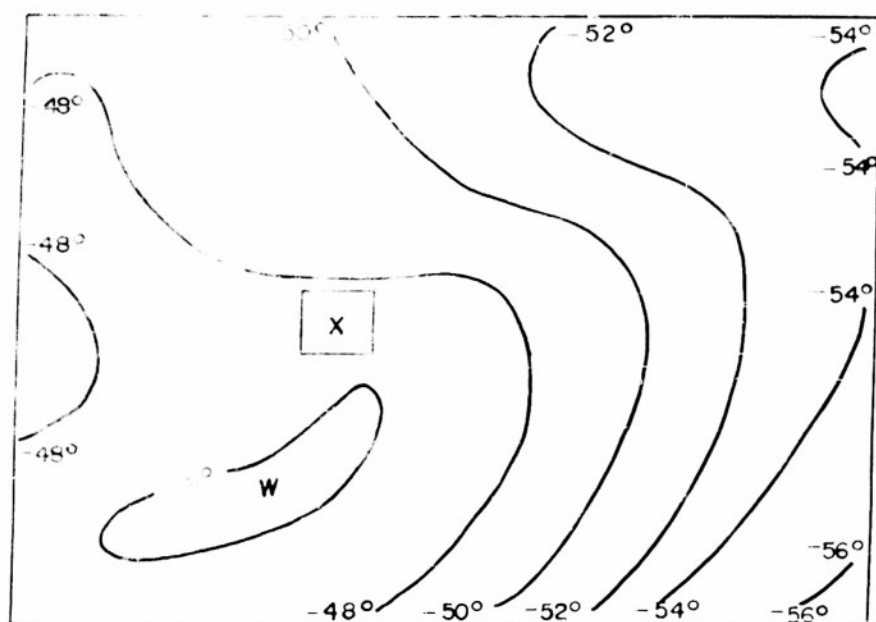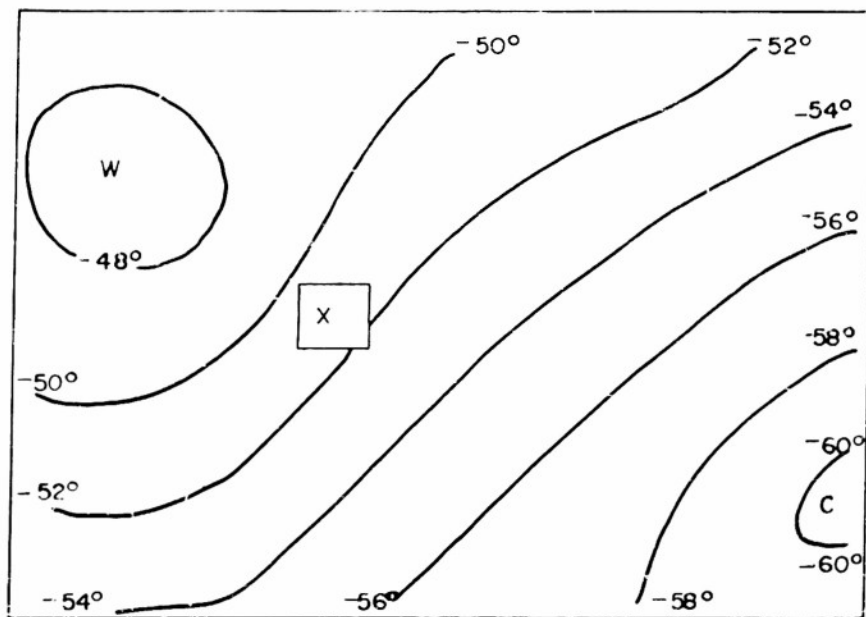Fig. 13. Average 200 mb temperature above group 1 cyclones at zero + 12 hours.

Fig. 14. Average 200 mb temperature above group 2 cyclones at zero + 12 hours.

of a warm tongue. Considerably more warming in this period to the southeast
of the primary cyclone is also evident in the temperature change field for
group 1 (fig. 15) than for group 2 (fig. 16). However, figure 15 is not
reliable since only three out of the six cyclones were used to construct
the zero-plus-12 hour temperature field for group 1.

The 200 mb temperature field at zero hour relative to the secondary
cyclones which developed out of the group 1 primary lows is shown in figure
17. Again the warm tongue extending southeastward from the warm pool is evi-
dent. The structure of the temperature field is now not unlike that connect-
ed with the primary cyclones in their earlier stages. The warm pool lies to
the northwest and the cold pool to the east or southeast. Of course, later
the warm pool will either move to a position closer to the new cyclone or a
new warm pool will develop east of the original one. This "jumping" of the
warm pool from the primary to the secondary has been described by Fleagle
(1947).

The composite maps were constructed from relatively few cases and there-
fore suffer from the usual deficiencies of small samples. In particular the
statistical stability of the averages is in doubt. Point values of the stand-
ard deviation about point means were found to be as high as 6 degrees centi-
grade and the average standard deviation was about 4.5 degrees centigrade.

The large standard deviation indicates that no significance can be attach-
ed to small details of the composite maps or to small differences between the
group 1 and group 2 composite maps. However, the observed differences between
the group 1 and group 2 temperature fields are too large to be ignored, and un-
doubtedly indicate the existence of different physical processes in the two
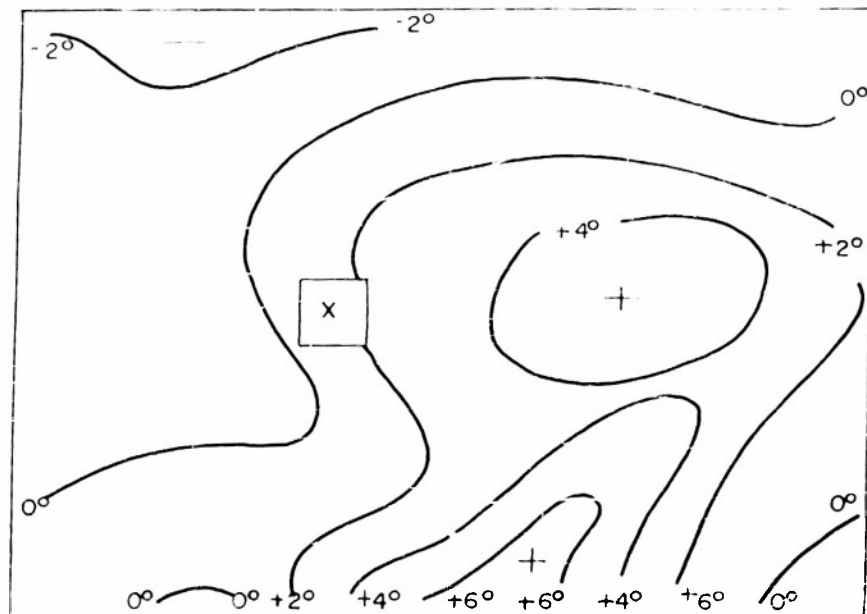groups of cyclones.

Fig. 15.   Average 200 mb temperature change above group 1 cyclones
between zero hour and zero + 12 hours.
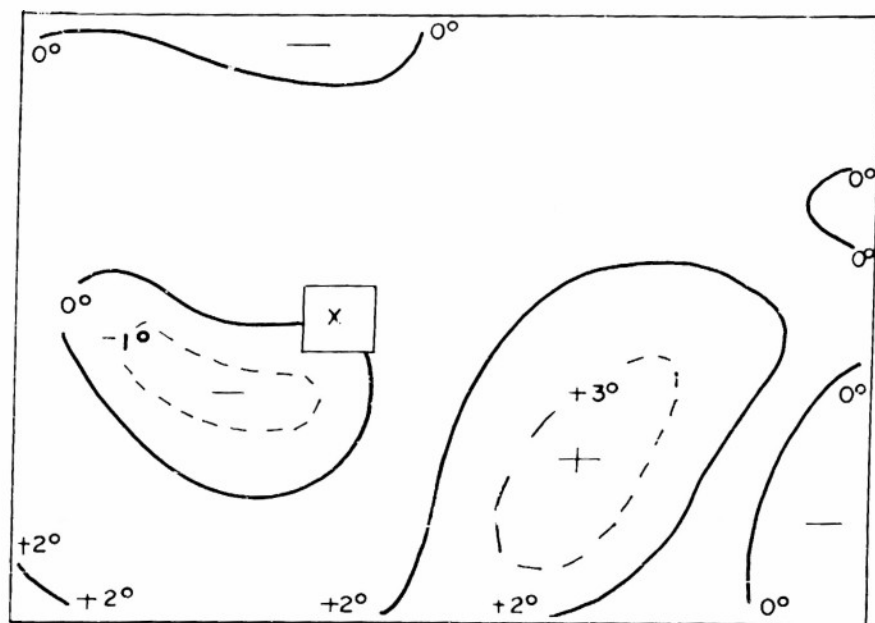
Fig. 16.   Average 200 mb temperature change above group 2 cyclones
between zero hour and zero + 12 hours.
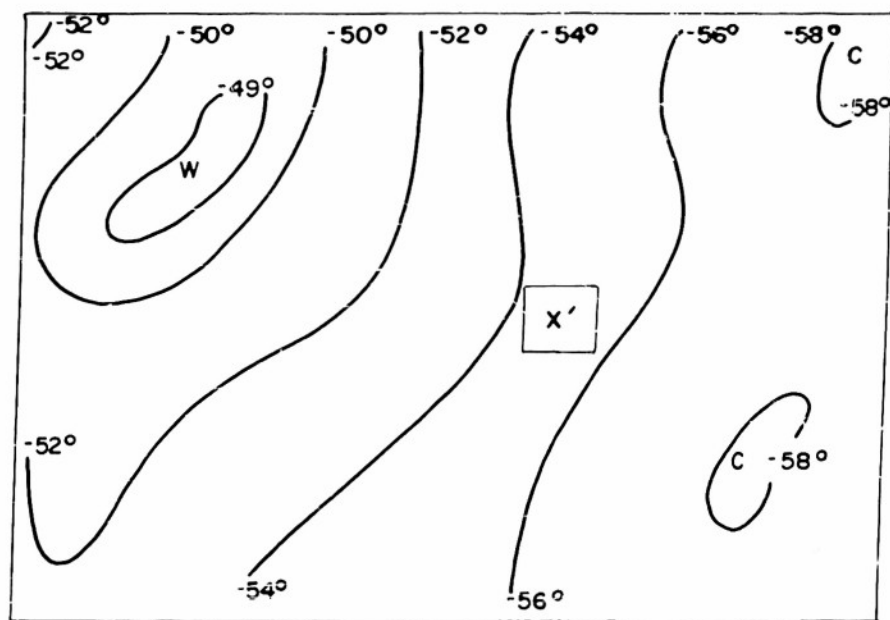
Fig. 17. Average 200 mb temperature above secondary cyclone at zero hour.

Summary

The main purpose of this study was to determine the prognostic value of the 200 mb temperature field for the prediction of secondary cyclone formation along the east coast of the United States, southeast of a primary cyclone. The working hypothesis was that cyclogenesis would be preceded by a characteristic deformation of the temperature field at 200 mb and the appearance of a stratospheric warm tongue or secondary warm pool southeast of the parent cyclone.

Twenty-four hours before formation of the secondary it was not possible to distinguish those cyclones which produced secondaries from those which did not. In both cases a 200 mb warm pool was found to the west and a 200 mb cold pool to the east of the primary surface cyclone.

Beginning at twelve hours before formation of the secondary, the thermal characteristics of cyclogenesis began to appear. A warm tongue at 200 mb developed southeast of the primary low, the 200 mb warm pool drifted to the south of the primary low, and the cold pool retreated toward the east. These developments were not observed in the cyclones which failed to produce secondaries.

Thus, although the working hypothesis appears to be verified, the short time lag between thermal developments at 200 mb and surface cyclogenesis places a practical limit on the usefulness of the results.

References

Austin, J. M., 1952: Development in the pressure field. Tech. Rep. No. 11.
    ONR Contract N5ori-07804. Mass. Inst. of Tech.

Dines, W. H., 1919: The characteristics of the free atmosphere. Geophys.
    Mem., No. 13. Met. Off., London.

Fisher, E. L., 1954: Upper level temperature fields associated with east
    coastal cyclogenesis. Tech. Pap. No. 1, Project SCUD. Contract
    Nonr-285 (09). New York Univ.

Fleagle, R. G., 1947: The fields of temperature, pressure and three-
    dimensional motion in selected weather situations. J. Meteor.,
    4, 165-185.

Miller, J. E., 1945: Cyclogenesis in the Atlantic coastal region of the
    United States. Dept. of Meteor. New York Univ. Mimeographed.
    77 pages.

Stüve, G., 1927: Thermozyklogenese. Beitr. z. Phys. d. fr. Atmos., 13,
    23-36.

Wulf, O. R. and Obloy, S. J., 1944: The utilization of the entire course
    of radiosonde flights in weather diagnosis. Misc. Rep. No. 10.
    Inst. of Meteor., Univ. of Chicago.

VERTICAL MOTIONS IN AN UPPER LEVEL CYCLONE

Benjamin M. Herman and John J. R. Kinney

Introduction

In the last decade an increasingly dense network of upper-air observations has become available to the meteorologist. These observations have revealed the existence of certain upper-level phenomena which are not readily detectable from surface analyses. One of the more important of these phenomena is the high level cold cyclone. These disturbances are observed to develop in the southern end of a trough in the westerlies and, upon intensifying, may become cut-off from the main stream and propagate down to the surface. Consistent feature of these disturbances are a pool of cold air in the troposphere, a low tropopause and a warm stratosphere.

Palmèn (1949) has described the formation of a cold upper-level cyclone, or cut-off low, as a wave-like deformation in the upper flow which increases in amplitude until the cold air in the southern part of the trough becomes cut off from the cold air to the north. This cutting off may be accomplished by subsidence within the cold air in the central and northern parts of the trough. If the subsidence is intense enough, it may eventually result in a lowering of the top of the cold air mass below a particular level, say 500 mb, with the cold air still remaining at this level farther to the south.

On upper air charts the cut-off polar air appears as a cold, cyclonic vortex in the southern part of the original upper trough. Farther to the north a new belt of strong westerly winds can be observed. Thus, the whole process can be regarded as a special case of cyclone formation on the south side of the strongest westerlies. A corresponding transport of warm air masses to the north can often be observed in the formation of warm cut-off highs.

Palmèn and Nagler (1949) have analyzed a selected cold vortex of the cut-off type, and have shown that, as the cyclone deepens, the temperature decreases within the cold core in the upper troposphere, while there is a rapid lowering of the tropopause (and subsequently the stratosphere) directly above the disturbance. They observed that a warm pool forms in the

area of the lowering stratosphere while a cold pool forms in the upper tropo-
sphere beneath. It was shown that the warm pocket could not have been a result
of any purely horizontal advective processes, but must have been due mainly to
subsidence. Similarly, it was concluded that the cooling of the cold air in the
troposphere was brought about by ascending motion. (On the other hand, Nyberg
(1949) has stated that in no cases studied by him, did he find any upward
motion of the cold air in an upper trough.)

Palmen's hypotheses regarding the development of the cold low and the
associated temperature field are supported by the analysis of Hsieh (1941) who
has described not only the development of the low aloft but also the downward
propagation of the upper level cyclone to the surface.

While numerous computations of vertical motions have been performed re-
cently (see, e.g., Fleagle, 1947), there is as yet not available a complete
description of the field of vertical motion associated with the life history
of an upper level cyclone. In this study computed fields of vertical velocity
at 500 and 200 mb are presented for such a cyclone during a two and one-half
day period when the cyclone was moving southeastward across the north central
United States. The 500 mb and 200 mb levels were selected in order to show
the vertical motion fields in both the troposphere and stratosphere.

Computation Methods

The method used to compute vertical velocities is a modified form of the graphical method of computing the adiabatic warming from constant pressure charts devised by Miller (1945).

Miller has shown that

$$W_t = -0.236 \; \Delta T \tag{1}$$

where W_t is the vertical velocity of a particle with respect to the isobaric surface, in cm sec^{-1}, and ΔT is the adiabatic warming of the air particle in degrees Centigrade per 12 hours. In order to obtain the vertical velocity, W, of a particle with respect to the earth, the vertical velocity, W_p, of the isobaric surface along the horizontal trajectory must be added to W_t. Thus,

$$W = W_t + W_p \tag{2}$$

When 12 hour trajectories are used, W_p can be gotten from the equation

$$W_p \; (\text{cm sec}^{-1}) = 7 \times 10^{-4} \; \Delta H(\text{ft}) \tag{3}$$

where ΔH is the change in height of the isobaric surface along the 12 hour trajectory. Therefore the vertical velocity of a particle along a 12 hour trajectory with respect to the earth is given by:

$$W(\text{cm sec}^{-1}) = -0.236 \; \Delta T + 7 \times 10^{-4} \; \Delta H$$

To determine W_t from 12 hour trajectories, **end** points were selected and horizontal trajectories of the air particles were traced back to determine their origin 12 hours earlier. This was done by moving the end point back a distance corresponding to 6 hours travel parallel to the contour lines with a speed equal to that of the observed winds on the chart for time t_f. This point was marked as the mid-point of the 12 hour trajectory and was then transferred to the map for time $t_o = (t_f - 12$ hours). The process was repeated for another 6 hour period and the final point was marked as the origin of the 12 hour trajectory. In areas where observed winds were lacking, gradient winds were computed.

In and around the low center, the configuration of the contour lines underwent considerable change during the 12 hour periods, thus giving rise to errors in trajectories determined in the above manner. In order to minimize these errors, an interpolated mean chart was constructed for time t_m ($t_m = t_f - 6$ hours) and was used as an aid in determining trajectories.

The t_m charts were constructed by averaging the temperature and height values for time t_o and t_f. Pilot balloon wind observations for time t_m were used to supplement the interpolated data. In areas where no observed winds were available an average wind was used. Additional accuracy was gained by interpolating the t_m position of significant features such as pressure centers, trough and ridge lines, and temperature centers.

Twelve-hour trajectories in and around the low center could now be computed with the use of the t_m chart. The end point was selected on the t_f chart as before, but moved back for a period of only 3 hours in the same manner as described above. This point was then transferred to the t_m chart and the particle moved back for a period of 6 hours. This end point was then transferred to the t_o chart and moved back the remaining 3 hours to its origin. The mid-point of this 12 hour trajectory was taken as the mid-point of the 6 hour trajectory on the t_m chart.

The value of the temperature and height at the origin (T_o, H_o) and end (T_f, H_f) of the 12 hour trajectory were noted and ΔH and DT were determined.

ΔH, as stated above, is the height change of the isobaric surface along the horizontal trajectory $(H_f - H_o)$ and DT is the isobaric temperature change $(T_f - T_o)$ resulting from the adiabatic warming.

The end points of the trajectories were chosen at stations where soundings were available, whenever possible. As this was not possible for all trajectories, some soundings were constructed by interpolation from available data. These soundings, therefore, represent the vertical structure of the atmosphere through the end point of the trajectory. It was now assumed that the air in the layer affected by the vertical motion moves with a constant horizontal velocity. Therefore, this layer consists of the same air particles at both the beginning and end points, thereby eliminating advection. The temperature changes within this layer are thus the result of vertical motion, if non-adiabatic effects may be considered negligible.

To determine ΔT from DT, the temperature of the beginning point, T_o, was plotted at the appropriate level (in this study either 500 mb or 200 mb) on the

thermodynamic diagram containing the soundings for this trajectory for time t_f. The adiabat through T_o to the intersection with the end point sounding was then drawn. If the temperature at this intersection point is denoted T_a, then

$$\Delta T = T_a - T_o \tag{5}$$

ΔH and ΔT now having been determined, W, the vertical velocity of the particle with respect to the earth's surface may be determined from equation (4).

Due to the methods employed, the values of W thus obtained are actually mean values for the 12 hour time interval and are consequently plotted at the midpoints of the trajectories. Also, since the adiabatic paths between T_o and T_a are entirely in the layer immediately above or below the level in question, depending upon whether the particle rises or sinks, the values of W represent mean values for this layer, and not actually for the level in question. The midpoint of this layer, however, is generally close enough to the level in question so that the deviation can be neglected.

The Vertical Velocity Distribution

On the 4th and 5th of December 1950 a strong polar anticyclone moved south-eastward from Canada into the Great Plains of the United States. At 1230 GMT on the 5th (fig. 18) the polar anticyclone was separated from a weaker ridge to the east by a surface pressure trough in the Mississippi valley, but there was no closed cyclone in the area. However, as will be seen in figure 20, a very deep cyclone did exist aloft over the surface high. Forty-eight hours later (fig. 18) the cyclone was found also at the surface and the high had split into two cells, one over the Gulf of Mexico and the other over Quebec. Subsequently, both the upper level and surface cyclones moved northward over the Great Lakes while the surface low deepened and the upper low filled slightly.

Vertical velocities at the 500 and 200 mb levels in and around the upper level cyclone were computed for the five twelve-hour periods beginning at 1500 GMT on the 5th and ending at 0300 GMT on the 8th when the cyclone moved out of the U. S. radiosonde network. The 500 and 200 mb maps and the corresponding vertical velocity distribution are shown in figures 19 - 29.

The solid lines on the constant pressure maps are contours (drawn for an interval of 200 geopotential feet) and the dashed lines are isotherms (drawn for an interval of 4 degrees Centigrade). On the vertical velocity maps the thin solid lines are isopleths of positive vertical velocity and dashed lines are isopleths of negative vertical velocity (subsidence). The vertical velocity isopleths (sometimes called isanabats) are drawn for an interval of 0.5 cm sec^{-1}. Centers of rising motion are labelled R and centers of subsidence are labelled S. On the 200 mb vertical velocity maps the tropopause intersection is shown as a heavy solid line. The interpolated positions of the cyclones at the appropriate isobaric level are indicated on the vertical velocity maps by the letter L.

The vertical velocity maps for 2100 GMT on the 5th (fig. 20) are shown between the constant pressure maps for 1500 GMT on the 5th (fig. 19) and 0300 GMT on the 6th (fig. 21). During this period the cyclone, both at 200 mb and 500 mb, moved southward and filled slightly. At 500 mb the cold core of the cyclone became warmer while at 200 mb the warm core cooled. However, the warm pool in the trough south of the low center at 200 mb warmed about 2 degrees and remained almost stationary over Kansas.
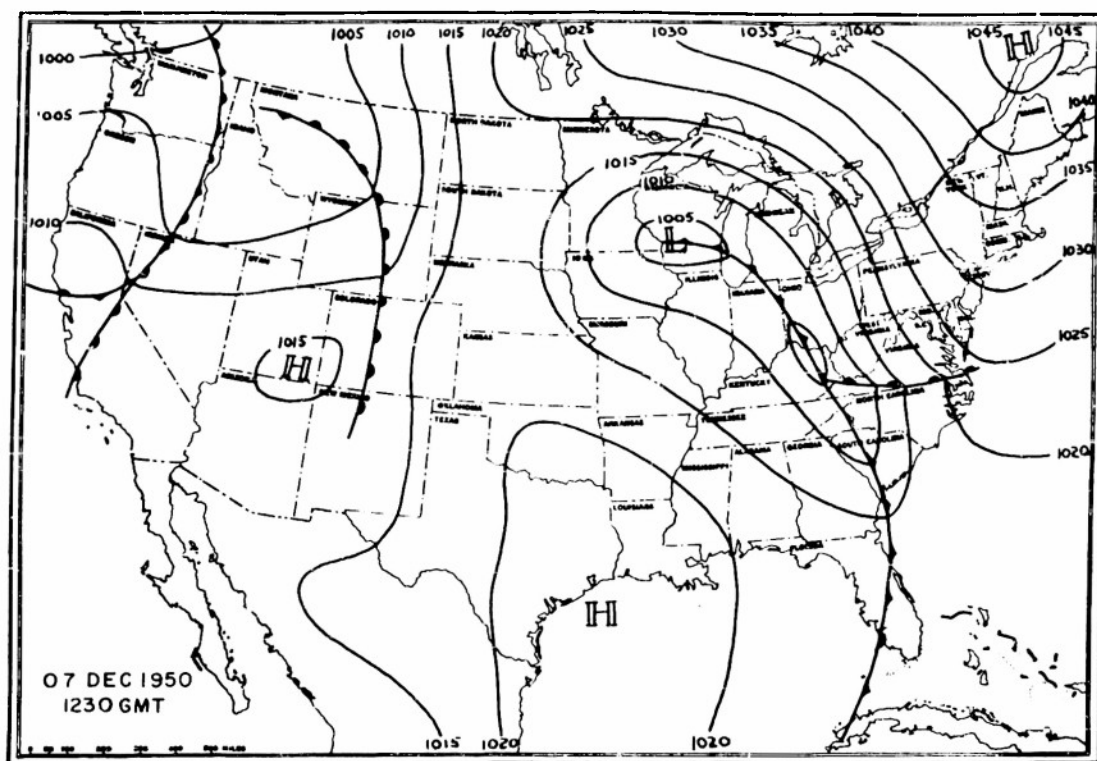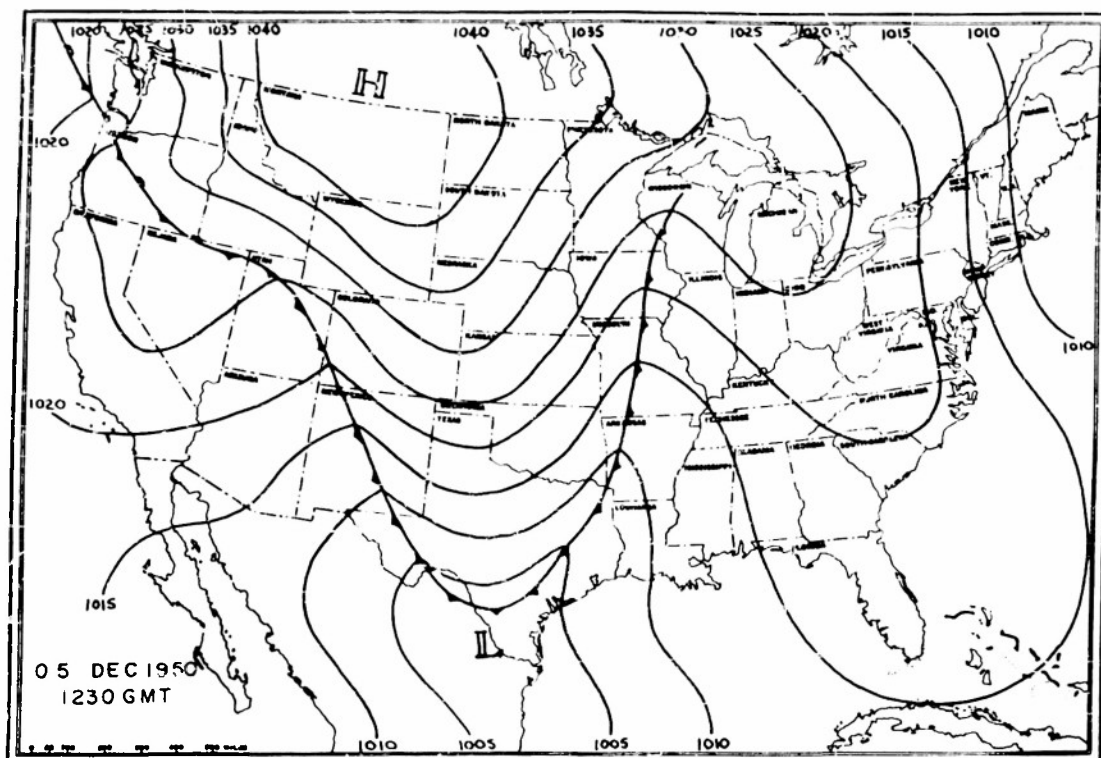
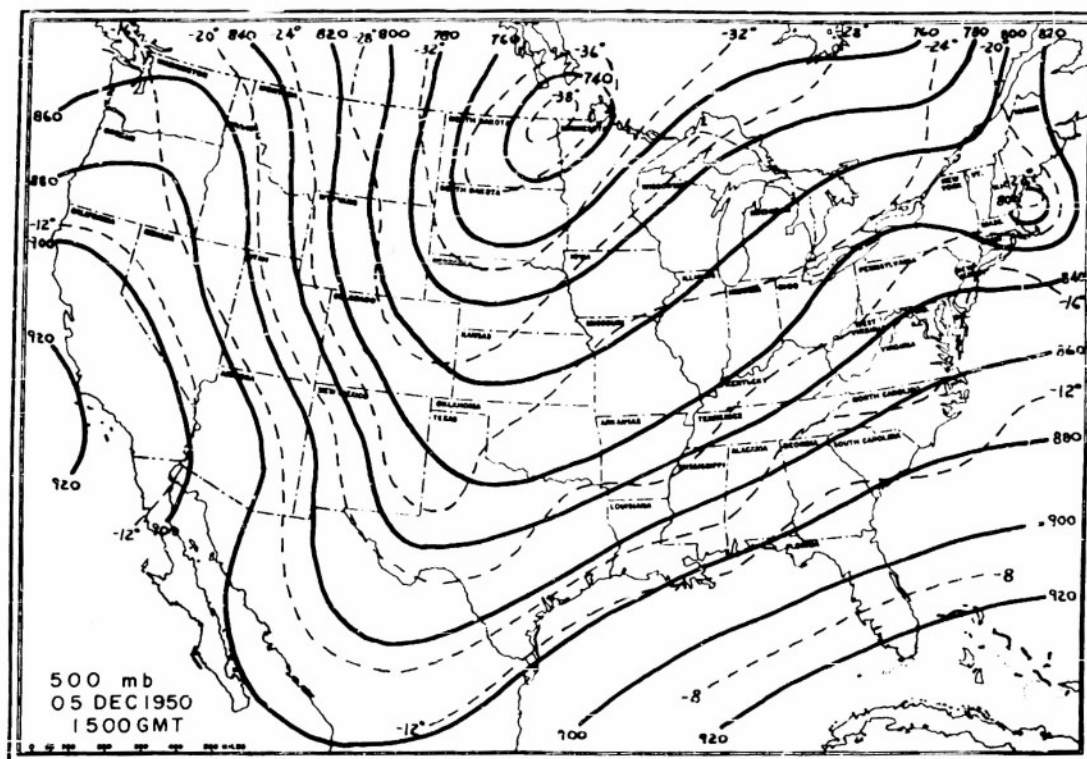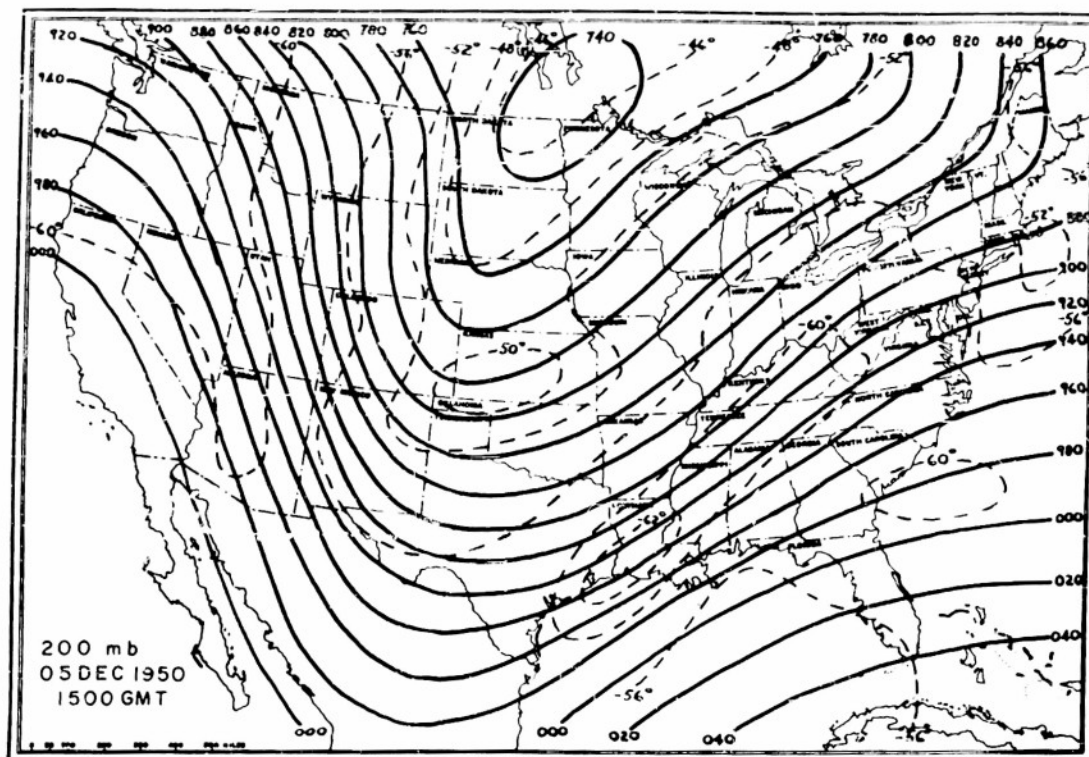Fig. 18.   Surface weather maps.   1230 GMT, 5 and 7 December 1950.

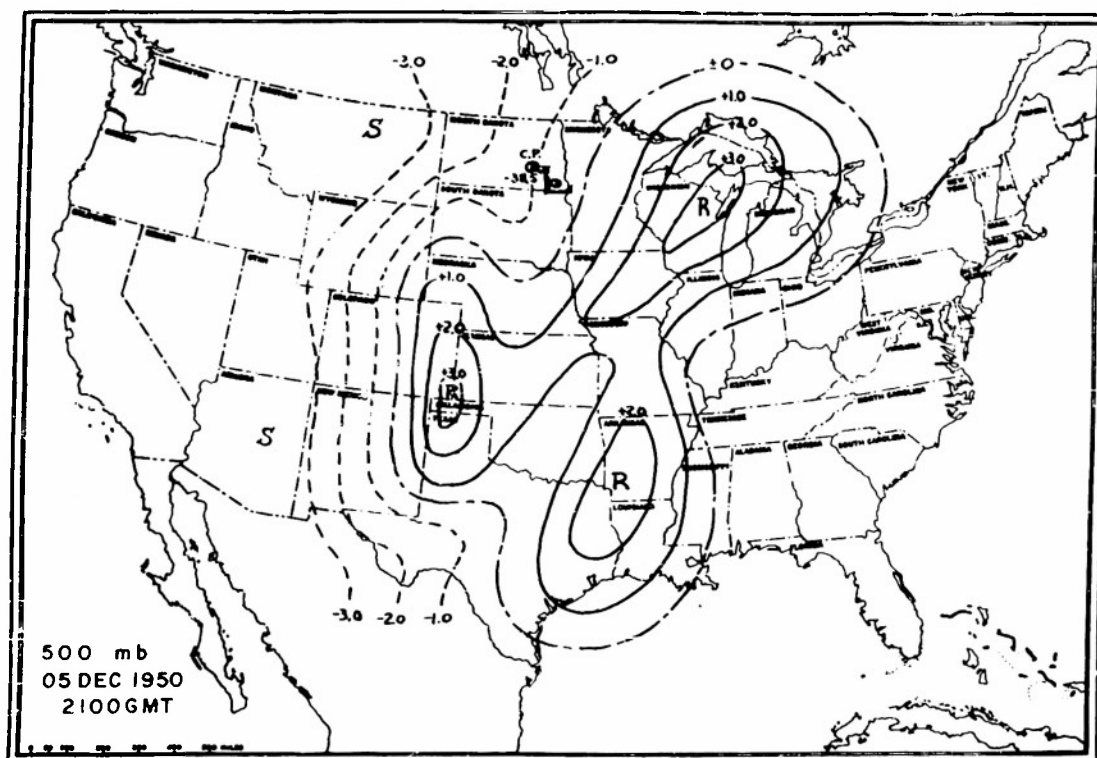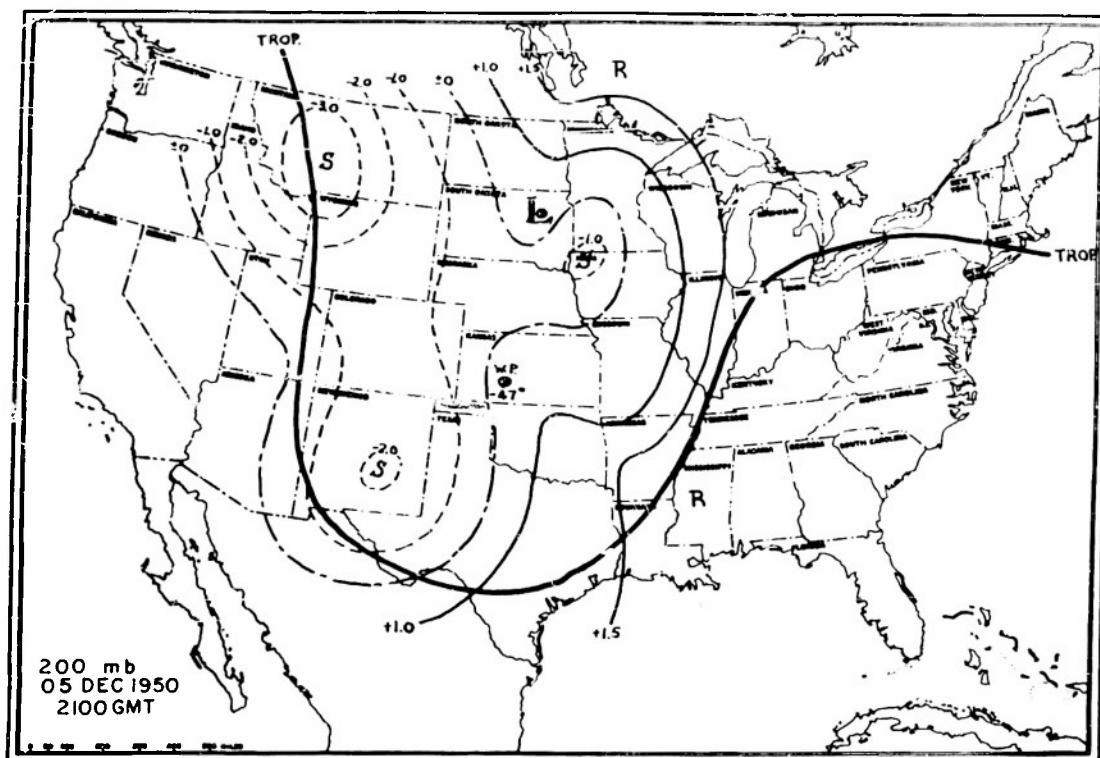Fig. 19.   200 mb and 500 mb maps.   1500 GMT, 5 December 1950.

Fig. 20. 200 mb and 500 mb vertical velocity maps.
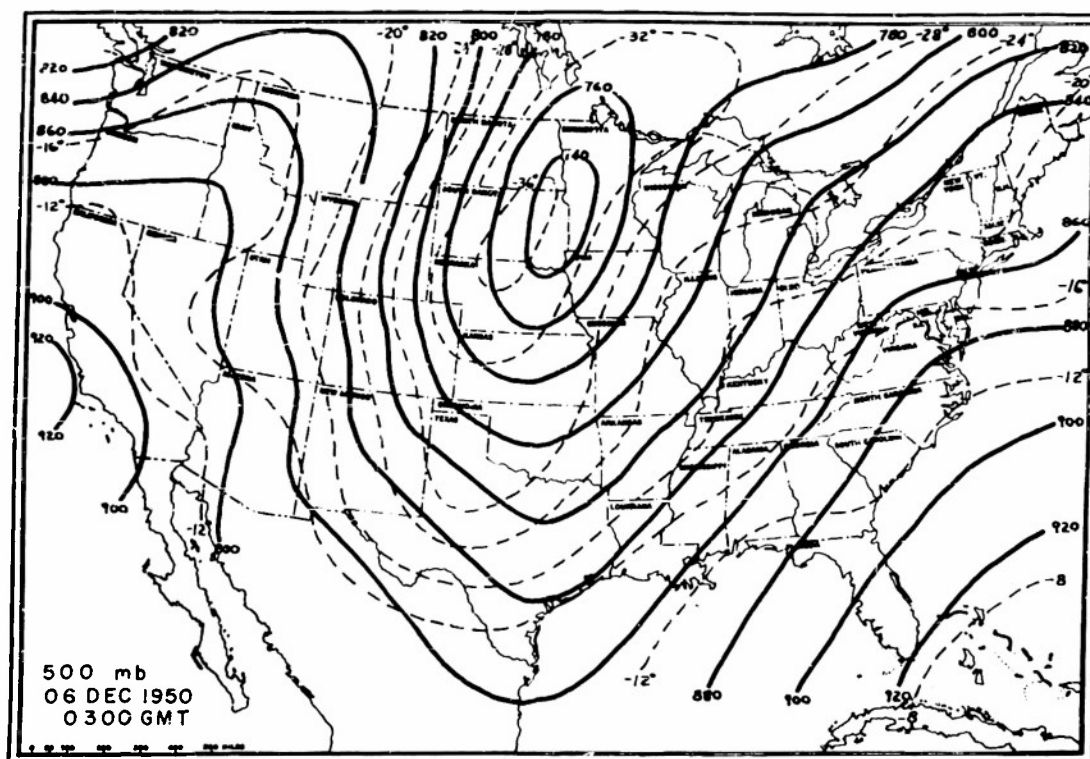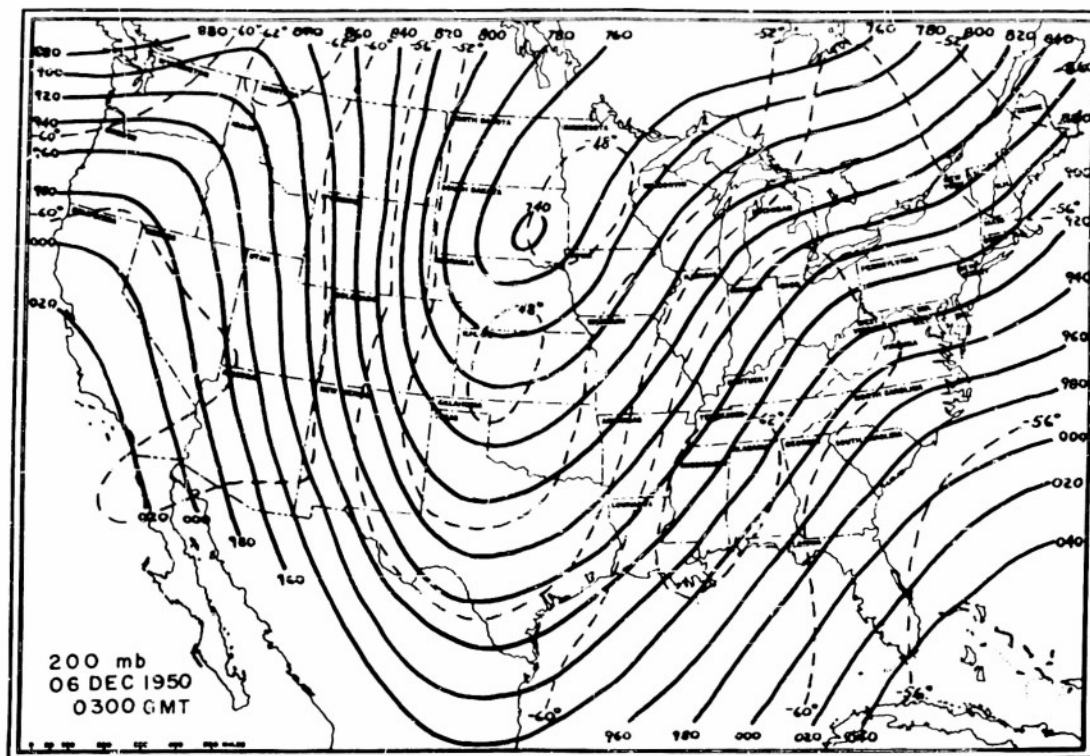2100 GMT, 5 December 1950.

Fig. 21. 200 mb and 500 mb maps. 0300 GMT, 6 December 1950.

The vertical velocity map for 0900 GMT on the 5th shows three centers of rising motion at 500 mb (fig. 20) to the east, southeast and south-southeast of the low. West and southwest of the low the air was sinking at 500 mb, while in the low itself the vertical velocity was almost zero.

At 200 mb (fig. 20) the air was subsiding to the west and southwest of the cyclone and also to the southeast. However, in the cyclone itself the vertical velocity was almost zero.

Twelve hours later, at 0900 GMT on the 6th (fig. 22), the air at 500 mb was still rising to the east and southeast of the low. However, to the south and west of the low subsidence was found at 500 mb.

The 200 mb vertical motion chart for 0900 GMT on the 6th again shows subsidence southwest of the low center. However, to the northwest the air was ascending at 200 mb over a region of rather strong subsidence at 500 mb. The pattern of a stratospheric lifting over tropospheric sinking motion indicates the existence of horizontal convergence in the vicinity of the tropopause, which in turn suggests that the low center will move southeastward away from the center of high level convergence. A center of subsidence was also found at 200 mb over Tennessee, well to the southeast of the low. Below the 200 mb sink there existed ascending motion at 500 mb indicating the existence of horizontal divergence between these two levels. This pattern again suggests movement of the low toward the southeast, away from the convergence and towards the divergence aloft. (A quantitative analysis of the divergence will be discussed below.)

Between 0300 and 1500 GMT on the 6th the low at 500 mb (fig. 23) moved southward with little change in intensity except for an increase in the gradient flow to the east and southeast. At 200 mb (fig. 23), however, filling and cyclogenesis occurred simultaneously. Although the height of the 200 mb surface generally increased over the plains, a new cyclone center appeared southeast of the original low. The sinking motion of the air at 200 mb raised the temperature of the two pools of warm air. At the same time the gradient flow southeast of the cyclone increased considerably and the trough showed signs of developing toward the southeast.

At 2100 GMT on the 6th the air was ascending at 500 mb (fig. 24) in two centers, one northeast and one southwest of the cyclone. The development of ascending motion southwest of the low is rather surprising since the air had been sinking in this quadrant at 500 mb. There was also a marked change in

fig. 22.   200 mb and 500 mb vertical velocity maps.
0900 GMT, 6 December 1950.

200 mb
06 DEC 1950
1500 GMT

500 mb
06 DEC 1950
1500 GMT

Fig. 23. 200 mb and 500 mb maps. 1500 GMT, 6 December 1950.
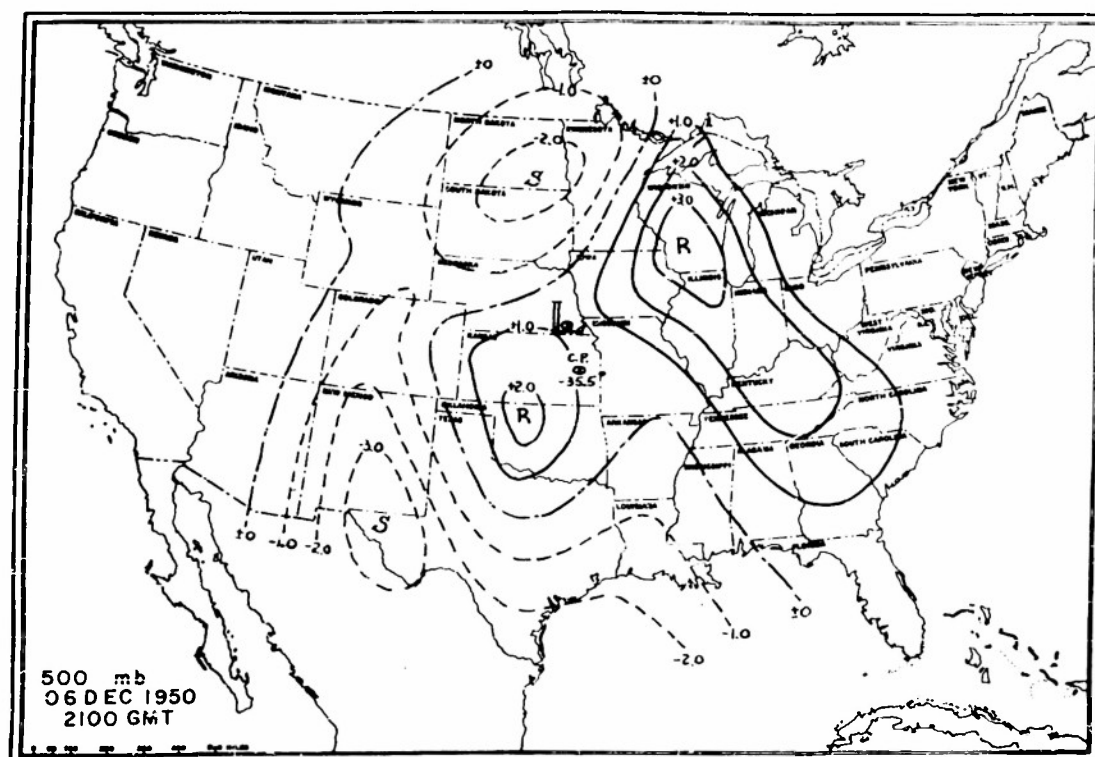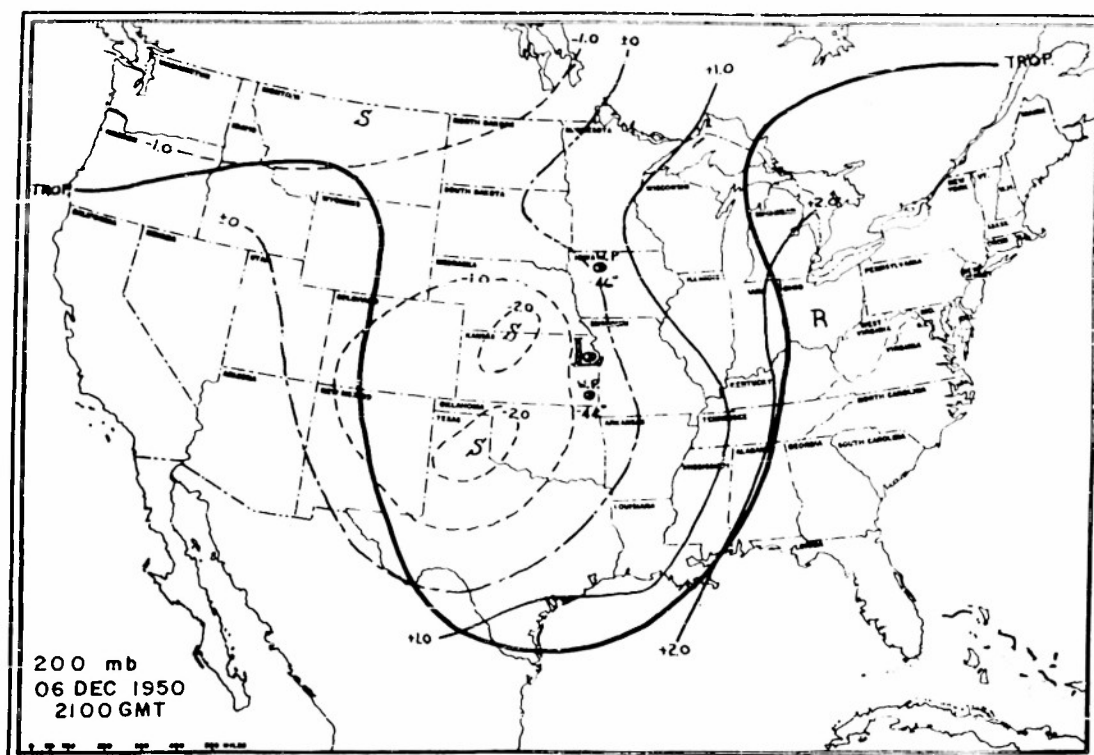
Fig. 24.   200 mb and 500 mb vertical velocity maps.
2100 GMT, 6 December 1950.

the distribution of vertical motion at 200 mb at this time (fig. 24). Above the ascending air southwest of the low at 500 mb, there appeared subsidence in the stratosphere. A qualitative consideration of the horizontal velocity divergence corresponding to this field of vertical motion indicates the existence of positive divergence near the tropopause southwest of the low.

Between 1500 GMT on the 6th and 0300 GMT on the 7th (fig. 25), the low at 500 mb deepened slightly and continued its southward movement. The gradient steepened noticeably in the southwest quadrant of the cyclone. At 200 mb (fig. 25) there was little change in the position or intensity of the low, although the temperature in the center increased.

At 0900 GMT on the 7th, the center of ascending motion southwest of the low at 500 mb (fig. 26) disappeared. The dominant area of ascending motion northeast of the low moved northward over the Great Lakes and the upward velocities increased markedly. To the west of the low the air was subsiding. The vertical velocities at 200 mb (fig. 26) were generally quite small at this time with sinking motion northwest, south and east of the low and rising motion to the northeast.

The 500 mb low had apparently begun to recurve before 1500 GMT on the 7th (fig. 27). At this time the low was already moving northeastward toward the region of ascending motion over the Great Lakes. Similarly, the 200 mb low (fig. 27) began moving northeastward. At both levels there was little change in the depth of the cyclone.

By 2100 GMT on the 7th, the center of subsidence at 500 mb (fig. 28), which had been west of the low, moved to the south. The center of ascending motion moved eastward across the lakes and remained north-northeast of the cyclone center. At this time (fig. 28) the air at 200 mb was sinking northeast of the cyclone. However, the vertical velocities were far greater at 500 mb than at 200 mb.

The low subsequently moved northeastward both at 500 mb and 200 mb, as can be seen on maps for 0300 GMT of the 8th (fig. 29), and began once again to deepen.

During the period studied the air at 200 mb was generally sinking around the low center. The sinking motion was not confined to any one quadrant and at various times pockets of subsidence developed in all quadrants of the cyclone.

200 mb
07 DEC 1950
0300 GMT

500 mb
07 DEC 1950
0300 GMT

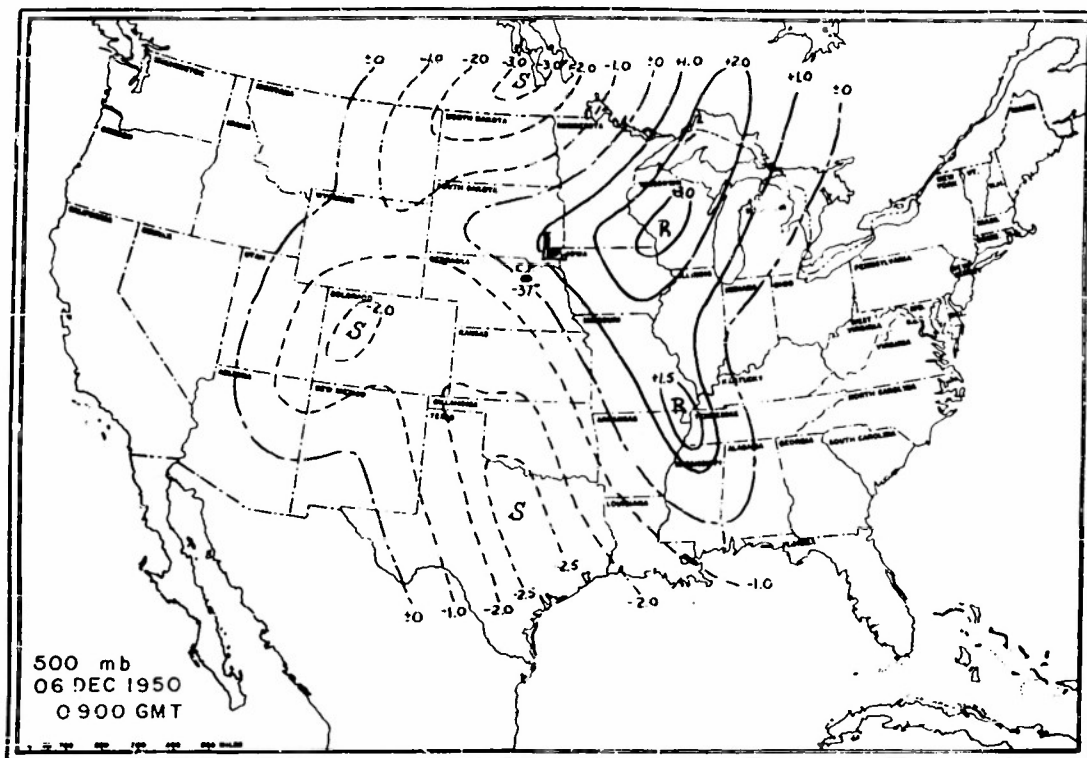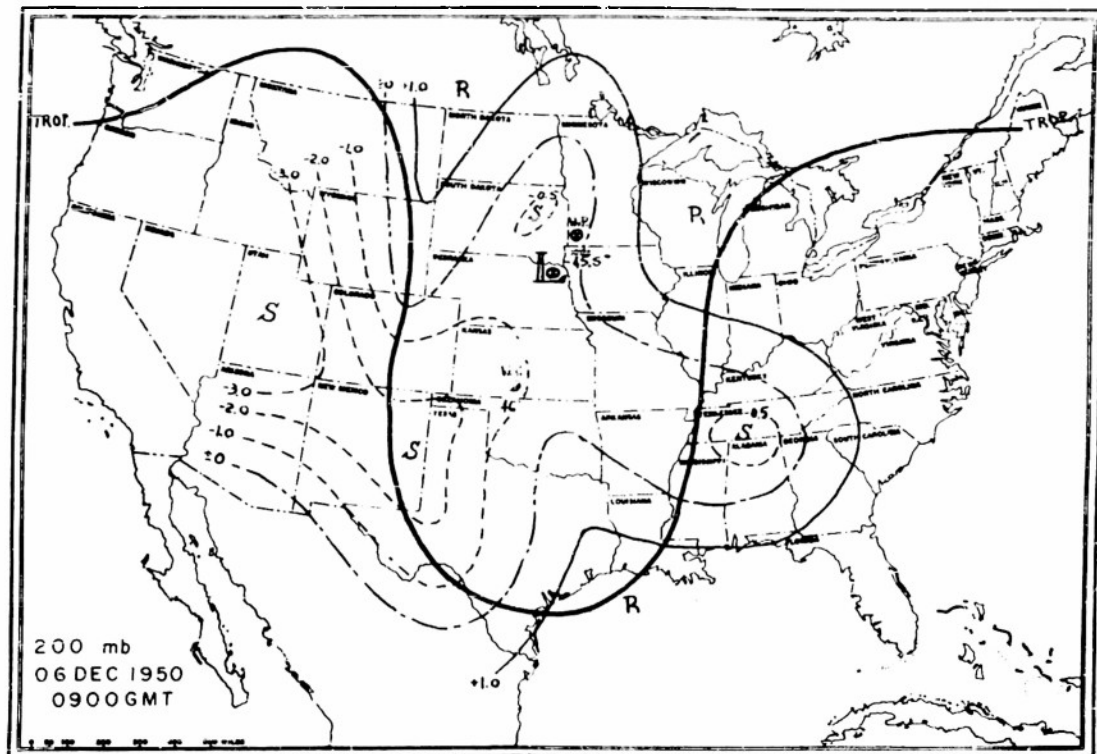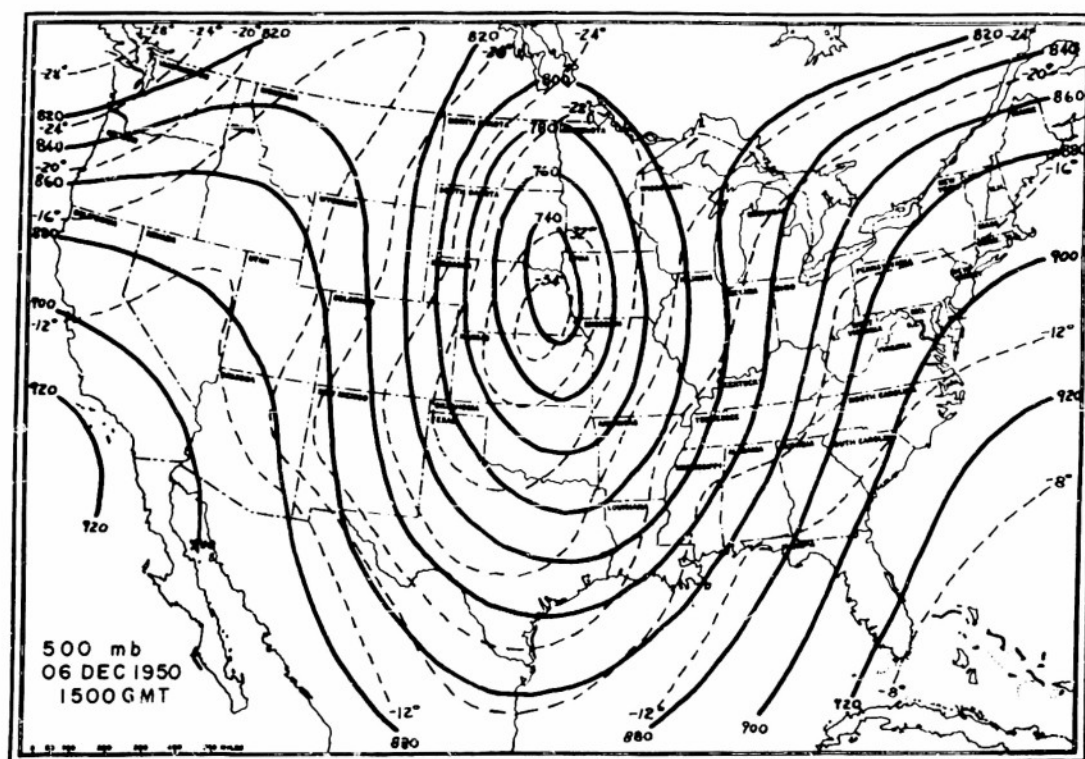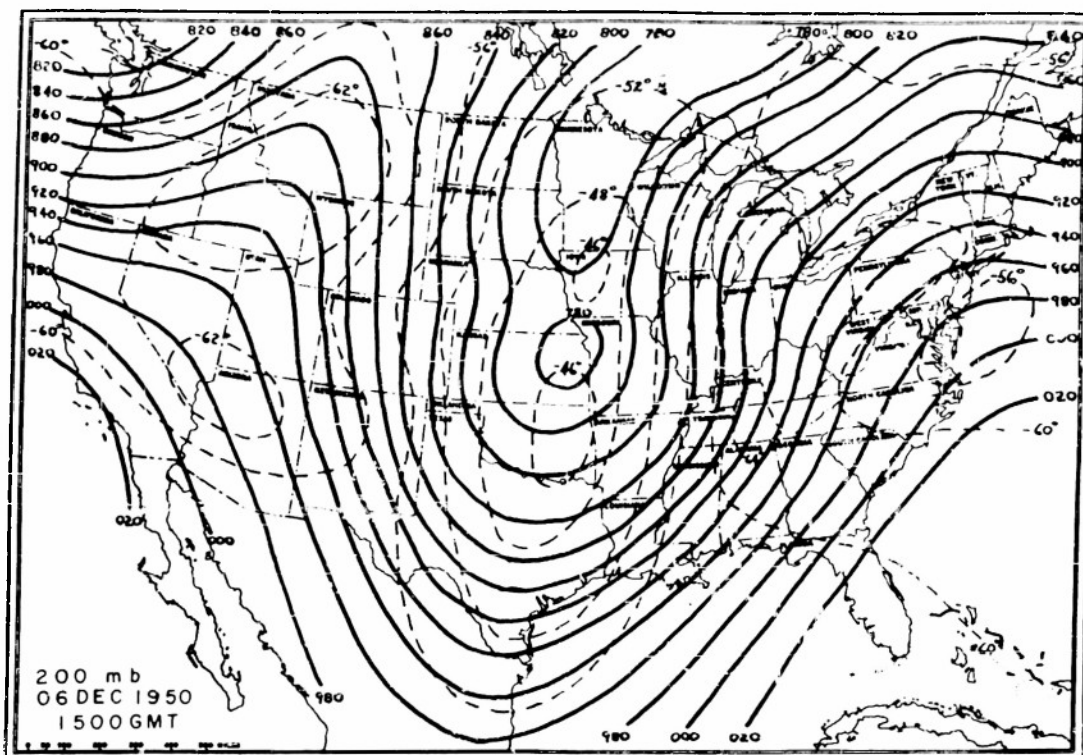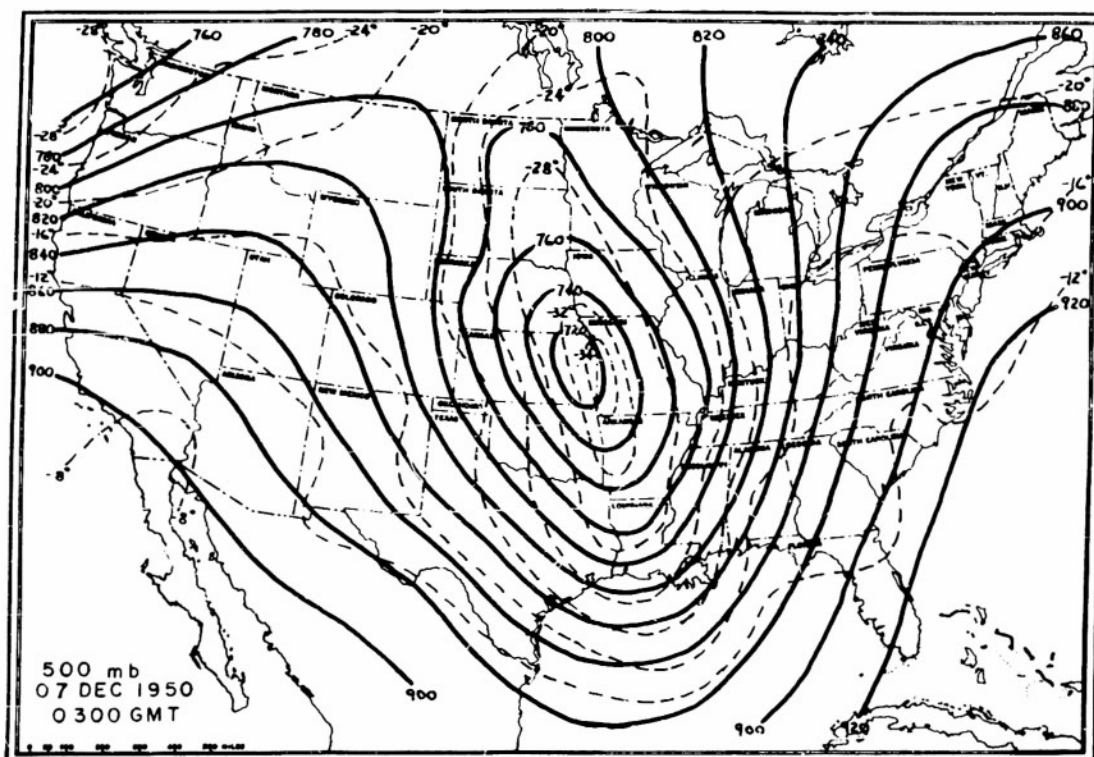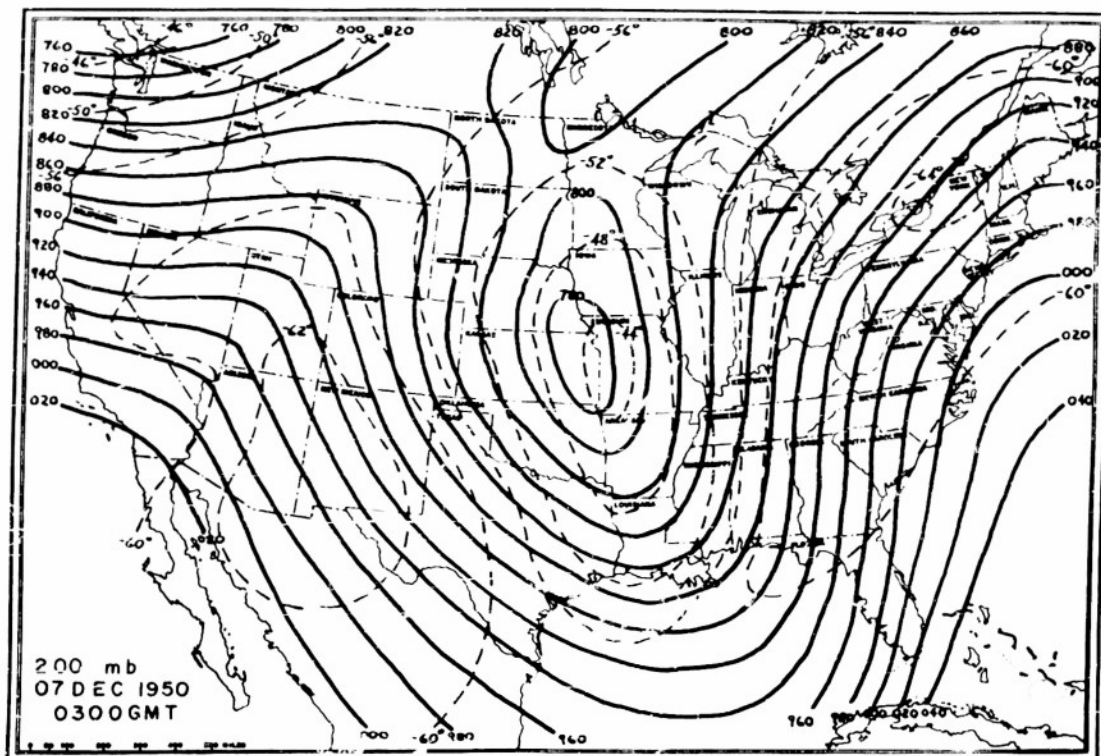Fig. 25.   200 mb and 500 mb maps.   0300 GMT, 7 December 1950.
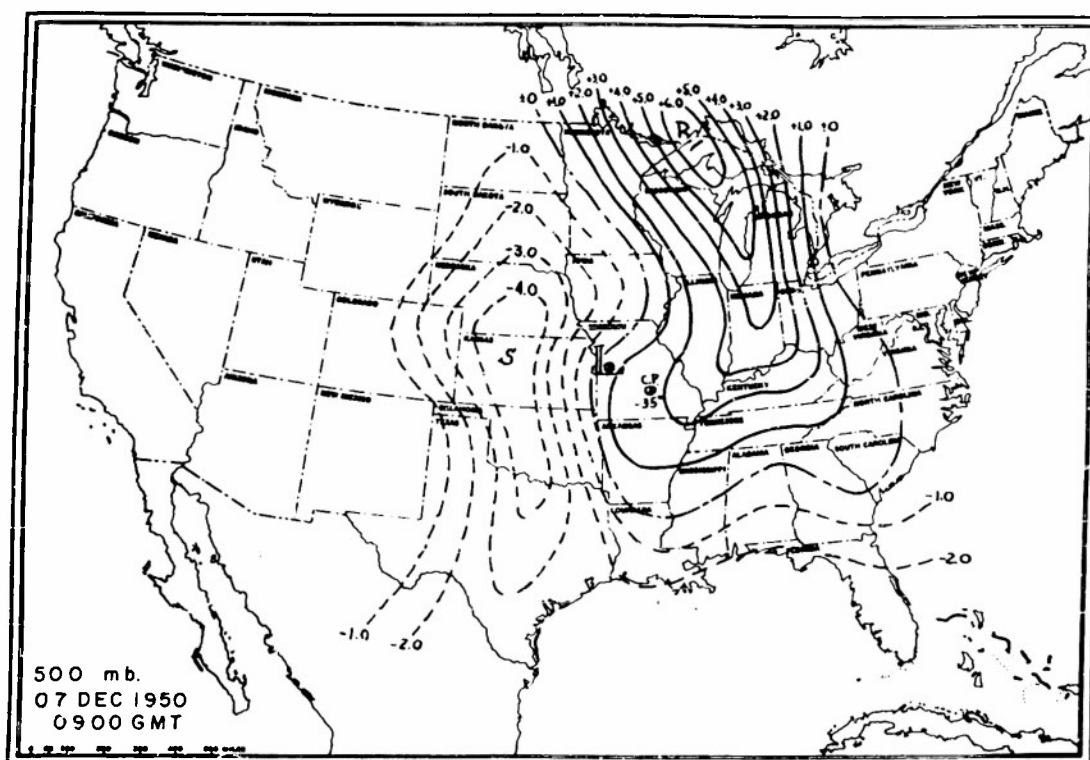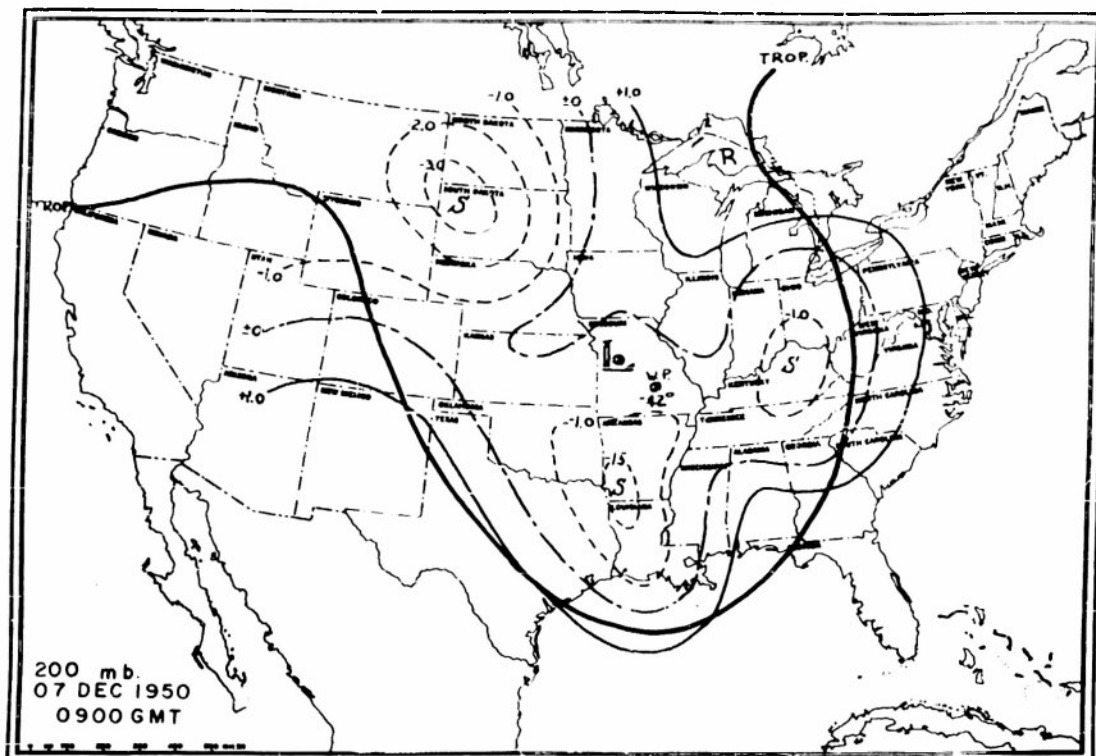
Fig. 26. 200 mb and 500 mb vertical velocity maps.
0900 GMT, 7 December 1950.
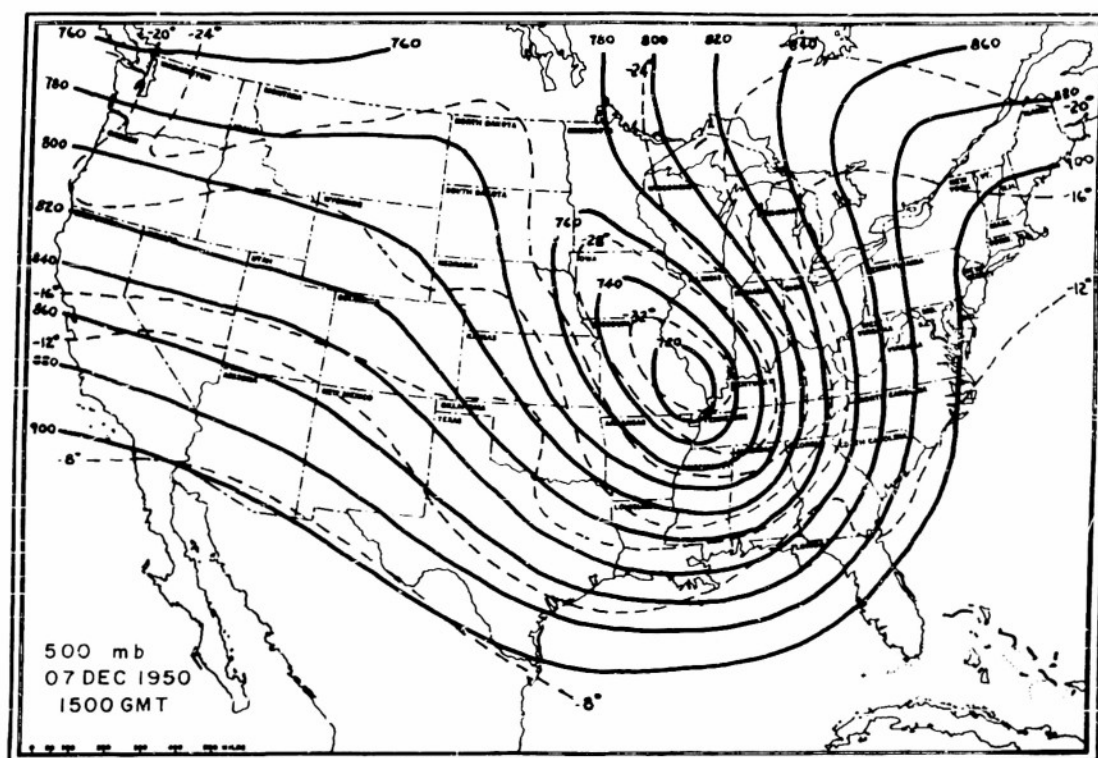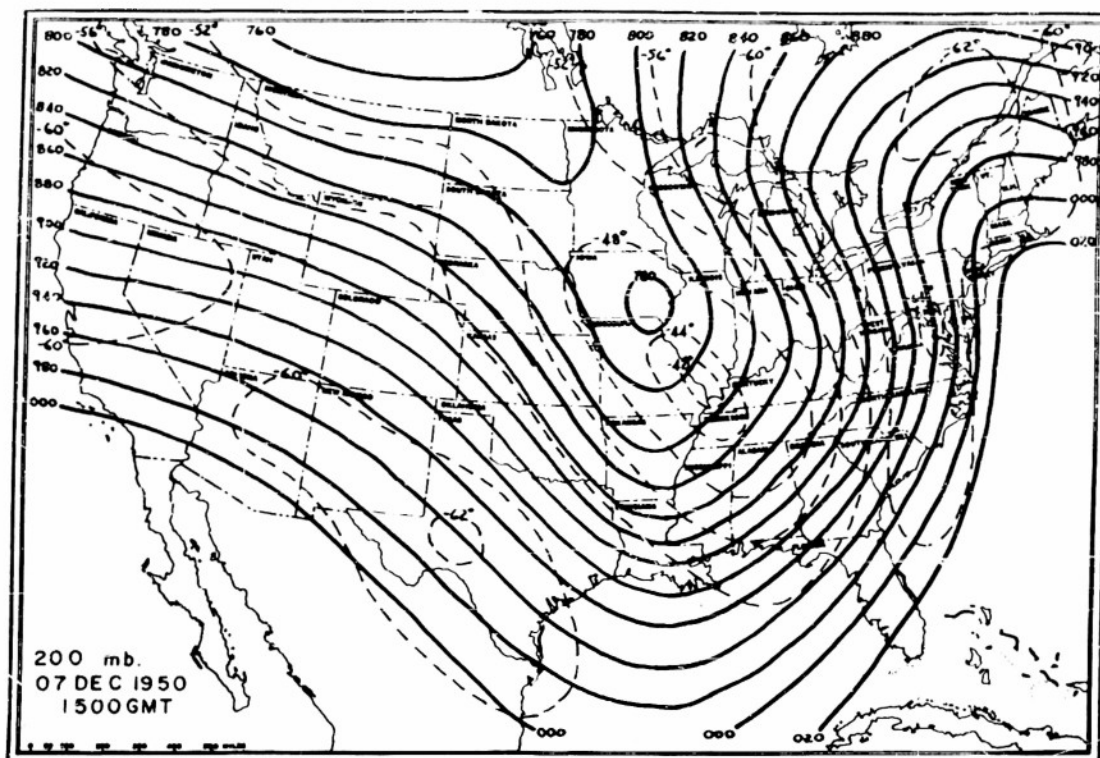
Fig. 27. 200 mb and 500 mb maps. 1500 GMT, 7 December 1950.
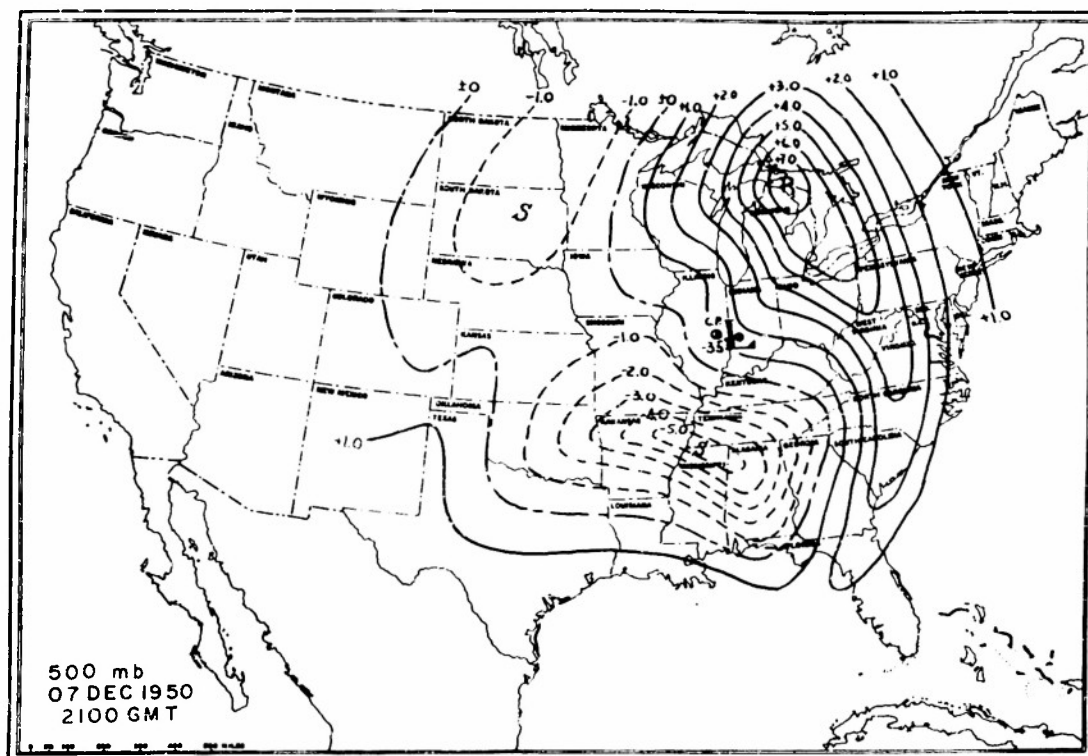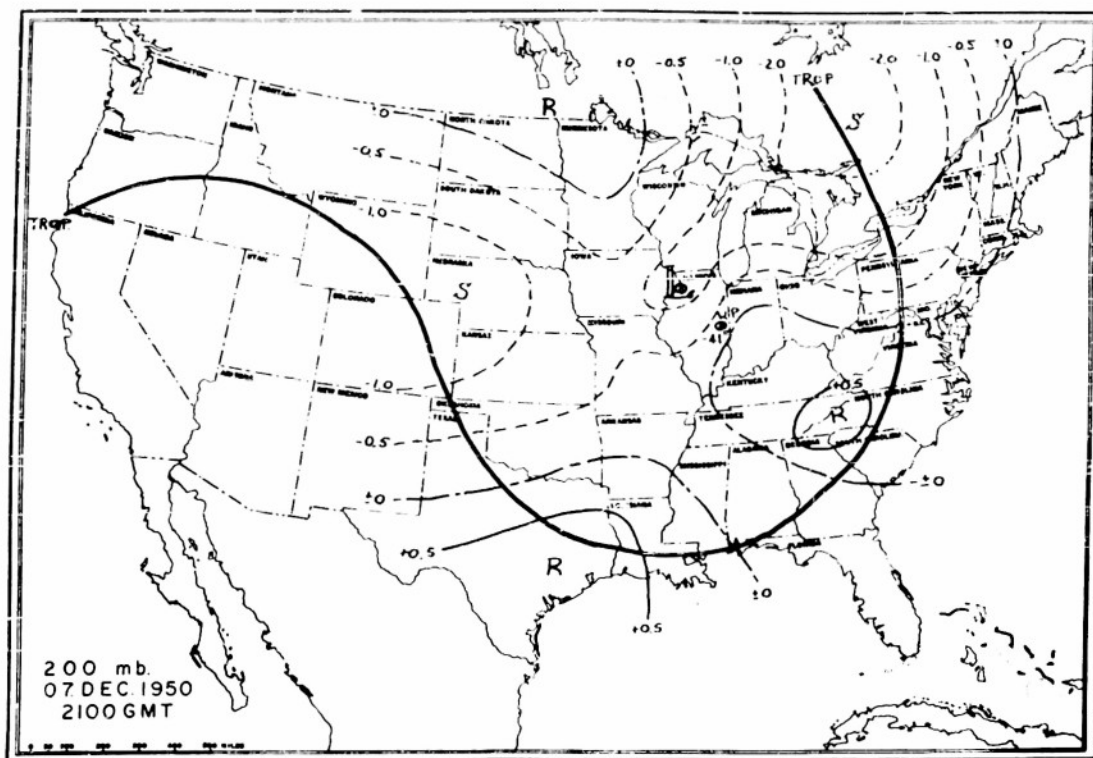
Fig. 28. 200 mb and 500 mb vertical velocity maps.
2100 GMT, 7 December 1950.
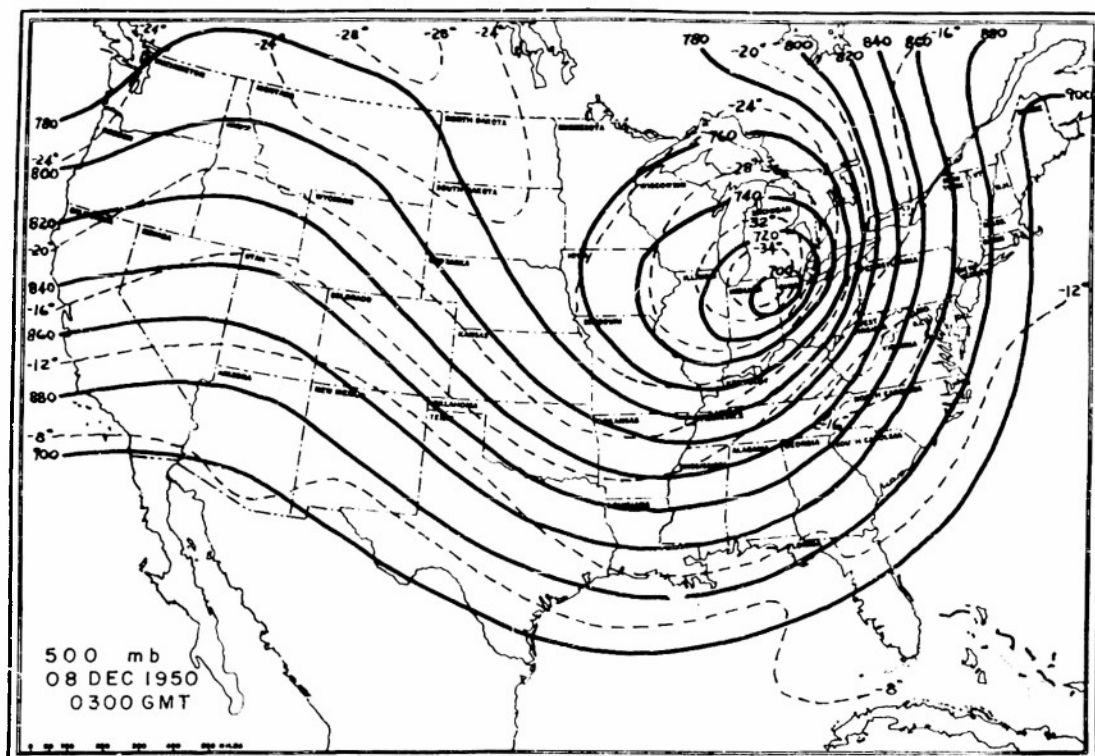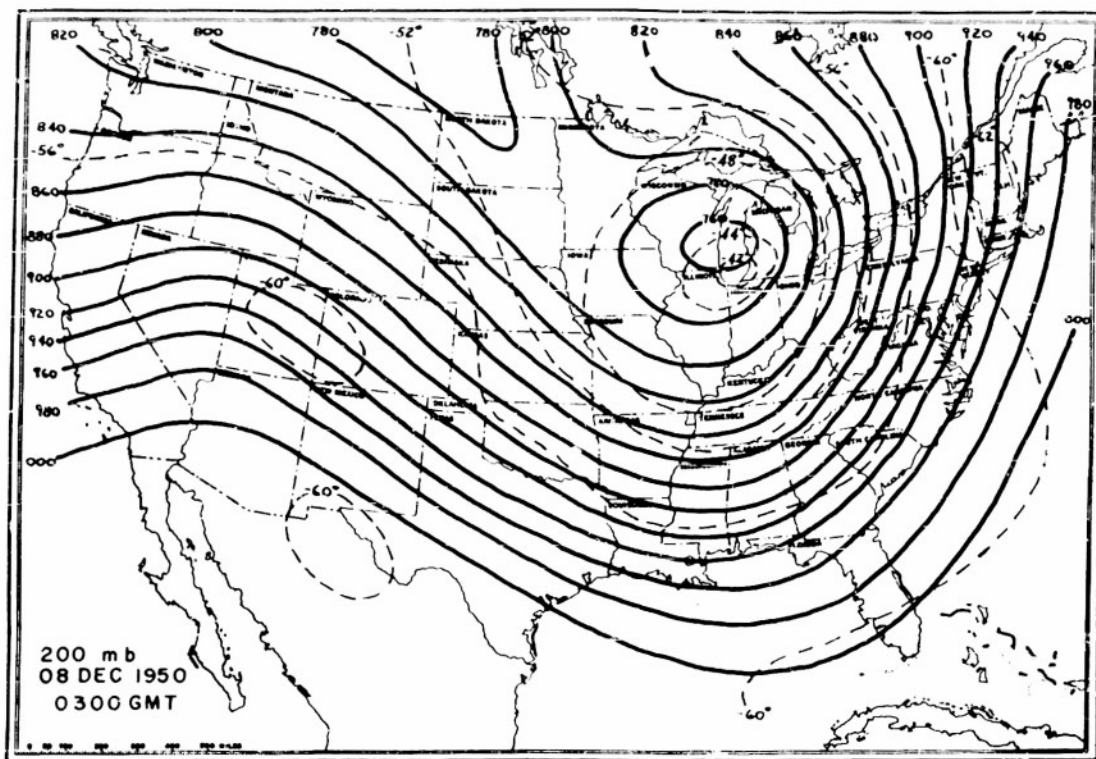
Fig. 29.   200 mb and 500 mb maps.   0300 GMT,   8 December 1950.

At 500 mb there appeared definite areas of rising as well as sinking air around the cyclone. At the beginning of the period, the pattern of vertical motion at this level resembled the well known long wave tropospheric model with ascending motion to the east and descending motion to the west of the trough line. However as the low began to recurve northward toward the end of the period, a center of rapidly ascending air developed ahead (north-northeast) of the low center. At the same time the air began to subside rapidly behind (south of) the low center. By this time, of course, the north-south trough line had virtually disappeared, the vortex was fully developed, and the locus of zero vertical motion had rotated from a north-south orientation to about west northwest - east southeast across the cyclone center.

The Horizontal Velocity Divergence

According to the equation of continuity,

$$\frac{\partial \rho}{\partial t} + \frac{\partial}{\partial x}(\rho u) + \frac{\partial}{\partial y}(\rho v) + \frac{\partial}{\partial z}(\rho w) = 0 \tag{6}$$

where is the air density, x, y and z are in the east, north and upward vertical directions, and u, v and w are the east, north and upward vertical components of the wind velocity. The continuity equation may also be written as,

$$\frac{1}{\rho}\frac{d\rho}{dt} + \left(\frac{\partial u}{\partial x} + \frac{\partial v}{\partial y}\right) + \frac{\partial w}{\partial z} = 0 \tag{7}$$

If we neglect the first term, which represents the compressibility and which is generally of smaller magnitude than the remaining terms, equation (7) reduces to

$$\frac{\partial w}{\partial z} = -\left(\frac{\partial u}{\partial x} + \frac{\partial v}{\partial y}\right) = -\ \text{div}_2 V \tag{3}$$

where $\text{div}_2 V$ represents the horizontal divergence.

Assuming a monotonic change of w from 500 mb to 200 mb, it follows from equation (8) that rising motion at 500 mb and sinking motion at 200 mb indicate horizontal divergence between these levels. Conversely, sinking motion at 500 mb and rising motion at 200 mb indicate horizontal convergence between the levels. In the areas where the vertical motion at both levels is of the same sign, the relative magnitudes of the vertical velocities at the two levels determine the sign of the divergence.

There are four possible combinations of vertical velocities between the two levels. Upon inspecting the vertical velocity charts it was noted that the areas comprising these different combinations have about the same location relative to the path of the 500 mb low center on each chart. In the area vacated by the low, 200 mb rising over 500 mb sinking motion predominates. Ahead of the low we find sinking at 200 mb over rising at 500 mb. To the left of the path (looking in the direction of movement) there exists rising motion at both levels, while to the right of the path we find sinking motion at both levels. These areas rotate as the path of the low curves to the east and then northeast.

In order to get some quantitative estimate of the magnitude of the divergence, equation (8) was used with $\partial w/\partial z$ replaced by $\Delta w/\Delta z$. Δ w was taken as $(w_{200\ mb} - w_{500\ mb})$, and Δ z was taken as 20,000 ft, the average height difference between the two levels. This approximation is valid under the assumption of a linear change of w with height. Computations were made at points of maximum difference of vertical velocity between the two levels. These points along with the magnitudes of $\text{div}_2 \mathbf{W}$ in $\sec^{-1}$ are shown on the divergence charts (figs. 30 - 34). This divergence may be interpreted as the mean divergence in the layer between 500 and 200 mb.

In general it can be seen from the divergence charts that the low moves away from an area of convergence and toward an area of divergence. (The six-hourly cyclone positions shown on the divergence maps are for the 500 mb level). An interesting example of this can be seen on the map for 0900 GMT of the 7th (fig. 33). The area of convergence, previously to the north of the low center (figs. 30, 31, 32) moved to the west and southwest of the low along the path previously taken by the low. This was reflected in a change in the path of the low towards the southeast and east. On the following chart (fig. 34) it can be seen that the area of convergence intensified and moved to the southeast. The low then recurved towards the northeast and finally to the north, directly into an area of strong divergence over the Great Lakes.
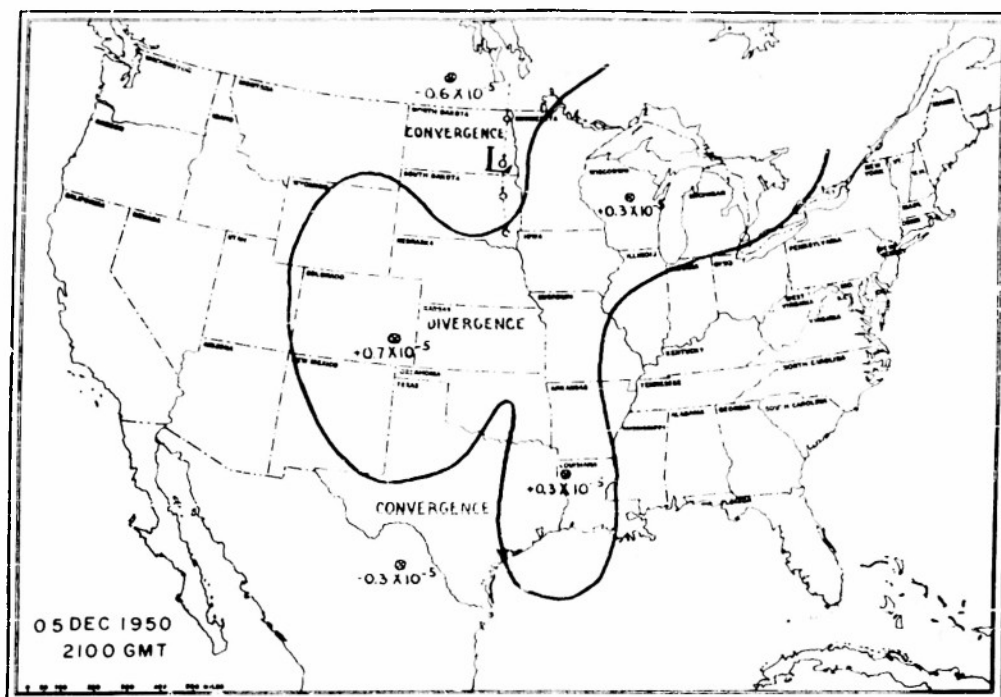
Fig. 30. Horizontal divergence between 200 and 500 mb.
2100 GMT, 5 December 1950.
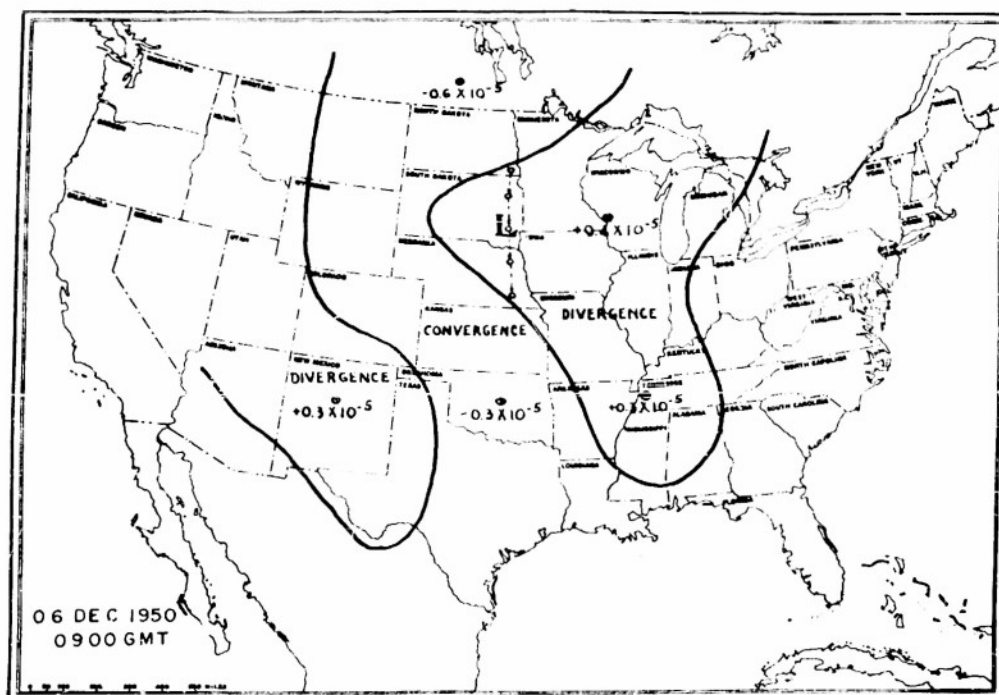
Fig. 31. Horizontal divergence between 200 and 500 mb.
0900 GMT, 6 December 1950.
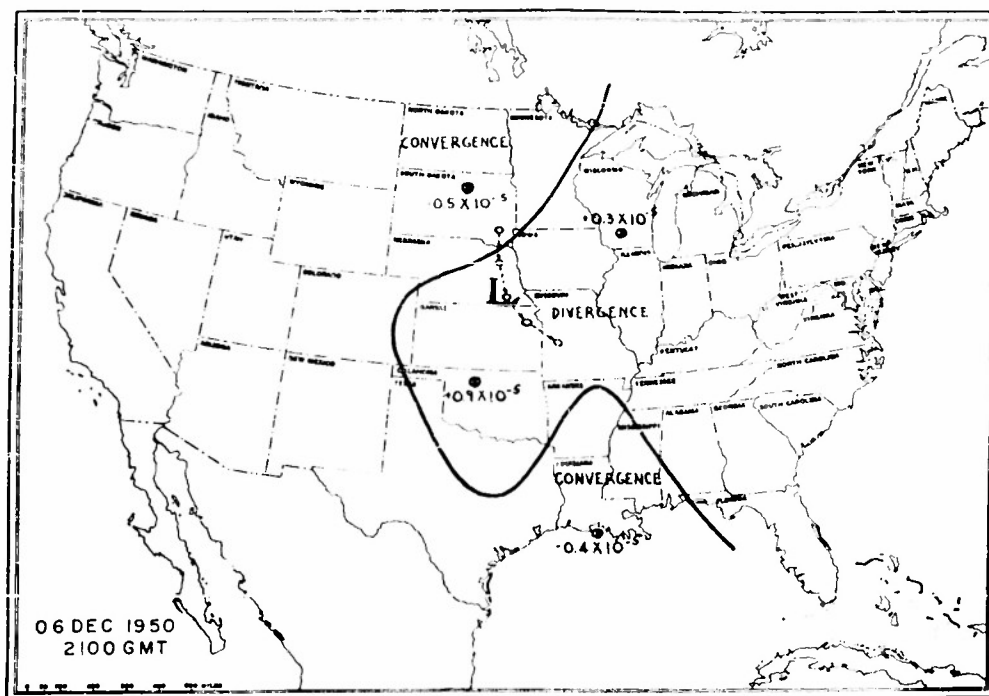
Fig. 32. Horizontal divergence between 200 and 500 mb.
2100 GMT, 6 December 1950.
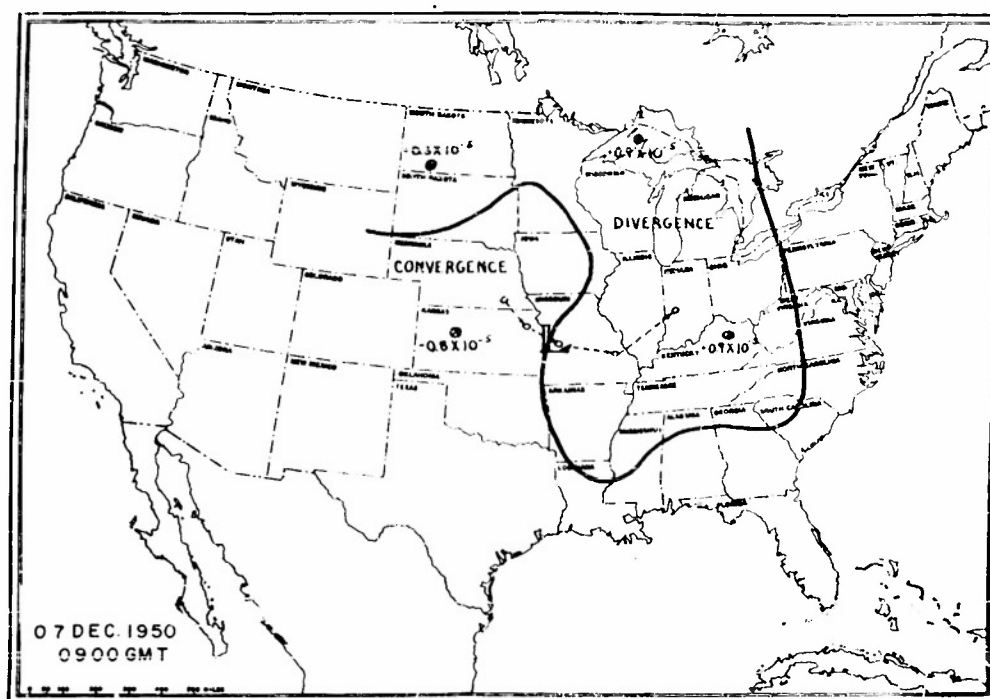
Fig. 33. Horizontal divergence between 200 and 500 mb.
0900 GMT, 7 December 1950.

References

Fleagle, R. G., 1947: The fields of temperature, pressure and three-dimensional motion in selected weather situations. _J. Meteor._, v. 4, 165-185.

Hsieh, Yi-ping, 1949: An investigation of a selected cold vortex over North America. _J. Meteor._, v. 6, 401-410.

Miller, J. E., 1945: Computation of vertical motion from constant-pressure charts. Department of Meteorology, College of Engineering, New York University, New York, N. Y. 14 pp.

Nyberg, A., 1949: An aerological study of large-scale atmospheric disturbances. _Tellus_, v. 1, no. 1, 44-53.

Palmén, E., 1949: On the origin and structure of high-level cyclones south of the maximum westerlies. _Tellus_, v. 1, no. 1, 22-31.

Palmén, E., and K. M. Nagler, 1949: The formation and structure of a large-scale disturbance in the westerlies. _J. Meteor._, v. 6, 227-242.
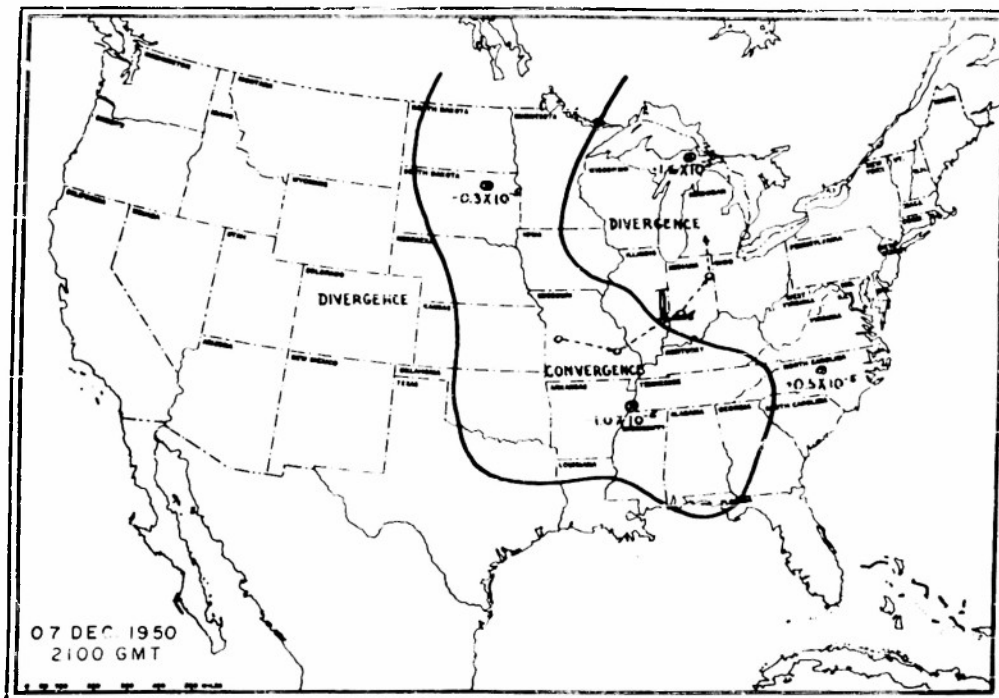
Fig. 34. Horizontal divergence between 200 and 500 mb.
2100 GMT, 7 December 1950.

COMPUTATIONS OF LONG WAVE RADIATIONAL
COOLING IN EXTRATROPICAL CYCLONES

GEORGE OHRING

Introduction

There has been much research on mean infrared radiational cooling in the atmosphere. These studies, which present an average picture of atmospheric radiational processes, tend to smooth out the irregularities which occur daily in various synoptic situations. One of the most important synoptic situations in need of further understanding is the cyclone. The aim of this paper is to determine the effect of the synoptic conditions within a storm upon the radiational cooling rates. This in turn may lead to a better understanding of the role of radiational cooling on cyclone structure and development.

Summary of Earlier Work

The greater part of previous research on infrared radiational cooling has been concentrated upon the computation of cooling rates for mean or idealized conditions. For clear Arctic conditions, the mean summer maximum cooling rate is 1.2°C/day and the mean winter maximum cooling rate is 0.8°C/day (Penner,1948). For middle latitudes, average clear sky cooling rates have a maximum of 1° to 2°C/day (Möller, 1950 and London, 1952). In clear equatorial air, mean maximum cooling rates are 2 to 3°C/day (Elsasser, 1940).

Studies of radiational cooling, assuming mean cloud conditions as well as mean lapse rates, indicate that with the presence of clouds the cooling rate increases. In an average middle latitude cyclone the cooling rate at the top of the lower cloud layer is 2°C/day and at the top of the higher overcast is 5°C/day (Möller, 1950). With mean cloudy conditions in the Northern Hemisphere the cooling rate is greater than 2°C/day at the tops of the clouds (London,1952).

The theoretical infrared radiational properties of a cloud layer 50m thick, in a normal atmosphere, were investigated by Möller (1943). At a height of 2 km

the cloud top cooled at a rate of 6.5° C/hr and the base warmed at a rate of 1.7°C/hr. When placed at 6 km. the cloud top cooled at a rate of 9.6°C/hr and the base warmed at a rate of 6.9°C/hr. Möller noted that such a large cooling at the top and a warming at the base would result in a very unstable lapse rate within the cloud.

Synoptic studies of long wave radiational cooling have been made by Alder (1951) and by Neiburger and Thompson (1953). Alder investigated a polar outbreak over the United States and reported that maximum cooling rates were found above clouds, that maximum heating in the vicinity of clouds occurred at the bases, that atmospheric heating was found at the bases of inversions, and that atmospheric cooling was found at the tops of inversions. In their study of the subtropical anticyclone in the Pacific Ocean, Neiburger and Thompson found maximum cooling rates greater than 2.5°C/day at the 700 mb level. These maximum rates occurred at the top of a subsidence inversion in the eastern part of the high pressure cell.

It is known that radiational cooling in the free air depends upon the temperature distribution, the moisture distribution and the cloudiness distribution. In a cyclonic situation the most important of these three is in the effect of cloudiness. From previous studies of longwave radiational cooling and theoretical reasoning one would expect to find large cooling at the top surfaces of the cloud layers within the cyclone. Also, one would expect to find a general warming at the bases of the cloud layers. At the frontal inversions in a cyclone the temperature distribution influences the cooling rates to a great extent. The rate of temperature change would be expected to change from a warming rate at the base of the inversion to a cooling rate at the top of the inversion.

Procedures and Methods of Computation

In all methods of computing radiational temperature changes, the cooling is determined from the divergence of the net radiational flux. The equation for the cooling is given by

$$\frac{\Delta T}{\Delta t} = \frac{g}{c_p} \frac{\Delta S_n}{\Delta p} \tag{1}$$

where $\Delta T/\Delta t$ is the local temperature change per unit time

g is the acceleration of gravity

c_p is the specific heat of dry air at constant pressure

$\Delta S_n/\Delta p$ is the change of net radiational flux S with changing pressure in the vertical direction.

This formula is derived from the first law of thermodynamics assuming that the effects of compression and advection can be neglected.

There are direct and indirect methods for computing radiational cooling. Elsasser's method (1942), for example, is an indirect one and requires a determination of the net flux graphically and a further computation to obtain the cooling. This method is not very practical for synoptic applications since it tends to smooth out irregularities. Bruinenberg's tabular method (1946), which is based upon a simplified water vapor spectrum, obtains the cooling directly from an integration of the flux divergence above and below the level at which the cooling is being computed. In this study, D. L. Brooks' tabular method (1950) was used, rather than Bruinenberg's, because of its availability. Brooks derived his method from Bruinenberg's equation (1946) for the instantaneous rate of temperature change due to infrared radiation. The essential difference between the two methods is that Brooks makes use of empirical emissivity measurements rather than the simplified water vapor spectrum theorized by Bruinenberg.

Brooks' working equation for the instantaneous rate of temperature change due to water vapor radiation at a reference level in the atmosphere is

$$\frac{\partial T}{\partial t} = -\frac{q}{c_p}\left(\frac{p}{1000}\right)^{\frac{1}{2}}\left[\sum_{k=1}^{N}\Delta(\sigma T^4)_n\left(\overline{\frac{\partial \varepsilon}{\partial w}}\right)_n \downarrow + \frac{\partial S_E}{\partial w}\downarrow - \sum_{k=1}^{\infty}\Delta(\sigma T^4)_m\left(\overline{\frac{\partial \varepsilon}{\partial w}}\right)_m \uparrow\right] \quad (2)$$

where $\frac{\partial T}{\partial t}$ is the local temperature change in degrees centigrade per minute at the reference level

q is the specific humidity at the reference level

c_p is the specific heat of dry air at constant pressure

$(p/1000)^{1/2}$ is the square root pressure correction factor to obtain the corrected optical path length at the reference level where the pressure is p. The need for a pressure correction factor is explained in the section on discussion of assumptions.

(σT^4) is the black body radiation of a slab. (σ is the Stefan – Boltzmann constant.)

S is the infrared radiational flux.

ε is the emissivity of water vapor and is defined as the actual emission divided by the black body emission. It is a function of the corrected optical path length w.

w is the corrected optical path length for water vapor.

$\partial S_E/\partial w$ is the value of $\partial S/\partial w$ at the upper boundary of the radiating atmosphere.

In equation (2), the summation over n is for layers above the reference level into which the atmosphere has been divided, and the summation over m is for layers below the reference level. The points on the radiosonde sound-

ing are considered to bound the layers into which the atmosphere has been divided for purposes of the summation of the individual contributions. Within the brackets of equation (2), $\Delta (\leqslant T^4)$ is the change in ($\leqslant T^4$) in each layer, $\overline{\partial \varepsilon / \partial w}$ is the average slope of the emissivity curve for an increment of w for each layer, and $\partial S_E/\partial)w$ is equal to ($\leqslant T^4$) $(\partial \varepsilon /\partial)w$ evaluated at the top of the water vapor atmosphere. The term $\partial S_E/\partial)w$ becomes zero at a black body surface such as the ground or a cloud since w becomes infinite and $\partial \varepsilon / \partial w$ becomes zero.

This method was applied in the following manner. The first step, as in all methods of computing radiative fluxes and cooling rates, is to determine w, the corrected optical path length, for each layer of the sounding. For small layers this is given by (Brooks, 1950)

$$w \text{ (corrected)} = - \bar{q} \; \frac{\Delta p}{g} \left(\frac{\bar{p}}{1000} \right)^{1/2} \tag{3}$$

where w is the corrected optical path length in g/cm^2

  $\bar{q}$ is the mean specific humidity for the layer in g/kg

  p is the thickness of the layer in mb

  g is the acceleration of gravity in cm/sec^2

  $\bar{p}$ is the mean pressure of the layer.

Next, the increments of path length (w) are summed up with respect to the level at which the temperature change is being computed, i.e., the reference level. At the reference level w is taken as zero and increases in either direction. From Brooks' tables the values of $\Delta (\leqslant T^4)$, $\overline{(\partial \varepsilon /\partial w}$, and $\partial S_E/\partial)w$ are obtained. If there are no cloud decks, the summation of equation (2) extends to the top of the water vapor atmosphere. It is sufficient to go up as high as 200 mb or 150 mb since above these levels there is very little contribution to the cooling at lower heights. If there is a cloud deck the summation is carried out up to the base of the cloud. Since the cloud is a black body, the term $\partial S_E/\partial)w$ becomes zero and does not have to be included in equation (2).

The summation of equation (2) is then carried out and the rate of temperature change is obtained. For partially cloudy skies a weighted cooling

rate was obtained by weighting the cooling rates computed for clear skies and total cloudiness according to the amount of clouds present. This weighted cooling rate formula is

$$\frac{\partial T}{\partial t_w} = N\left(\frac{\partial T}{\partial t}\right)_{cloudy} + (1-N)\left(\frac{\partial T}{\partial t}\right)_{clear} \tag{4}$$

where $\partial T/\partial t_w$ is the weighted cooling rate,

N is the amount of clouds in tenths,

$(\partial T/\partial t)_{cloudy}$ is the cooling rate assuming total cloudiness, and

$(\partial T/\partial t)_{clear}$ is the cooling rate assuming clear skies.

Long wave radiational cooling rates within the clouds were computed in the following manner. Assuming that each 50 mb layer within a cloud acts as a perfect black body, the cooling is given by

$$\frac{\Delta T}{\Delta t} = K \frac{\Delta^2 T}{\Delta p^2} \tag{5}$$

where $\frac{\Delta T}{\Delta t}$ is the rate of temperature change per day, and

$\frac{\Delta^2 T}{\Delta p^2}$ is the curvature of the temperature sounding .

K is a constant which depends upon the thickness of cloud chosen as a complete black body radiator (in these calculations, 50 mb), and upon the mean temperature of the layer.

The method by which equation (5) can be derived is discussed by Brunt (1952). The thickness of cloud that will behave as a complete black body is not precisely known at the present time. However, no matter what thickness is assumed, it will only change the magnitude of the radiational cooling, not the sign or the distribution.

From the previous discussion of the method for obtaining the radiational cooling, it can be seen that three quantities must be known in order to carry out the computation. These are

1) The temperature distribution in the vertical

2) The moisture distribution in the vertical

3) The amount of clouds and heights of bases and tops of clouds.

Temperatures were obtained from radiosonde data and plotted on tephigrams. Where the temperature soundings did not extend up to 150 mb they were extrapolated to that point on the basis of the temperature fields on the 200 mb and 150 mb facsimile maps. Dew points, obtained from radiosonde data, were used as a measure of the moisture distribution. They were extrapolated to 150 mb assuming a humid stratosphere with saturation at the tropopause (see Hoffer, 1951). All the assumptions made in this section are discussed below.

Cloud distributions were based on synoptic data, three-hourly data, pilot reports and radiosonde data. Wherever cloud data were lacking, cloud distributions were determined by using the soundings and on the basis of continuity in a cyclonic cloud distribution.

Discussion of Assumptions

The warming of the atmosphere due to absorption of short wave solar radiation was ignored in this study because, for the most part, it is negligible compared to the temperature changes due to long wave radiation. In a clear atmosphere, warming by absorption of solar radiation amounts to only a few tenths of a degree per day. With cloudy skies, according to a sample calculation, the absorption of solar radiation may produce a warming of 2.5° C/day in the top 20 mb of the cloud. This warming turns out to be almost as large as the infrared cooling rates computed in this paper near the cloud tops. However, it should be pointed out that the long wave cooling rates at the top of the cloud are much larger than those presented in this paper, just as the temperature of the ground surface is much higher than the temperature of the air a few centimeters above it during the daytime. Also, solar radiational processes operate only while the sun is shining, while long wave radiational processes operate throughout the day.

The extrapolation of temperature on the basis of the temperature field on upper level constant pressure charts is fairly accurate since the temperature field is continuous. The extrapolation of dew points up to 150 mb is based upon the presumption of a humid stratosphere. At the present time our knowledge of the stratosphere leads us to believe that there is an equal probability of there being a humid or dry stratosphere. Hoffer (1951) computed tropospheric radiational cooling curves for both dry and humid stratospheric conditions. His results indicate that there is little difference between the tropospheric cooling computed from both assumptions. The humid stratospheric assumption was chosen in this study as a matter of mechanical convenience in the extrapolation of dew points.

A pressure correction factor is necessary in the atmosphere because it has been found that the absorption coefficients of water vapor depend, in a rather complex manner, upon the air pressure. Previous investigators have used a square root pressure correction factor (see, for example, Elsasser, 1942). This type of pressure correction was used in this paper. Recent studies (see, for example, Kaplan, 1952) indicate that a linear pressure correction, more correctly defines the pressure dependence of absorption. This new correction would not

influence the results of this study except at high levels and even there it would not change the pattern of radiative cooling.

The long wave radiational cooling of carbon dioxide in the atmosphere was ignored in this study because it is insignificant when compared to the water vapor radiational cooling. According to Brooks (1950), CO_2 cooling is generally about 3% as large as water vapor cooling.

Some of the computations made in this study with Brooks' method were checked by the use of Bruinenberg's tabular method. The largest difference in cooling rates computed by both methods was about $0.7^{\circ}C/day$. When Brooks (1950) compared his method with Bruinenberg's, he found that Bruinenberg's tables gave consistently lower values -- generally about 2/3 as great. The reason for this difference, according to Brooks, is the variation in emissivity with temperature derived theoretically by both of these researchers. Our present knowledge cannot tell us which of these methods gives more accurate results.

Synoptic Situations Investigated and Sources of Data

Cooling rates were computed in two different cyclones. The first cyclone (No. I) was centered in southern Illinois at 0330 GMT, 1 April 1953. Within a period of 24 hours it moved eastward across the country to northeastern Virginia and occluded (figs. 35, 36, 37). In general, there were overcast sky conditions and rain areas north of the cyclone center. Cooling rates were computed above Buffalo, New York; Mount Clemens, Michigan; Rantoul, Illinois; and Omaha, Nebraska, for 0300 GMT, 1 April 1953. For 1500 GMT, cooling rates were computed above Rantoul, Mount Clemens, Buffalo, Pittsburgh, Pennsylvania and Washington, D.C. For 0300 GMT 2 April 1953, cooling rates were computed above Dayton, Ohio, Pittsburgh, and Lakehurst, New Jersey.

The second storm (No. II) was centered in eastern Kansas at 0300 GMT, 20 November 1953. In 12 hours it moved northward to northeastern Nebraska and its central pressure dropped from 1002 mb to 996 mb (figs. 38, 39). Widespread cloudiness, rain and snow were prevalent at the center f the storm and to the north of the center. For 0300 GMT, 20 November 1953, cooling rates were computed
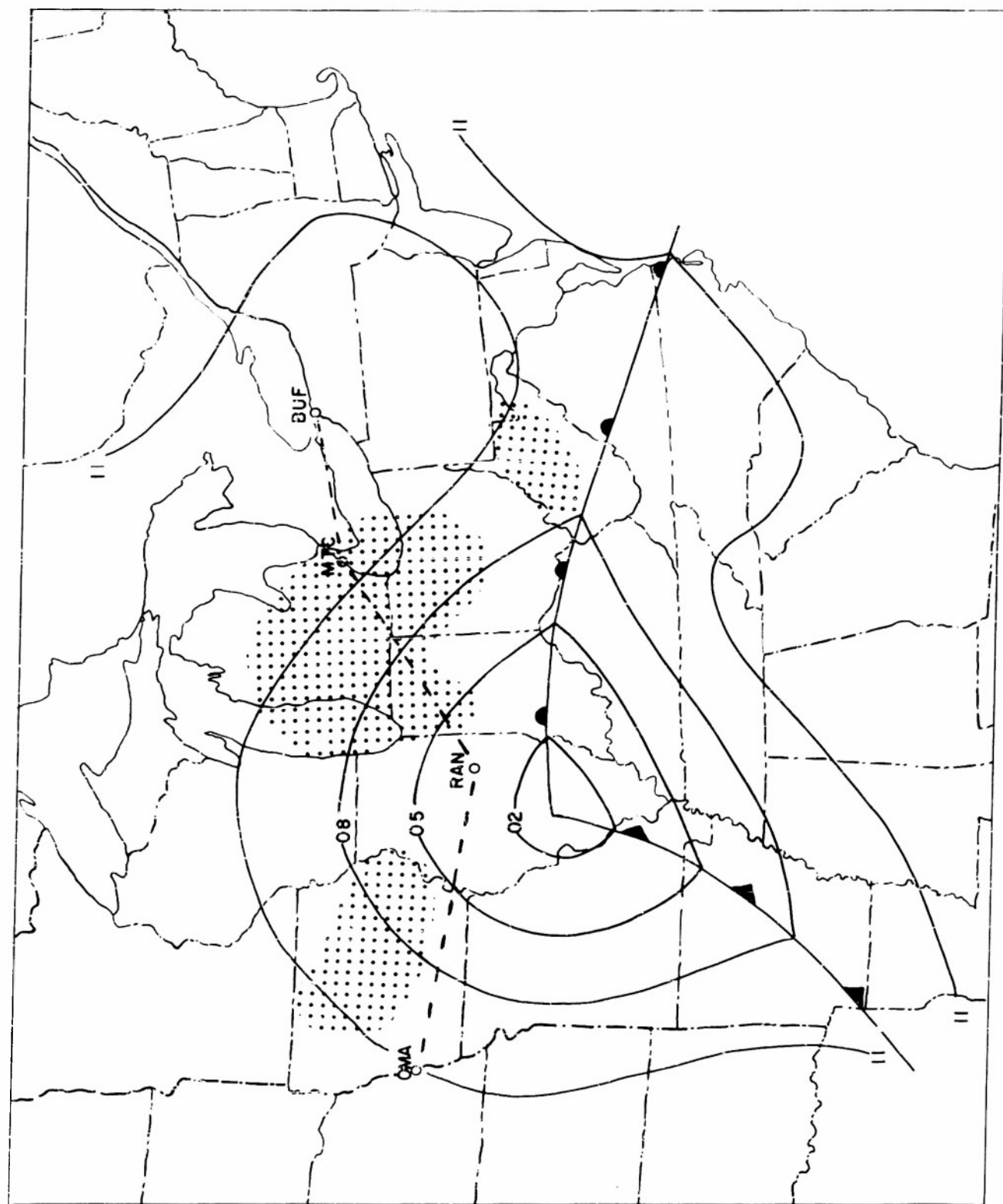
Fig. 35. Surface weather map. Cyclone I. 0300 GMT, 1 April 1953.
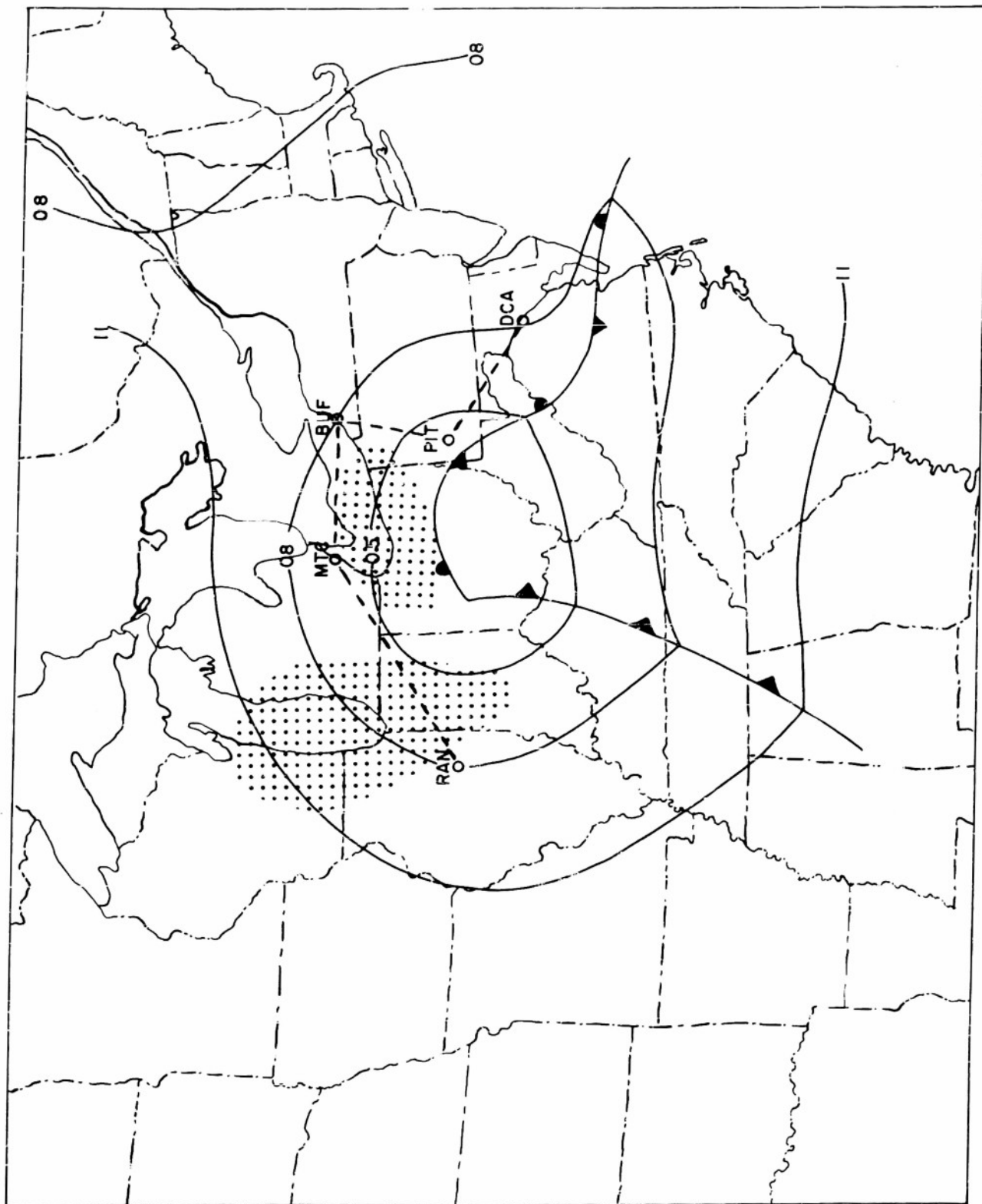
Fig. 36. Surface weather map. Cyclone I. 1530 GMT, 1 April 1953.
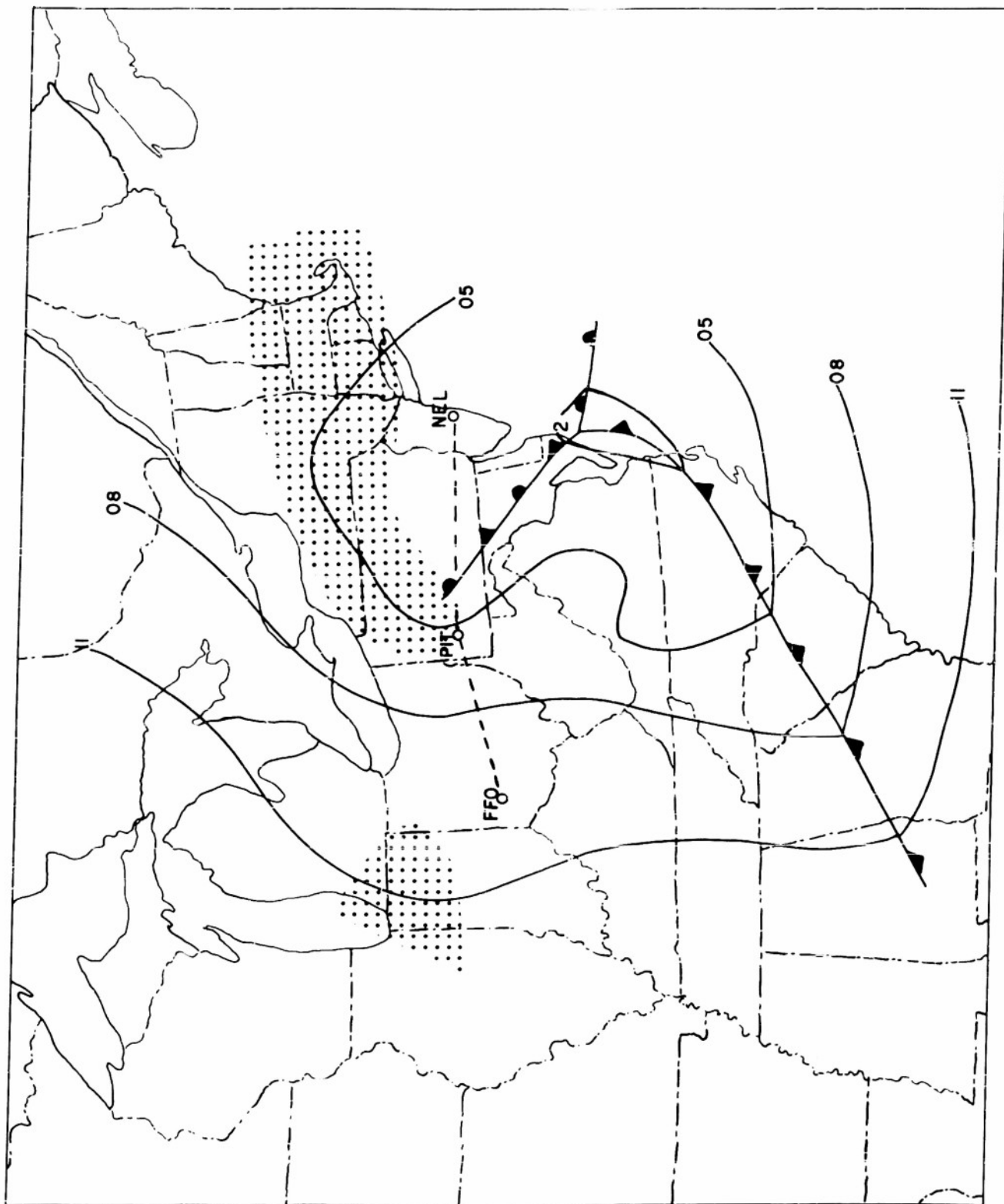
Fig. 37. Surface weather map. Cyclone I. 0300 GMT, 2 April 1953.
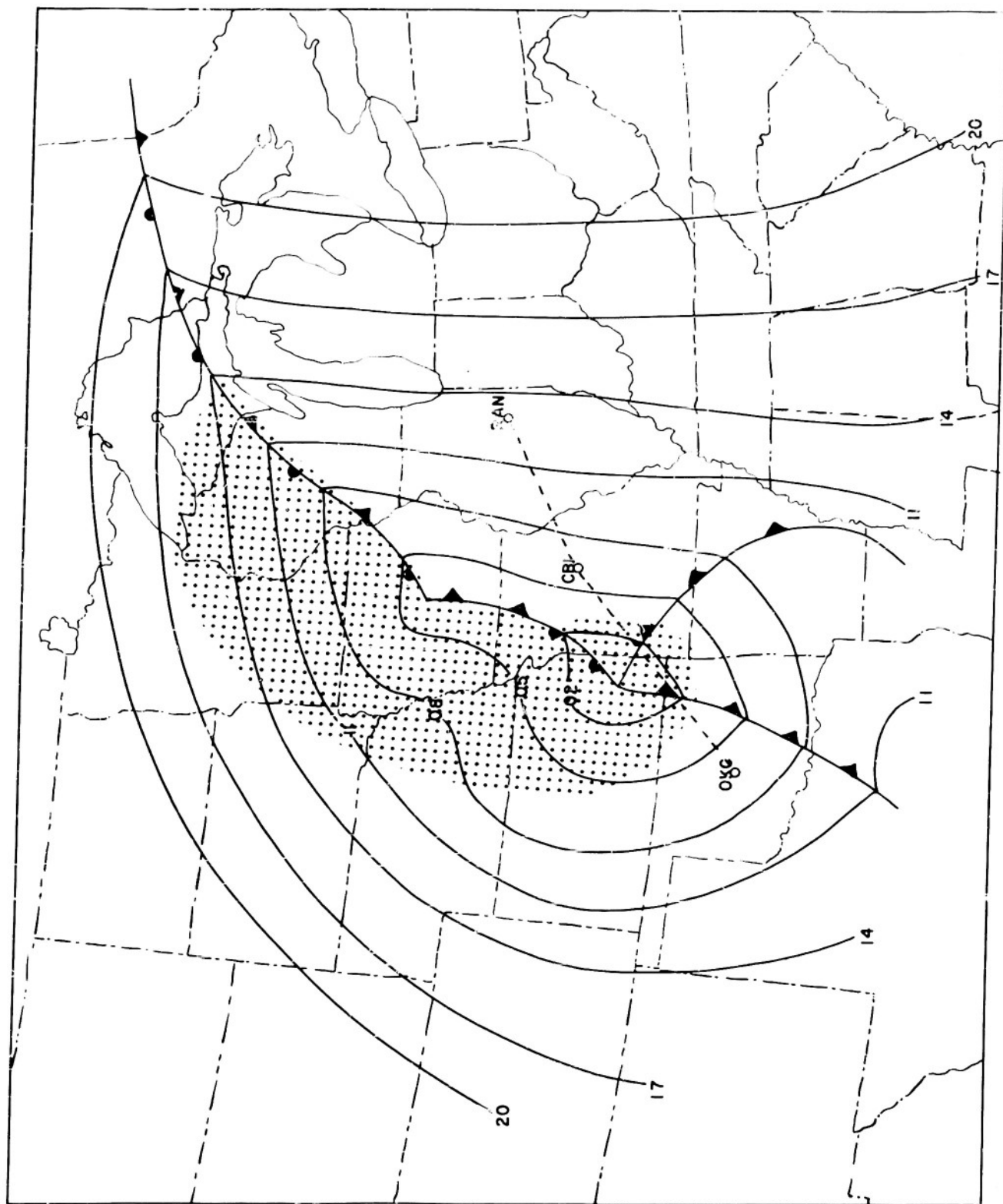
Fig. 38. Surface weather map. Cyclone II. 0300 GMT, 20 November 1953.
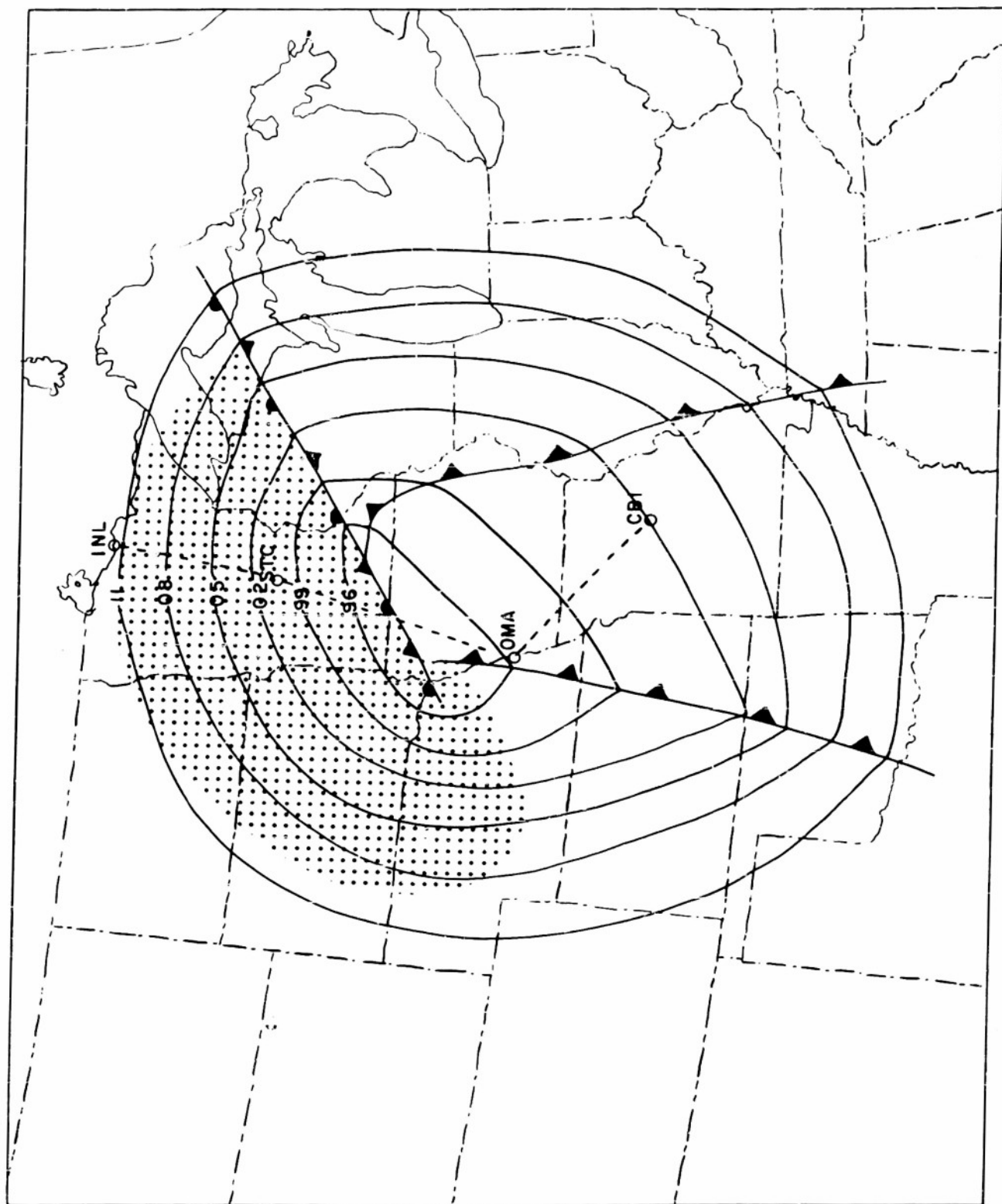
Fig. 39. Surface weather map. Cyclone II. 1530 GMT, 20 November 1953.

above Oklahoma City, Oklahoma; Columbia, Missouri; and Rantoul. For 1500 GMT
cooling rates were computed above International Falls, Minnesota; Saint Cloud,
Minnesota; Omaha and Columbia.

Results

The most important effect on the radiational cooling in a cyclone is caused
by the distribution of cloudiness within the storm. With cloudy skies, the air
below the clouds does not cool as rapidly as it would with clear skies. The
air immediately above the clouds cools at a greater rate than it would with
clear skies. These two effects, slight cooling or warming immediately below
the clouds in a cyclone, and large cooling immediately above the clouds, can
be seen in the cooling rate curves (figs. 40 - 44).

The cooling rate curves show the temperature and dewpoint soundings and
the computed cooling rates on one diagram. The positions and amounts of clouds,
and the frontal zones are also indicated on these diagrams. Wherever there is
partial cloudiness the cooling rates are weighted cooling rates.

Large cooling rates are found at the tops of the overcast layers. In
cyclone I (figs. 40 - 42) cooling rates of 3° C/day are found above the thick
altostratus - altocumulus overcasts of the storm. Warming rates in cyclone I
(figs. 40 - 42) are equal to about 1° C/day at the bases of the cloud decks of
the storm.

The cooling curves for cyclone II are shown in figures 43 and 44. The
most striking feature of these curves is the cooling rate of more than 8° C/day
at the top of the cloud layer at Columbia (fig. 43). This large rate resulted
from the fact that there was a steep inversion at the top of the cloud. The
cooling rate was computed at the top of this inversion which was about 15 mb
above the cloud top. This level is at a higher temperature than the cloud
top or any point above the inversion and will therefore lose a great deal of
heat by radiation. Cooling rates at the tops of the cloud systems in this
cyclone are also generally about 3° C/day. Warming of as much as 1.8° C/day
(fig. 44) is found immediately below the cloud bases at Omaha.
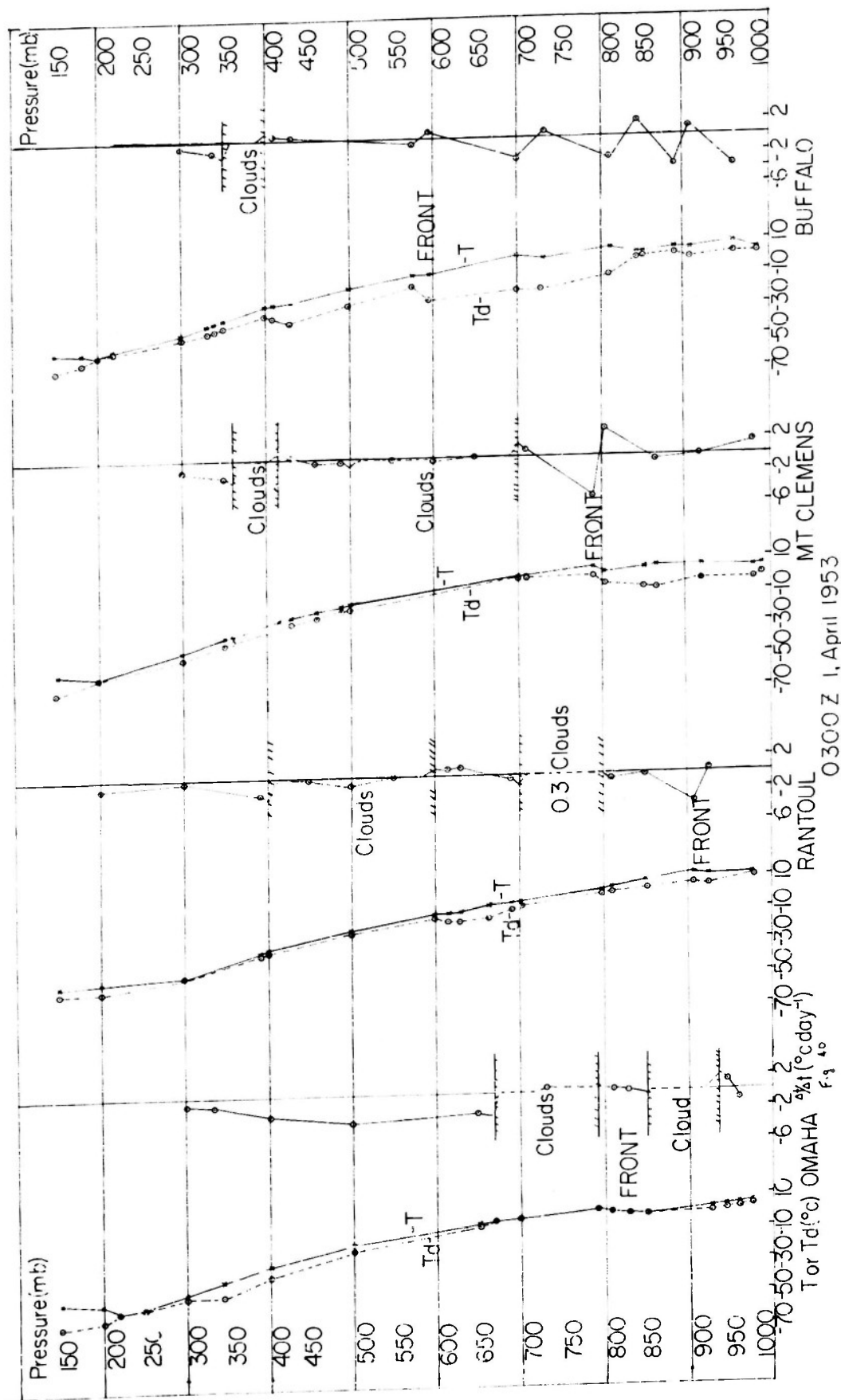
Fig. 40. Lapse rate and cooling rate curves. 0300 GMT, 1 April 1953.
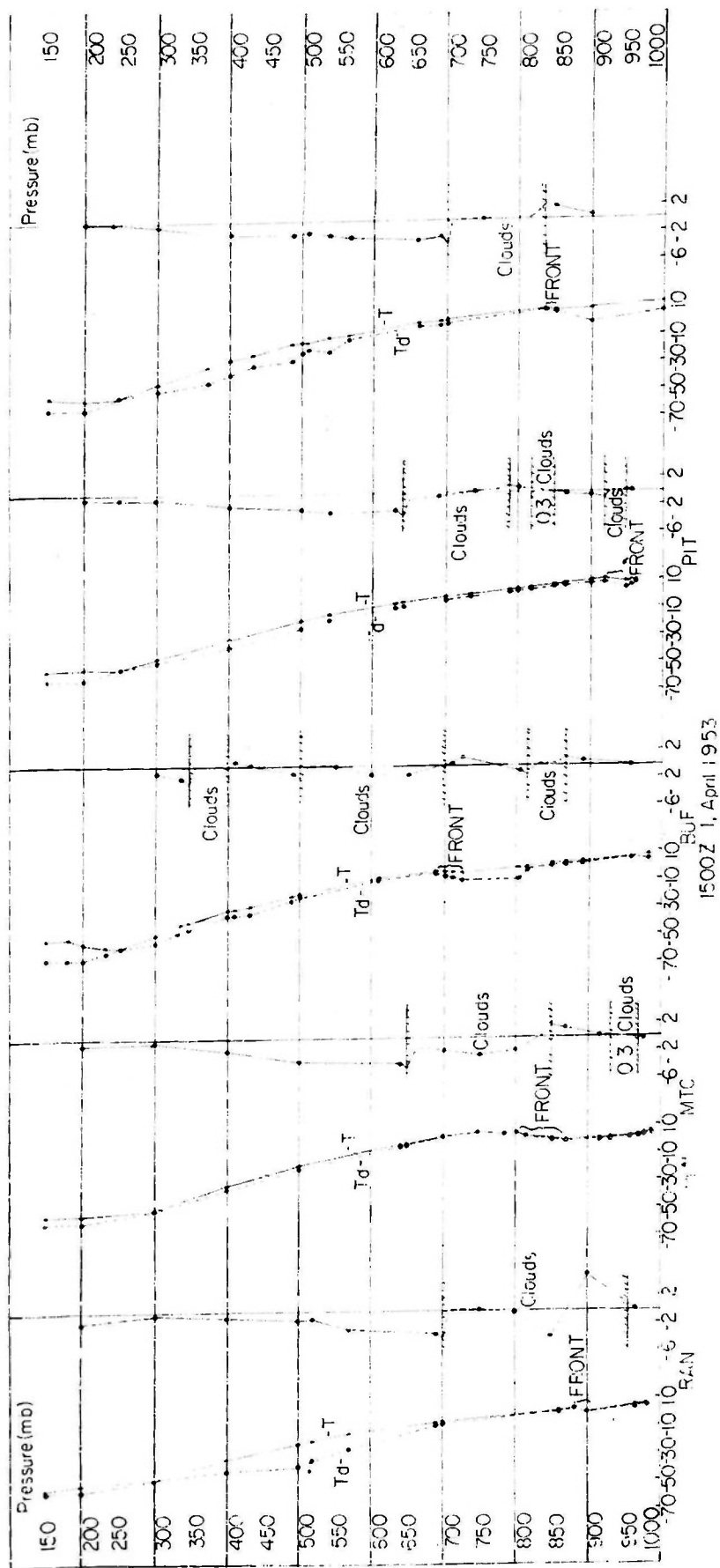
Fig. 41. Lapse rate and cooling rate curves. 1500 GMT, 1 April 1953.
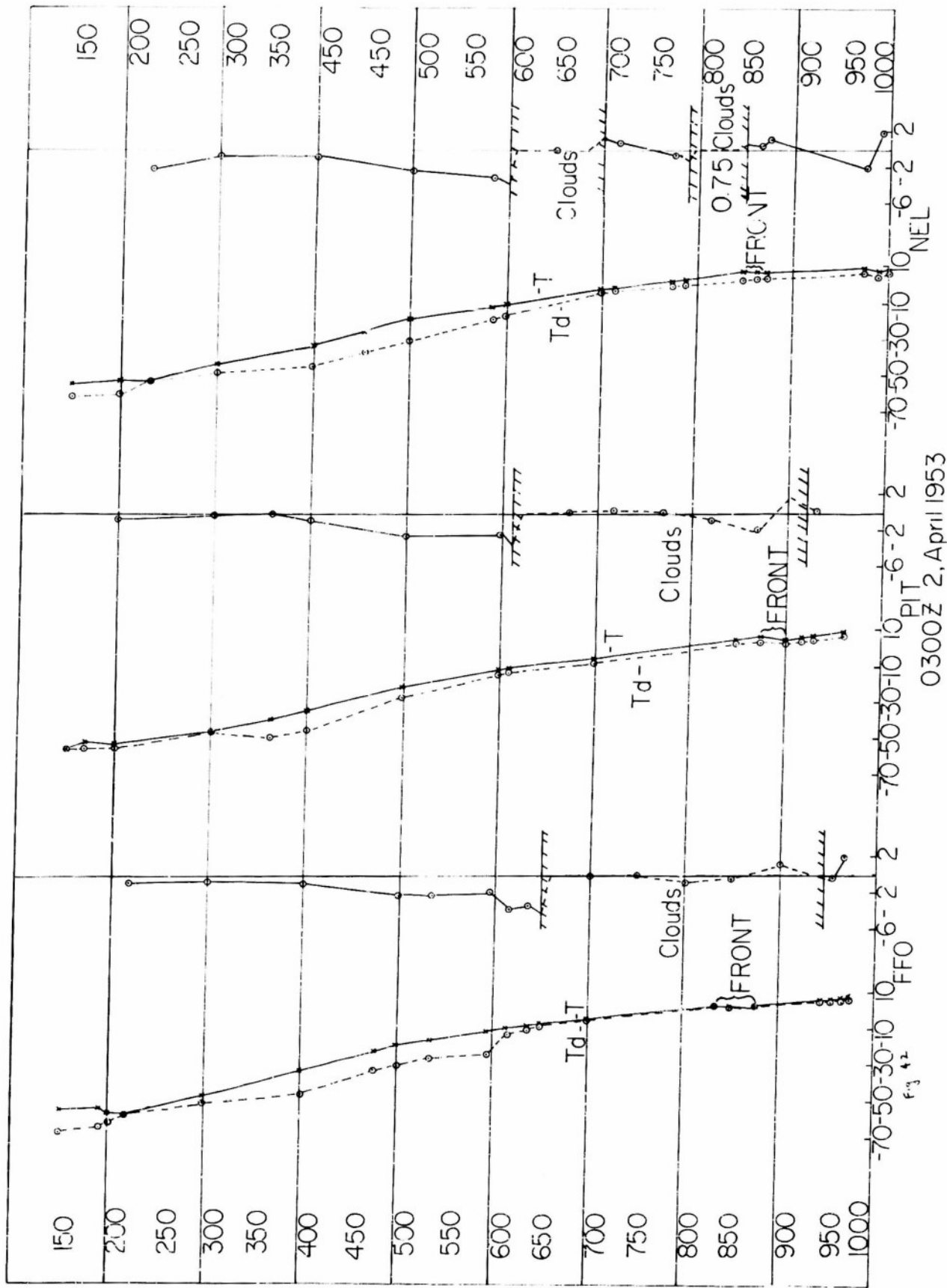
Fig. 42. Lapse rate and cooling rate curves. 0300 CM, 2 April 1953.
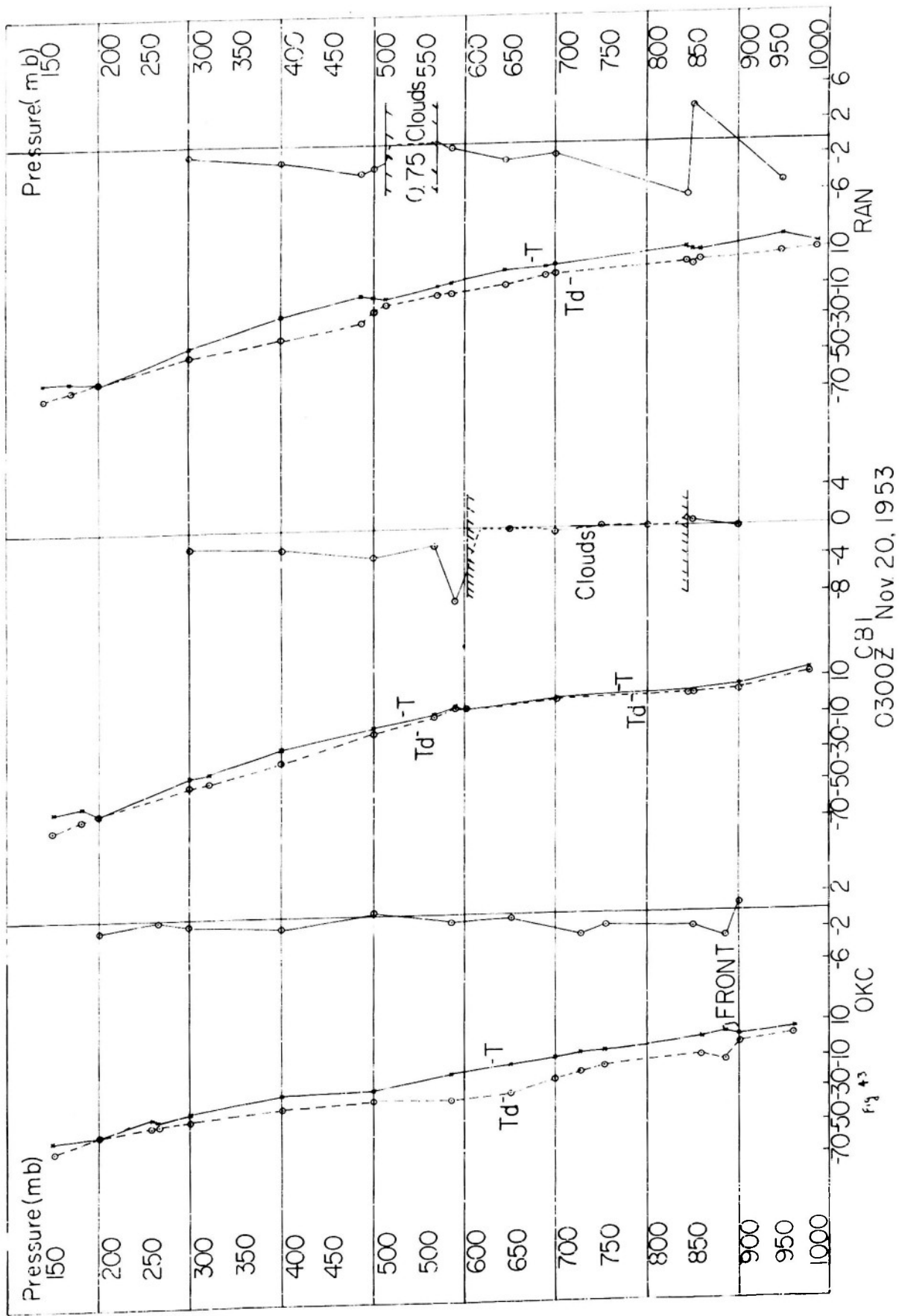
Fig. 43. Lapse rate and cooling rate curves. 0300 GMT, 20 November 1953.
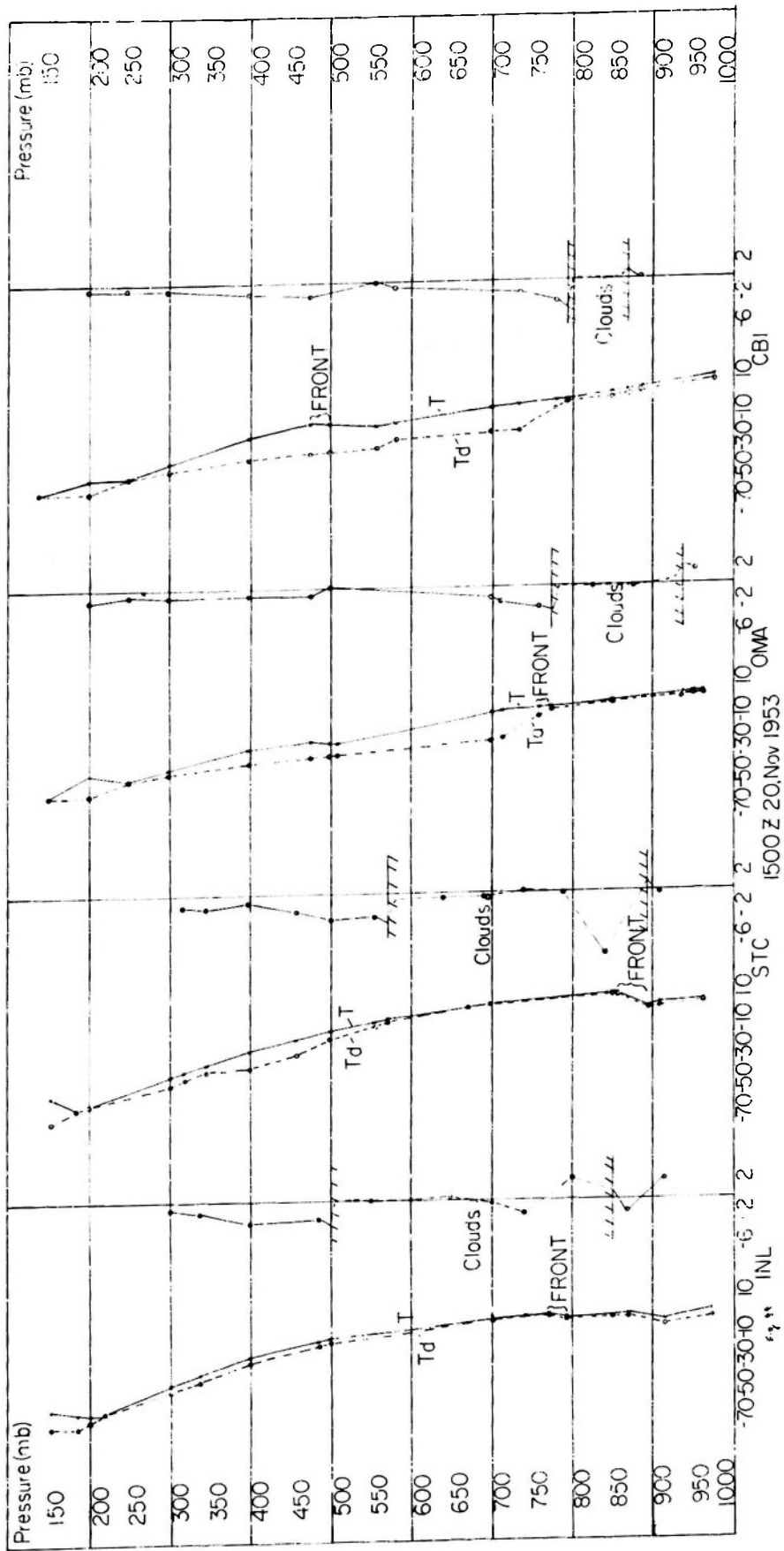
Fig. 44. Lapse rate and cooling rate curves. 1500 GMT, 20 November 1953.

The effect of frontal inversions, which cause radiational cooling at their tops and warming at their bases, can also be seen in the cooling areas. Examples of these large changes from warming to cooling as one goes from the base of the frontal inversion to the top can be seen at Mount Clemens in figure 40 and at Oklahoma City in figure 43.

Within clouds of normal temperature distribution, there is warming near the base, cooling near the top and a tendency for zero cooling throughout the remainder of the cloud.

Irregular temperature soundings caused the erratic cooling and warming rates above Buffalo (fig. 40).

As was indicated previously the radiational cooling is a function of the temperature, the moisture, and the cloud distributions. The effects of cyclonic cloudiness on the cooling rates were discussed in the previous section. Now the effects of temperature and moisture variations upon the radiational cooling rates shall be discussed.

It can be shown that the radiational cooling depends upon the change of the temperature lapse rate. It is to be expected, therefore, that maxima and minima of cooling would occur at places of large curvature of the temperature profile, such as inversions. Large cooling would be expected at the tops of inversions and warming would be expected at the bases of inversions. These effects have already been shown for frontal inversions. This temperature dependence of radiational cooling can be seen in the cooling curves.

Figure 40 contains the Buffalo cooling curve for 0300 GMT, 1 April 1953. Maximum cooling rates are found at the tops of all four inversions in the troposphere and maximum warming rates are found at the bases of these inversions.

Figure 43 contains the cooling curves for Rantoul at 0300 GMT, 20 November 1953. Through the steep inversion from 850 mb to 840 mb the rate of temperature change varies from a warming rate of 4° C/day at the base to a cooling rate of over 6° C/day at the top. A 5° C/day cooling rate at 948 mb is due to the fact that this point is at the top of a ground inversion.

The dependence of radiational cooling upon moisture content can also be seen in the cooling curves. A moist layer radiating upward to a dry atmosphere will cool substantially. A dry layer radiating to a moist atmosphere will not cool as effectively. In figure 42, in the layers above the cloud, the curvature of the

temperature profile at Dayton does not change substantially and therefore does not change the amount of radiational cooling. At 615 mb, the top of a moist layer, the cooling rate is 3.7° C/day. At 595 mb, the top of the dry layer that is located immediately above the moist layer, the cooling rate decreases to 1.9° C/day. This change in cooling rate is due to the sharp change in the dew point lapse rate in the layers involved.

Conclusions

Just above overcast cloud layers the cooling is quite large, generally 2 to 4° C/day. Cloud tops behave as black bodies and radiate very efficiently at their own temperatures. The downward radiation from the water vapor above the cloud is not nearly enough to compensate for the upward radiation of the cloud top. This results in a large net flux directed upward at the cloud top. This net flux increases rapidly with height immediately above the cloud top, since the upward flux decreases at a lower rate than the downward flux. These processes cause a large positive flux divergence immediately above the cloud and therefore a large cooling rate.

Immediately below cloud decks there is slight radiational heating, about 1° C/day. There is heating in the vicinity of cloud bases because the divergence of the net flux is negative, i.e., there is a convergence of the net flux immediately below the cloud base. This convergence of net flux results from the fact that the upward radiation from the layers immediately below the cloud decreases more rapidly with increasing height than does the downward radiation from the cloud and layers immediately underneath it. It can easily be seen that radiational processes tend to make the air within the clouds more unstable, perhaps aiding in the further development of the cloud.

There is a tendency for zero radiational cooling to take place in the interior of clouds. This neutral condition is caused by the fairly constant lapse rates generally observed within clouds. With constant lapse rates, there is no curvature of the temperature profile and therefore no cooling.

Fronts, inversions and discontinuities of lapse rate in general are characterized by a change in the curvature of the temperature profile. This results in great changes in the cooling, since the radiational cooling is a function of the curvature of the temperature profile. Large cooling rates are found at the tops of frontal inversions and other inversions. Warming is generally found at the bases of these inversions. The magnitudes of these rates of temperature change depend upon the steepness of the inversion. In this study, the extremes ranged from +4° C/day at the base of an inversion to -6° C/day at the top of an inversion. Thus long wave radiational processes tend to destabilize the air or destroy the inversion. However, the magnitude of the radiational destabilizing process will decrease in intensity as the inversion is destabilized.

The large radiational cooling rates found in this study, especially at cloud tops and at the tops of inversion layers, may help to explain some of the erratic temperature changes which are occasionally observed on upper air maps. They also suggest a possible source of error in the computation of vertical velocities by the adiabatic method as well as in the advective temperature forecasts.

It is clear that the role of radiational cooling is to "smooth out" the lapse rate curve. Inversions tend to be destroyed by the large radiational cooling at the top and the radiational warming at the bottom. Thus, soundings on which appear a multiplicity of inversion layers are probably quite transitory since they are constantly undergoing modification by radiational processes.

The alteration of inversion layers by radiational cooling, however, is greatly modified by the existence of clouds. A cloud layer with its top at the base of the inversion layer (e.g., stratus and stratocumulus) cause radiational cooling to prevail at the base of the inversion and so maintain the inversion layer. Similarly, a cloud layer with its base at the top of an inversion layer (e.g., frontal altostratus) may prevent the destruction of the inversion by diminishing the radiative cooling which generally prevails at tops of inversions.

Finally, the cooling curves indicate that inversions, including frontal inversions, may move up or down in response to radiative cooling. This fact may explain the difficulty which analysts often experience in establishing continuity between vertical cross sections. Apparently frontal surfaces in the free atmoshere are not always substantial surfaces.

Bibliography

Alder, J. E., 1951: The distribution of water vapor radiative cooling in an outbreak of polar air. Atmospheric Research Project, University of Utah, Quarterly Progress Report No. 5.

Brooks, D. I., 1950: A tabular method for computation of temperature change by infrared radiation in the free atmosphere. Jour. of Meteor., v. 7, 313-321.

Bruinenberg, A., 1946: Een Numerieke methode voor de bepaling van temperature-veranderingen door straling in de vrije atmosfeer. (A numerical method for the calculation of temperature changes by radiation in the free atmosphere.) Koninklijk Nederlandsch Meteorologisch De Bilt. Mededeelingen en Verhandelingen, Serie B, Deel 1, 1-103.

Brunt, D., 1939: Physical and Dynamical Meteorology. Cambridge University Press, London, pp. 131-133.

Elsasser, W. M., 1940: Radiative cooling in the lower atmosphere. Monthly Wea. Rev., v. 68, 185-188.

_____, 1942: Heat transfer by infrared radiation in the atmosphere. Harvard Meteorological Studies No. 6, Harvard University, 107 pages.

Hoffer, T. E., 1951: A study of the long wave radiation balance in certain typical air masses. Atmospheric Radiation Project, University of Utah, Quarterly Progress Report No. 5, Appendix A, 46 pp.

Kaplan, L. D., 1952: On the pressure dependence of radiative heat transfer in the atmosphere. Jour of Meteor., v. 9, 1-12.

London, J., 1952: The distribution of radiational temperature change in the Northern Hemisphere during March. Geophysical Research Papers, No. 18, 64 pp.

Möller, F., 1943: Labilisierung von schichtwolken durch strahlung. Meteorologische Zeitschrift, vol. 60, 212-213.

_____, 1950: Long wave radiation, pp. 34-49 in Compendium of Meteorology, ed. by T. F. Malone, A.M.S., Boston, Mass. ix + 1344 pp.

Neiburger, M., and A. M. Thompson, 1953: The radiational temperature changes over the eastern North Pacific Ocean in July 1949. Jour. of Meteor., v. 10, 167-174.

Penner, C. M., 1948: Note on radiative cooling in the free atmosphere over Arctic Bay. Jour. of Meteor., v. 5, 65-70.

MONTHLY FREQUENCIES OF CYCLOGENESIS IN THE EAST
COASTAL REGION OF THE UNITED STATES

Monthly frequencies of east coastal cyclogenesis have been determined by Miller (1946) for the months October through April on the basis of data from the period 1929-1939. In the present study Miller's data have been supplemented by the addition of cyclones from the ten-year period 1942-1952. The cyclone season has also been extended to include the months September and May.

For the purpose of this study, the east coastal region of the United States was defined by the same boundaries employed by Miller (see Miller's figure 1).

The cyclone types described by Miller were adopted in this study. These include the type A or cold frontal cyclone and the type B or warm frontal cyclone, both of which are illustrated in Miller's paper. It was found necessary, however, to introduce another cyclone type, called type C, which forms at the peak of the warm sector (or point of occlusion) of an occluded cyclone. Type C cyclones may also form on or near north-south oriented cold fronts. These cyclones, which closely resemble the Skagerak cyclones described by Bjerknes and Solberg (1922), generally form near the southern end of the Appalachian Mountains. Since type C cyclones were included in the type B category by Miller, it was necessary to regroup the data for 1929-1939. Therefore the frequency distribution presented below for this period does not correspond exactly to Miller's.

The complete tabulation of the three cyclone types for the twenty-year period studied is given in table 1. The twenty-year averages for each month and for each year are shown in figure 45. A minor adjustment for the variable number of days in each month was made in computing the averages.

The variation of cyclone activity from year to year is shown clearly in the table. In the least active year (1946-1947) only 14 cases of cyclogenesis occurred during the nine-months period, whereas the most active year (1948-1949) saw 39 cases. The average number of cyclones was 29.9 per season of which 12.6 were type A, 19.8 were type B and 5.4 were type C.

It can be seen from figure 45 that September and October are the least active months in terms of cyclone frequency with only 1.8 cyclones per month compared with 4.0 cyclones per month in February and March, the most active
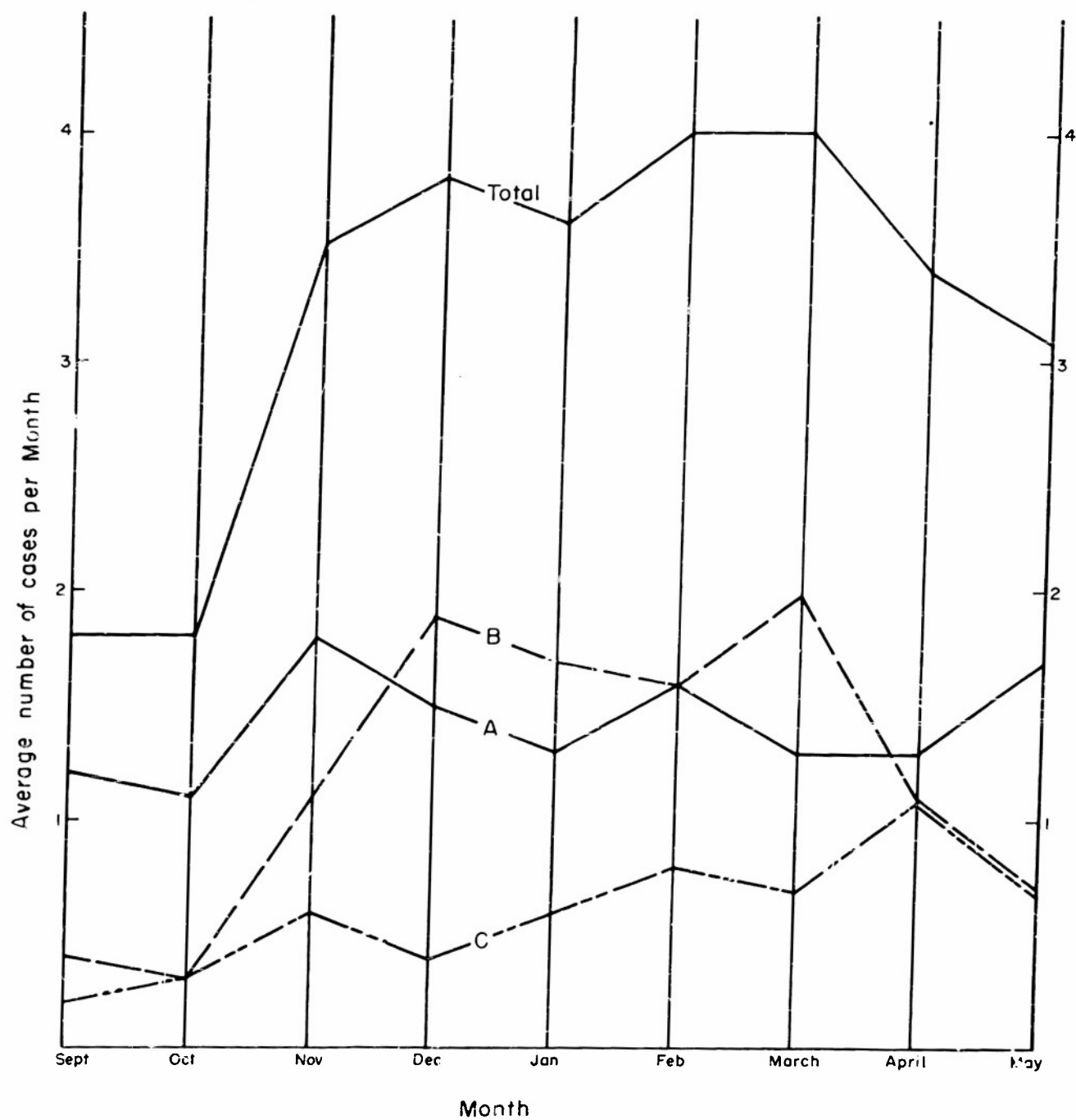
Fig. 45. Monthly frequencies of east coastal cyclogenesis.
Based on data for the years 1929 – 1939 and 1942 – 1952.

months. The seasonal variation of cyclone frequency is due largely to the variation in the number of type B cyclones which ranges from 0.3 in October to 2.0 in March. The type A cyclones range in frequency from 1.1 per month in October to 1.8 per month in November, while the frequencies of type C cyclones range from 0.2 per month in September to 1.1 per month in April. More than two-thirds of the B cyclones occur in the four months December through March, whereas the A and C type cyclones show no such preference for the winter months. It is interesting to note that the secondary minimum of type B cyclone frequency in February which was discovered by Miller, also appears in the 1942-1952 data.

A study was also made of those type B regimes which failed to produce type B cyclogenesis. A type B regime is characterized by a primary cyclone west of the Appalachian Mountains, generally in the Great Lakes region, and a warm or stationary front extending eastward across the coastal plain with a ridge of high pressure to the north. Those type B regimes which did not produce secondary cyclones in the east coastal region are here denoted type D situations.

The monthly frequencies of type D cases are shown in table 2 for the twenty year period investigated. Also shown is the ratio of number of type B cyclones to the sum of type B and D cases for each month. The last statistic may be considered to be a measure of the probability of type B cyclogenesis when the more obvious type B characteristics are present on the surface map.

The table shows clearly that not only are September, October and May months of low type B frequency, but also the probability of type B cyclogenesis under apparently favorable conditions is low in these months. Similarly the months of high type B frequency, December and March, are also the months in which type B cyclogenesis is most probable under these same conditions. On the average, in the nine-months period only thirty percent of the favorable situations produce type B cyclones in the region.

References

Miller, J. E., 1946: Cyclogenesis in the Atlantic coastal region of the United States. J. Meteor., 3, 31-44.

Bjerknes, J. and H. Solberg, 1922: Life cycle of cyclones and the polar front theory of atmospheric circulation. Geofys. Publ., vol. III, No. 1.

TABLE 1. NUMBER OF CASES OF CYCLOGENESIS

MONTH / Type	SEPT. A	SEPT. B	SEPT. C	SEPT. All	OCT. A	OCT. B	OCT. C	OCT. All	NOV. A	NOV. B	NOV. C	NOV. All	DEC. A	DEC. B	DEC. C	DEC. All	JAN. A	JAN. B	JAN. C	JAN. All
1929-30	1	0	0	1	0	0	0	0	5	1	1	7	1	4	0	5	2	0	0	2
30-31	2	0	0	2	2	0	0	2	3	1	0	4	2	1	0	3	0	0	0	0
31-32	1	0	0	1	1	0	1	2	0	0	0	0	1	2	0	3	0	0	0	0
32-33	2	0	0	2	1	0	1	2	1	1	0	3	1	1	0	2	1	1	0	2
33-34	1	0	1	2	1	1	0	2	3	0	0	3	2	1	1	4	2	1	2	5
34-35	0	1	0	1	2	1	0	3	1	0	1	2	3	4	0	7	0	3	1	4
35-36	1	1	0	2	2	0	0	2	4	0	0	4	2	2	2	6	2	3	2	7
36-37	0	0	1	1	1	1	0	2	1	0	1	2	0	0	0	0	2	5	0	7
37-38	2	0	0	2	2	0	0	3	1	1	0	2	2	0	0	2	2	1	2	5
38-39	2	0	1	3	1	0	1	2	1	1	1	3	1	3	2	6	0	4	3	7
Sub-total	**12**	**2**	**3**	**17**	**14**	**2**	**4**	**20**	**21**	**5**	**4**	**30**	**15**	**18**	**5**	**38**	**11**	**18**	**10**	**39**
1942-43	1	1	0	2	0	0	1	1	2	0	0	2	2	1	0	3	2	0	0	2
43-44	3	0	0	3	0	0	0	0	0	0	0	0	0	0	0	0	1	4	0	5
44-45	0	1	0	1	1	1	0	2	1	2	1	4	0	3	1	4	1	2	0	3
45-46	0	0	0	0	2	0	0	2	3	1	0	4	3	3	0	6	1	2	0	3
46-47	1	1	0	2	0	0	0	0	0	0	1	1	1	0	0	1	2	2	0	4
47-48	0	1	0	1	0	1	0	1	1	3	1	5	2	3	0	5	3	2	0	5
48-49	2	1	0	3	2	1	1	4	0	4	2	6	2	5	1	8	0	1	0	1
49-50	2	0	0	2	0	0	0	0	2	5	1	8	0	1	0	1	2	2	1	5
50-51	0	1	1	2	4	1	0	5	4	0	0	4	2	3	1	6	1	0	0	1
51-52	2	0	0	2	0	0	1	1	2	1	1	4	4	1	1	6	2	3	0	5
Sub-total	**9**	**6**	**1**	**18**	**9**	**4**	**3**	**16**	**15**	**16**	**7**	**38**	**16**	**20**	**4**	**40**	**15**	**17**	**2**	**34**
Grand total	**23**	**8**	**4**	**35**	**23**	**6**	**7**	**36**	**36**	**21**	**11**	**68**	**31**	**38**	**9**	**78**	**26**	**35**	**12**	**73**
Av. No. per month (adjusted for no. days per month):	1.2	0.4	0.2	1.8	1.1	0.3	0.3	1.8	1.8	1.1	0.6	3.5	1.5	1.9	0.4	3.8	1.3	1.7	0.6	3.6

	FEB.				MARCH				APRIL				MAY				TOTAL			
	A	B	C	All	A	B	C	All	A	B	C	All	A	B	C	All	A	B	C	All
	2	0	0	2	2	1	1	4	1	3	0	4	1	1	0	2	15	10	2	27
	1	1	0	2	1	1	2	4	2	0	1	3	2	2	2	6	13	7	4	24
	3	1	0	4	1	0	0	1	2	0	2	4	3	1	0	4	10	6	3	19
	1	1	0	5	0	0	2	2	3	1	2	5	2	1	0	2	13	5	8	26
	0	0	0	0	5	0	0	5	3	1	1	5	2	1	0	3	18	5	7	30
	2	2	2	4	0	4	1	5	1	2	0	3	2	0	1	3	11	17	6	34
	2	2	3	4	1	2	1	4	0	2	0	3	0	0	0	0	13	12	7	32
	0	3	3	6	1	3	0	4	0	0	3	2	0	0	1	3	9	12	7	28
	3	0	0	3	2	3	0	5	0	1	1	3	2	1	0	3	17	5	4	26
	1	2	0	3	0	2	1	3	2	2	2	6	3	0	1	4	12	14	11	37
	12 : 14	7	33	13 : 16	8	37	15	11	12	38	18	7	5	31	131	93	59	283		
	1	1	1	3	2	3	0	5	1	0	0	1	1	1	2	3	10	8	4	22
	1	2	1	4	0	2	1	3	1	2	0	3	0	0	0	0	6	10	2	18
	2	1	2	4	0	2	0	2	0	3	0	3	1	1	1	3	4	17	4	25
	1	1	1	4	0	3	1	4	0	2	3	5	4	1	0	5	11	14	8	33
	0	2	0	2	1	1	0	2	1	0	0	1	1	0	0	1	6	4	4	14
	2	0	1	6	1	2	0	3	4	3	2	4	0	3	1	4	11	19	4	34
	3	3	1	6	1	1	1	2	1	0	1	3	3	0	2	5	15	17	7	39
	2	2	1	5	1	4	1	3	3	1	2	5	3	1	0	4	22	13	3	38
	1	1	0	4	3	3	2	8	1	1	1	2	2	1	0	3	21	9	5	35
	1	2	0	2	2	3	2	7	2	0	2	4	1	0	3	4	16	11	8	35
	:17	:15	8	40	:13 :24	7	44	:10	12	9	31	16	8	8	32	122	122	49	293	
	29 : 29	15	73	:26 :40	15	81	25	23	21	69	34	15	13	63	253	215	108	576		
	2.6 : 1.6	0.8	4.0	1.3 : 2.0	0.7	4.0	1.3	1.1	1.1	3.4	1.7	0.7	0.7	3.1						

Table 2. <u>NUMBER OF TYPE D CASES AND RELATIVE FREQUENCY OF TYPE B CYCLONES</u> (1929 - 1939; 1942 - 1952)

	<u>SEPT.</u>	<u>OCT.</u>	<u>NOV.</u>	<u>DEC.</u>	<u>JAN.</u>	<u>FEB.</u>	<u>MARCH</u>	<u>APRIL</u>	<u>MAY</u>	<u>TOTAL</u>
Number of D Cases	37	33	56	53	77	61	59	58	64	498
Average Number per month - (D)	1.9	1.65	2.8	2.65	3.85	3.35	2.95	3.0	3.2	
Number of B plus D cases	45	39	77	91	112	90	99	81	79	713
Average Number per Month (B plus D)	2.3	1.9	3.9	4.5	5.5	4.9	4.9	4.1	3.9	
B/B plus D (percent)	18	15	27	42	31	32	40	28	19	30

Armed Services Technical Information Agency

AD 47616

Reproduced by

DOCUMENT SERVICE CENTER
KNOTT BUILDING, DAYTON, 2, OHIO

UNCLASSIFIED